Design of Experiments on a Semiconductor Plasma Ashing Process: Methods and Analysis

by

Tanay Rahul Nerurkar

Bachelor of Science in Engineering (Mechanical Engineering)
The University of Michigan-Ann Arbor, 2015

Submitted to the Department of Mechanical Engineering in Partial Fulfillment of the Requirements for the Degree of

MASTER OF ENGINEERING IN ADVANCED MANUFACTURING AND DESIGN

AT THE

MASSACHUSETTS INSTITUTE OF TECHNOLOGY

SEPTEMBER 2016

© 2016 Tanay Rahul Nerurkar. All rights reserved.

The author hereby grants to MIT permission to reproduce
and to distribute publicly paper and electronic
copies of this thesis document in whole or in part
in any medium now known or hereafter created.

Signature of Author ______________________________

Tanay Rahul Nerurkar
Department of Mechanical Engineering
August 19th, 2016

Certified by______________________________

Duane S. Boning
Professor of Electrical Engineering and Computer Science
Thesis Supervisor

Accepted by______________________________

Rohan Abeyaratne
Quentin Berg Professor of Mechanics
Chair, Committee of Graduate Students

This page is intentionally left blank.

Design of Experiments on a Semiconductor Plasma Ashing Process: Methods and Analysis

by

Tanay Rahul Nerurkar

Submitted to the Department of Mechanical Engineering on August 19th, 2016
in Partial Fulfillment of the Requirements for the Degree of
Master of Engineering in Advanced Manufacturing and Design

Abstract

Characterizing and controlling process variations in semiconductor manufacturing processes is crucial to ensure the extremely low defect and scrap rates that are needed for semiconductor manufacturing companies to maximize profitability. As semiconductor device critical dimensions become smaller and chips become more complex, and with customers enquiring about process capability metrics to make sure they get the highest quality product, there is a need for chip manufacturers to thoroughly analyze and define their process capabilities. The work in this thesis done in collaboration with Analog Devices Inc., a leading chip manufacturer, shows how the concept of design of experiments (DOE) and statistical regression modeling techniques can be implemented in a practical industrial setting to rigorously understand and mathematically characterize process variations in a semiconductor fabrication process (plasma ashing).

New approaches are introduced to Analog Devices Inc. in calculating wafer statistics. Methodologies are developed that will help the company to choose the right experimental designs based on the objective (e.g. accurate prediction of the response variable, process optimization, process robustness, etc.) while taking into account the process, time, and cost constraints. Multiple regression modeling techniques are utilized to analyze the outcomes of the experiment and the results of these techniques are compared to each other in order to choose the right model needed to satisfy the objective. The statistical software JMP is used to tease out subtle implications of the outcomes of the DOE and formulate hypotheses about any anomalies. The DOEs are performed on two Gasonics Aura 3010 machines that carry out the plasma ashing process using the same process parameters in order to highlight not only the similarities but also the differences in the machines which come from factors like the intrinsic build and state of the machines. The findings and results identify opportunities for the development of new process improvement strategies, faster root cause analysis of failures, methods to systematically calibrate new equipment, update standard operating procedures, and opportunities for machine matching. The purpose of this thesis is to serve as a pedagogical document and template for the process engineers at Analog Devices Inc. in the future to perform DOEs on other processes and machines in the fabrication center.

Thesis Supervisor: Duane S. Boning

Title: Professor of Electrical Engineering and Computer Science

Acknowledgements

The success of this project and thesis would not have been possible without the tremendous support and guidance of my advisors Prof. Duane S. Boning (MIT), Ken Flanders (Analog Devices Inc.), and Jack Dillon (Analog Devices Inc.). I would like to thank them for giving me such a fantastic opportunity and allowing me to work with them and learn from them.

Thank you to my teammates Tan Nilgianskul and Feyza Haskaraman for their ideas and collaboration throughout this project that made my work in this thesis even better and working with them has been a truly fabulous experience.

I owe a deep sense of gratitude towards the process engineering and equipment engineering teams at Analog Devices Inc. especially Megan Kromer, Pam Petzold, Peter Cardillo, Rich DeJordy, Dale Shields, and Brian Chouinard. They have all gone to great lengths in making sure I had access to all the tools and equipment in the fab whenever I needed them, and that I was properly given training on operating the machines.

I would like to thank Jose Pacheco, Prof. David Hardt, and Dr. Brian Anthony for believing in me and allowing me to pursue my graduate degree at MIT. The students, faculty, and staff that I have met and collaborated with in my cohort and the Institute in general have truly challenged me and encouraged me to develop skills and pursue opportunities beyond my wildest imaginations, and I leave Cambridge with many fond memories and lifelong friendships.

I would also like to thank Prof. Dawn Tilbury, Prof. Kira Barton, Nicholas Putman, and Miguel Saez at the University of Michigan for introducing me to many exciting research problems in manufacturing that made my decision to pursue graduate studies in the topic an easy one. I would also like to thank Prof. Allen Liu at the University of Michigan for his advice and guidance in helping me choose a graduate program that would match my needs and career ambitions.

Lastly but most importantly a big thank you to my family, especially my parents Rahul and Ashwini Nerurkar and my sister Shilarna Nerurkar, who have made many sacrifices to ensure I got the best possible education.

This page is intentionally left blank.

Table of Contents

CHAPTER 1: INTRODUCTION **15**

1.1 Background Information on Analog Devices Inc. 15

1.2 General Semiconductor Fabrication Process 16

1.3 Plasma Ashing Process 17

1.4 The Gasonics Aura 3010 Plasma Ashing Machine 18

1.5 Partial Recipe and Process Parameters 20

1.6 Data Collection and Logging 23

1.7 Calculation of Basic Statistics 25

1.8 Problem Statement 27

1.9 Outline of Thesis 29

CHAPTER 2: THEORETICAL REVIEW OF KEY CONCEPTS **30**

2.1 Statistical Process Control 30

2.1.1 Origin of SPC 30

2.1.2 Shewhart Control Charts 31

2.2 Analysis of Variance 32

2.3 Design of Experiments 35

2.4 Statistical Hypothesis Testing 37

2.4.1 Z-Test for Detecting Mean Shift 37

2.4.2 F-test 39

2.4.3 Bartlett's Test 40

CHAPTER 3: DESIGN OF EXPERIMENTS - METHODOLOGY **42**

3.1 Motivation and Need for Design of Experiments 42

3.2 A Standard Methodology for Design of Experiments 44

3.3 Experimental Designs for Linear Models 47

3.4 Experimental Designs for Non-Linear Models 52

CHAPTER 4: DESIGN OF EXPERIMENTS - ANALYSIS **54**

4.1 G53000: Multiple Response Surface Model 54

4.2 G53000: Single Response Surface Model 68

4.3 G53000: Quadratic Response Surface Model 74

4.4 G63000: Multiple Response Surface Model 80

4.5 G63000: Single Response Surface Model 90

4.6 G63000: Quadratic Response Surface Model 95

4.8 Comparison between G53000 and G63000 Machines 101

CHAPTER 5: CONTRIBUTIONS TO ANALOG DEVICES INC. 102

5.1 New Methodologies for Wafer Statistics Calculation 102

5.2 Root Cause Analysis and Machine Diagnostics 104

5.3 Process Improvement Strategies 112

CHAPTER 6: CONCLUSION AND FUTURE WORK 114

6.1 Conclusion 114

6.2 Future Work 114

REFERENCES 115

List of Figures

Figure 1-1: Overview of manufacturing operations at Analog Devices Inc.'s facilities. 16

Figure 1-2: General semiconductor fabrication process 17

Figure 1-3: Schematic of the plasma ashing process. 18

Figure 1-4: A file photo of the Gasonics tool. 19

Figure 1-5: A sample recipe on the display screen of the Gasonics tool. 21

Figure 1-6: Spatial distribution of the nine measured sites on a wafer. 23

Figure 1-7: Co-ordinate values of the nine measured sites on a wafer. 23

Figure 1-8: Areal Representation Ratio of nine sites on the wafer. 25

Figure 1-9: An example of within-wafer non-uniformity and run-to-run variation observed on the plasma ashing process. 27

Figure 1-10: X-bar control chart monitoring the plasma ashing process showing clear mean shifts. 28

Figure 2-1: Example of a Shewhart control chart. 31

Figure 3-1: Plasma ashing process block diagram. 43

Figure 4-1: Specifying model parameters in JMP. 56

Figure 4-2: Normal probability plot of effects affecting photoresist strip rate standardized to have equal variances across all runs in the G53000 machine. 57

Figure 4-3: Normal probability plot of effects affecting photoresist strip rate not standardized that have unequal variances across all runs in G53000 machine. 57

Figure 4-4: Singularity report as seen in JMP. 58

Figure 4-5: Observed values versus model predicted values plot for amount of photoresist removed from site 3 of the wafer in the G53000 machine. 59

Figure 4-6: Model coefficients and hierarchy of significance of factors affecting the amount of photoresist removed from a wafer in the G53000 machine (site 3 of wafer). 60

Figure 4-7: Normal probability plot of residuals for amount of photoresist removed from a wafer in the G53000 machine (site 3). 63

Figure 4-8: Residual versus predicted plot for amount of photoresist removed from a wafer in the G53000 machine (site 3). 63

Figure 4-9: Observed and predicted values of the amount of photoresist stripped at each site for treatment combination [--+-++].. 67

Figure 4-10: Observed and predicted values of the amount of photoresist stripped at each site for treatment combination [00+000] 67

Figure 4-11: Observed and predicted values of the amount of photoresist stripped at each site for treatment combination [+---+-] 67

Figure 4-12: Observed and predicted values of the amount of photoresist stripped at each site for treatment combination [+0+0+0] 67

Figure 4-13: Normal probability plot of effects affecting wafer non-uniformity standardized to have equal variances across all runs in the G53000 machine. 70

Figure 4-14: Observed values versus model predicted values plot for the wafer non-uniformity observed on the G53000 machine. 71

Figure 4-15: Model coefficients and hierarchy of significance of factors affecting the wafer uniformity observed on the G53000 machine. 71

Figure 4-16: Normal probability plot of residuals for wafer non-uniformity observed on the G53000 machine. 72

Figure 4-17: Residual versus predicted plot for wafer non-uniformity observed on the G53000 machine. 72

Figure 4-18: Observed values versus model predicted values plot for the wafer non-uniformity quadratic model obtained from the experiments done on the G53000 machine.................. 76

Figure 4-19: Quadratic model coefficients of factors affecting the wafer non-uniformity observed on the G53000 machine. 76

Figure 4-20: Normal probability plot of residuals for wafer non-uniformity observed on the G53000 machine (quadratic model)........ 77

Figure 4-21: Residual versus predicted plot for wafer non-uniformity observed on the G53000 machine (quadratic model). 77

Figure 4-22: Quadratic response surface for wafer non-uniformity with temperature and oxygen as controllable factors obtained from the experiments done on the G53000 machine. 79

Figure 4-23: Prediction profiler for the response of wafer non-uniformity to temperature and oxygen for the G53000 machine. 79

Figure 4-24: Normal probability plot of effects affecting photoresist strip rate standardized to have equal variances across all runs in the G63000 machine. 81

Figure 4-25: Observed values versus model predicted values plot for amount of photoresist removed from site 3 of the wafer in the G63000 machine. 82

Figure 4-26: Model coefficients and hierarchy of significance of factors affecting the amount of photoresist removed from a wafer in the G63000 machine (site 3 of wafer.) 83

Figure 4-27: Normal probability plot of residuals for amount of photoresist removed from a wafer in the G63000 machine (site 3). 86

Figure 4-28: Residual versus predicted plot for amount of photoresist removed from a wafer in the G63000 machine (site 3). 86

Figure 4-29: Observed and predicted values of the amount of photoresist stripped at each site for treatment combination [-++---] 89

Figure 4-30: Observed and predicted values of the amount of photoresist stripped at each site for treatment combination [000000]. 89

Figure 4-31: Observed and predicted values of amount of the photoresist stripped at each site for treatment combination [++-+--]. 89

Figure 4-32: Observed and predicted values of amount of the photoresist stripped at each site for treatment combination [++++++]. 89

Figure 4-33: Normal probability plot of effects affecting wafer non-uniformity standardized to have equal variances across all runs in the G63000 machine. 91

Figure 4-34: Observed values versus model predicted values plot for the wafer non-uniformity observed on the G63000 machine. 92

Figure 4-35: Model coefficients and hierarchy of significance of factors affecting the wafer non-uniformity observed on the G63000 machine. 93

Figure 4-36: Normal probability plot of residuals for wafer non-uniformity observed on the G63000 machine. 94

Figure 4-37: Residual versus predicted plot for wafer non-uniformity observed on the G63000 machine. 94

Figure 4-38: Observed values versus model predicted values plot for the wafer non-uniformity quadratic model obtained from the experiments done on the G63000 machine. 97

Figure 4-39: Quadratic model coefficients of factors affecting the wafer non-uniformity observed on the G63000 machine. 97

Figure 4-40: Normal probability plot of residuals for wafer non-uniformity observed on the G63000 machine (quadratic model). 98

Figure 4-41: Residual versus predicted plot for wafer non-uniformity observed on the G63000 machine (quadratic model). 98

Figure 4-42: Quadratic response surface for wafer non-uniformity with temperature and oxygen as controllable factors obtained from the experiments done on the G63000 machine. 100

Figure 4-43: Prediction profiler for the response of wafer non-uniformity to temperature and oxygen for the G63000 machine. 100

Figure 5-1: Spatial map of a wafer showing the distribution of sites 103

Figure 5-2: 3-D plot of a wafer showing the amount of photoresist removed at each of the 49 sites 103

Figure 5-3: Spatial distribution map of a wafer processed in the G53000 machine using the partial recipe........ 105

Figure 5-4: Map of the amount of photoresist removed from the wafer sites shown in Figure 5-3. 105

Figure 5-5: Temperature profile of a wafer being processed in the G53000 machine using the partial recipe........ 106

Figure 5-6: Spatial map of wafer processed in the G63000 machine using the partial recipe. .. 107

Figure 5-7: Temperature profile of a wafer being processed in the G63000 machine using the partial recipe........ 107

Figure 5-8: Flat effect on wafer processed in the G53000 machine using the partial recipe. 109

Figure 5-9: Flat effect on wafer processed in the G63000 machine using the partial recipe. 109

Figure 5-10: Amount of photoresist removed from each site in the plasma ashing process using the partial recipe on the G53000 machine. 110

Figure 5-11: Amount of photoresist removed from each site in the plasma ashing process using the partial recipe on the G63000 machine. 110

Figure 5-12: Prediction profiler for the amount of photoresist removed from site 1 of the wafer in the G53000 machine. 111

List of Tables

Table 1-1: Controllable process parameters of the partial recipe. 22

Table 1-2: Nanospec data logging spreadsheet. 24

Table 2-1: A standard ANOVA table for a single factor fixed effect model. 33

Table 2-2: 2^3 full factorial experimental design. 36

Table 2-3: 2^{3-1} factorial experimental design. 37

Table 3-1: The controllable factors and the levels at which they are run. 48

Table 3-2: The 2^{6-2} resolution IV factorial design run table. 48

Table 3-3: The controllable factors and specific levels at which the 3^2 full factorial experiments are run. 53

Table 3-4: 3^2 full factorial design run table. 53

Table 4-1: Values of replicate runs, replicate mean, and replicate variance for amount of photoresist stripped from a wafer in the G53000 machine. 55

Table 4-2: Adjusted R^2 values for observed versus predicted plot for the amount of photoresist removed from all sites on a wafer in the G53000 machine. 60

Table 4-3: Model coefficients for all nine sites for the amount of photoresist removed from a wafer in the G53000 machine. 61

Table 4-4: List of significant two factor interactions for the amount of photoresist removed from a wafer in the G53000 machine. 62

Table 4-5: Test cases for a variety of treatment combinations to validate the wafer non-uniformity model using the multiple response surface method. 65

Table 4-6: Values of replicate runs, replicate mean, and replicate variance for wafer non-uniformity observed on the G53000 machine. 69

Table 4-7: Test cases for a variety of treatment combinations to validate the wafer non-uniformity model using the single response surface method on the G53000 machine. 73

Table 4-8: Values of wafer non-uniformity obtained from the 3^2 full factorial experimental runs done on the G53000 machine. 75

Table 4-9: Test cases for a variety of treatment combinations to validate the wafer non-uniformity quadratic model obtained from the experiments done on the G53000 machine. 78

Table 4-10: Values of replicate runs, replicate mean, and replicate variance for amount of photoresist stripped from a wafer in the G63000 machine. 80

Table 4-11: Adjusted R^2 values for observed values versus predicted values plot for the amount of photoresist removed from all sites on a wafer in the G63000 machine. 83

Table 4-12: Model coefficients for all nine sites for the amount of photoresist removed from a wafer in the G63000 machine. 84

Table 4-13: List of significant two factor interactions for the amount of photoresist removed from a wafer in the G63000 machine. 85

Table 4-14: Test cases for a variety of treatment combinations to validate wafer non-uniformity model obtained from the experiments done on the G63000 machine. 87

Table 4-15: Values of replicate runs, replicate mean, and replicate variance for wafer non-uniformity observed on the G63000 machine. 90

Table 4-16: Test cases for a variety of treatment combinations to validate the wafer non-uniformity model using the single response surface method from the experiments done on the G63000 machine. 95

Table 4-17: Values of wafer non-uniformity obtained from the 3^2 full factorial experimental runs in the G63000 machine. 96

Table 4-18: Test cases for a variety of treatment combinations to validate the wafer non-uniformity quadratic model obtained from the experiments done on the G63000 machine. 99

Table 5-1: Statistics of nine month actual production data from the Gasonics tools with proposed control limits. 108

Chapter 1: Introduction

The work in this thesis presents a methodology to systematically perform design of experiments (DOE) analyses on a semiconductor plasma ashing process. It lays out the necessary tools required to build a statistical regression model and demonstrates potential implications and analyses that could be used to better understand, improve or optimize the process for various parameters of interest. This is an industrial thesis and the work was done in collaboration with Analog Devices Inc. in their Wilmington, MA fabrication center. Analog Devices Inc. is a world leader in the design, manufacture, and marketing of high performance analog, mixed-signal, and digital signal processing integrated circuits used in a broad range of electronic applications and is headquartered in Norwood, MA [1]. Currently, there is a need in the company to rigorously analyze various processes and machine capabilities in an effort to improve yield, throughput, and reduce machine downtime through early detection of equipment anomalies. The purpose of this chapter is to provide background information on Analog Devices Inc., an introduction to the plasma ashing process that was studied in this work, and the problem statement that this thesis attempts to address.

1.1 Background Information on Analog Devices Inc.

Analog Devices Inc. is an American multinational company that specializes in the design, manufacture, and marketing of high performance analog, mixed-signal, and digital signal processing integrated circuits used in a broad range of electronic applications. The company's products play a fundamental role in converting, conditioning, and processing real-world phenomena such as temperature, pressure, sound, light, speed, and motion into electrical signals to be used in a wide array of electronic devices [2].

The company was founded in 1965 by Ray Stata and Matthew Lorber and is headquartered in Norwood, MA. Analog Devices Inc. has operations in 23 countries and serves over 100,000 customers from various industries like consumer electronics, automotive, and defense to name a few. The annual revenue of the company in the fiscal year 2015 was approximately $3.44 billion [2].

The manufacturing and assembly of Analog Devices Inc.'s products is conducted in several locations worldwide. Figure 1-1 [2] shows an overview of the location and functions of the company's manufacturing and assembly facilities.

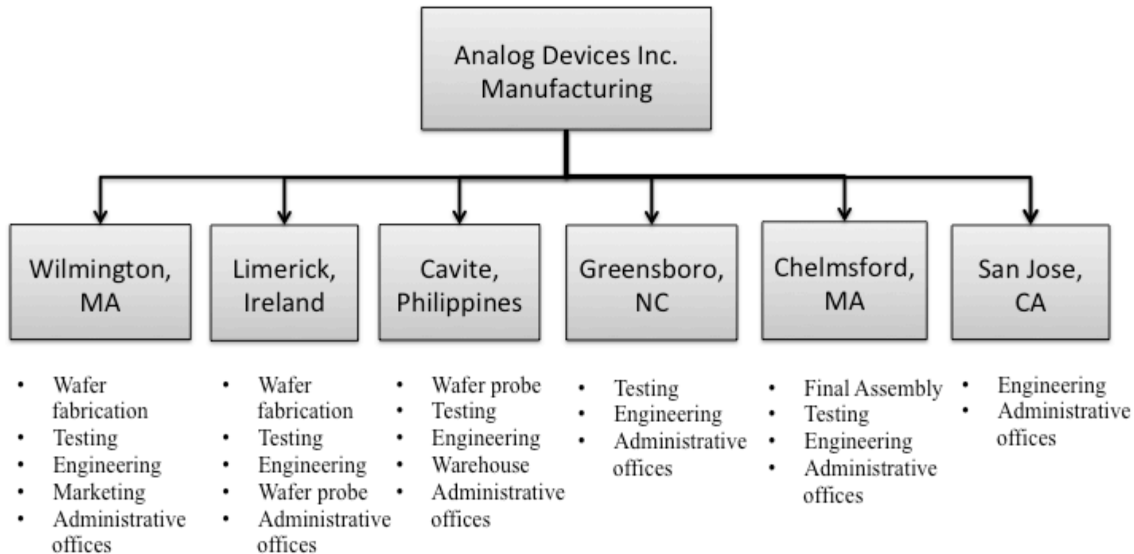

Figure 1-1: Overview of manufacturing operations at Analog Devices Inc.'s facilities.

The experiments in this thesis are carried out on the Gasonics Aura 3010 plasma ashing process tools in the Wilmington, MA fabrication center. This thesis is written in conjunction with the works of Tan Nilgianskul [3] and Feyza Haskaraman [4], and several sections and descriptions in this thesis are written in common with their works.

1.2 General Semiconductor Fabrication Process

Pre-doped wafers are supplied to the Wilmington, MA fabrication center as the starting material. The Wilmington, MA fabrication site is divided into five main sub-departments: thin-films, etch, photolithography, diffusion, and CMP (chemical mechanical polymerization). A key procedure used at many points in the manufacturing of a device is photolithography where photoresist is deposited and patterned on the surface of the wafer. In photolithography, photoresist is spun onto the wafer surface and exposed and developed to create open access to

the surface in some regions, and in other regions the photoresist remains as a blocking mask. The diffusion team then selectively implants impurity ions or the thin-films group deposits metals onto the designated parts of the silicon wafer. The etch group then strips the unwanted photoresist off from these wafers. The function of the CMP group is to use chemical-mechanical reaction techniques to smoothen the surface of the deposited materials. Figure 1-2 [5] gives an overview of the steps and processes involved in semiconductor fabrication.

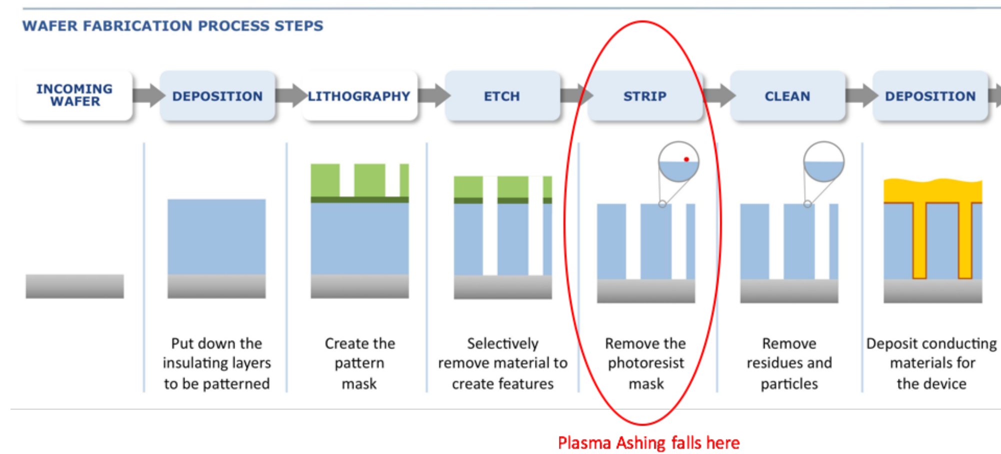

Figure 1-2: General semiconductor fabrication process.

These procedures do not have to go in any particular order. Different types of devices require different configurations of material layers with repeated sequences of photolithography, etch, implantation, deposition, and other process steps. The flexibility of these process steps is what enables the fabrication center to produce customizable electronic parts on a customer's short-term order.

1.3 Plasma Ashing Process

For the purpose of this thesis, the plasma ashing process is investigated. This process is used to remove photoresist (light sensitive mask) from an etched wafer using a monoatomic reactive species that reacts with the photoresist to form ash, which is removed from the vicinity of the wafer using a vacuum pump. The reactive species is generated by exposing a gas such as

oxygen or fluorine to high power radio or microwaves, which ionizes the gas to form monoatomic species [6], [7]. Figure 1-3 [6] shows a general schematic of the plasma ashing process with the key components indicated.

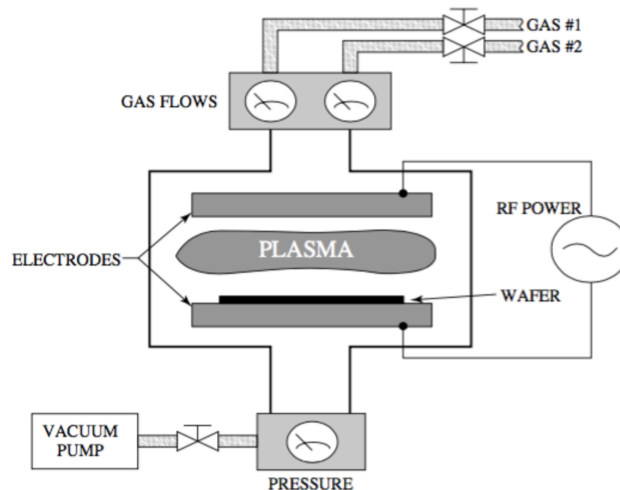

Figure 1-3: Schematic of the plasma ashing process.

Analog Devices Inc. uses the Gasonics Aura 3010 machines (hence forth will be referred to as Gasonics tools or Gasonics machines) to carry out the plasma ashing process. The reactive gas used by the company is oxygen and microwaves are used to ionize the gas. The Gasonics tool allows for the change of several variables including wafer temperature, chamber pressure, and power that make up a recipe to allow for different photoresist removal rates that may be needed for different products.

1.4 The Gasonics Aura 3010 Plasma Ashing Machine

The Gasonics Aura 3010 machine is used by Analog Devices Inc.'s Wilmington, MA fabrication center for photoresist ashing and cleaning of semiconductor wafers by creating a low-pressure and low-temperature glow discharge, which reacts chemically with the surface of the wafer [8]. The Gasonics system is composed of three main components:

i. The reactor chamber that contains the system controller, the electro-luminescent display, wafer handling robot, the microwave generator, and the gas box.
ii. The power enclosure wall box.
iii. The vacuum pump.

Figure 1-4 [9] below shows a picture of the Gasonics Aura 3010 machine.

Figure 1-4: A file photo of the Gasonics tool.

The machine is equipped with a three axis of motion wafer handling robot that picks up a single wafer from a twenty five wafer holding cassette and places it in the process chamber to execute the photoresist stripping process. After a particular recipe is executed, the robot removes the wafer and places it on a cooling station if required before returning the wafer back to its slot in the cassette. Inside the process chamber, the wafer rests on three sapphire rods and a closed loop temperature control (CLTC) probe which includes a thermocouple to measure the temperature of the wafer during the ashing process. Twelve chamber cartridges embedded in the chamber wall heat the process chamber. During the plasma ashing process, eight halogen lamps heat the wafer to the required process temperature. The process gases (oxygen or nitrogen) are mixed and delivered to a quartz plasma tube in the waveguide assembly where microwave energy generated by a magnetron ionize the gases into the monoatomic reactive species. The

machine is designed in a way to only allow the lower-energy free radicals and neutrals to come in contact with the wafer surface as higher energy radicals can damage the wafer. After the wafer has been stripped, the halogen lamps, microwave power, and the process gas flows are turned off and the process chamber is then purged with nitrogen before being vented to the atmosphere for wafer removal. The door to the process chamber is then opened and the robot removes the wafer to either place it on the cooling station or put it back in the cassette slot [8].

Analog Devices Inc.'s Wilmington, MA fabrication center has seven Gasonics machines which have a codename of GX3000 where X is a number between 1 and 7. The experiments and analysis that are presented in this work were conducted on G53000 and G63000 machines.

1.5 Partial Recipe and Process Parameters

A recipe is defined as a set of input settings that can be adjusted over an operating range on a tool or machine to execute a desired manufacturing process at those settings. For example, consider Figure 1-5 [8] which shows a sample recipe on the display screen of the Gasonics machine. The machine allows the operator to vary the quantities under the column "PARAMETER". The process engineers in the company are responsible for proposing and executing an optimal recipe taking into account product quality, throughput, and cost constraints. In addition to designing recipes for production wafers, Analog Devices Inc. also designs recipes to run qualification tests. Qualification tests are used to periodically monitor product quality and verify machine calibrations. In this thesis, the qualification test recipe that has been studied is named "partial" by Analog Devices Inc.

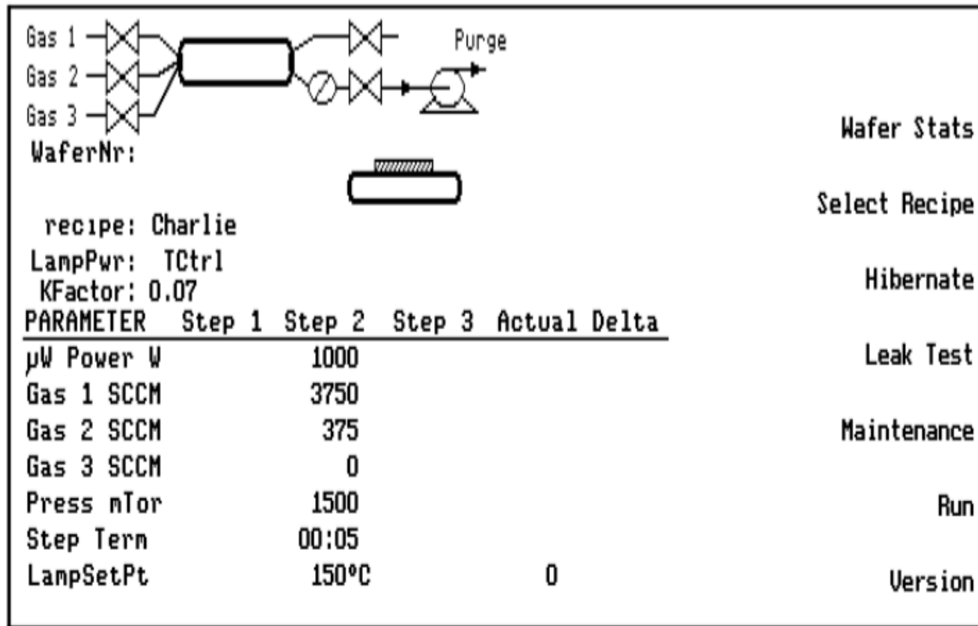

Figure 1-5: A sample recipe on the display screen of the Gasonics tool.

The partial recipe is used as a qualification test to calibrate the rate of photoresist removal on the Gasonics machine. The recipe is designed such that the photoresist mask is not completely removed from the wafer after the process. This is intentionally done so that the amount of photoresist removed and the time taken to do so can be recorded. An ideal Gasonics machine would remove 6000 Angstroms of resist in eight seconds. The entire process with the partial recipe takes approximately 63 seconds with the first 20 seconds being allocated to heating the wafer to the necessary conditions and bringing the machine to steady state (step-1), the next eight seconds being allocated to the stripping process (step-2), and the last 35 seconds being allocated to cooling the wafer. Table 1-1 shows the necessary machine parameters needed for the partial recipe.

Machine Parameter	Step-1	Step-2
Temperature (Celsius)	215	235
Pressure (mTorr)	2000	2000
Power (Watts)	0	1400
Blower Vacuum Pump Speed (k/min)	6	6
Main Vacuum Pump Speed (k/min)	5.5	5.5
Oxygen Gas Flow (SCCM)	3750	3750
Nitrogen Gas Flow (SCCM)	375	375
Step Term (Seconds)	20	8

Table 1-1: Controllable process parameters of the partial recipe.

The description of the partial recipe process parameters listed in Table 1-1 is as follows:

- ***i.*** ***Temperature:*** This is the temperature to which the wafer is heated to and maintained during the plasma ashing process.
- ***ii.*** ***Pressure:*** This is the pressure of the gases present inside the reacting chamber of the Gasonics machine during the plasma ashing process.
- ***iii.*** ***Power:*** This is the power needed by the magnetron to generate the necessary microwave energy to ionize the reacting gases.
- ***iv.*** ***Blower and Main Vacuum Pump Speeds:*** The main vacuum pump speed refers to the rate at which the residue ash and excess gases are removed from the reacting chamber. The blower pump is an addition to the main pump aiding in increasing the removal rate of the residue ash and gases. The speed of the main pump is kept constant while the speed of the blower pump is varied from recipe to recipe.
- ***v.*** ***Oxygen Gas Flow:*** This is the rate at which oxygen gas is allowed to flow into the reacting chamber during the process. The unit of measurement is standard cubic centimeter per minute (SCCM)
- ***vi.*** ***Nitrogen Gas Flow:*** This is the rate at which nitrogen gas is allowed to flow into the reacting chamber during the process. The unit of measurement is SCCM.
- ***vii.*** ***Step Term:*** This is the duration of each step in the plasma ashing process.

1.6 Data Collection and Logging

The key parameters that need to be measured in the plasma ashing process are the amount of photoresist removed from the wafer and the wafer non-uniformity after the process has been completed. The amount of photoresist removed divided by the time for which the Gasonics tool was set to function gives the photoresist removal rate, which Analog Devices Inc. uses to infer machine health. The tool used to measure the amount of photoresist removed in Analog Devices Inc.'s Wilmington fabrication center is the Nanospec 9200 measuring tool (Nanospec). The Nanospec tool has the capability to accurately measure wafer thicknesses in the Angstrom range. The Nanospec tool is programmed to measure nine sites on each wafer. Figures 1-6 and 1-7 shows the spatial distribution as well as the co-ordinate ordered pair values of the nine sites on each wafer. In the spatial distribution diagram, the blue dots indicate the sites where the measurements are taken.

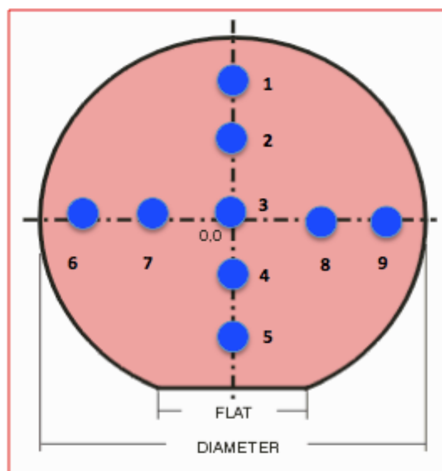

Figure 1-6: Spatial distribution of the nine measured sites on a wafer.

X co-ordinate (mm)	Y co-ordinate (mm)
0	65
0	32.5
0	0
0	-32.5
0	-60
-65	0
-32.5	0
32.5	0
65	0

Figure 1-7: Co-ordinate values of the nine measured sites on a wafer.

The measurement procedure of the thickness of the photoresist of the nine sites using the Nanospec tool is as follows:

i. The thickness of the photoresist is measured and recorded before the wafer undergoes the plasma ashing process. These are known as "*pre-measurements*".

ii. The thickness of the photoresist is measured and recorded after the wafer undergoes the plasma ashing process. These are known as "*post-measurements*".

iii. The difference between the pre-measurements and post-measurements gives the amount of photoresist removed during the process.

iv. The amount of photoresist removed can be divided by the duration of the plasma ashing process to give the rate of resist removal. The duration of the plasma ashing process is included as an input and monitored by the Gasonics tool.

The amount of photoresist removed for each of the nine sites on a single wafer is recorded in an excel spreadsheet on which further analysis can done. An example of the excel spreadsheet can be seen in Table 1-2. In Table 1-2, the columns in the spreadsheet represent the measurements taken on the nine sites within a single wafer while the rows represent different wafers measured. The Nanospec tool also logs the date and time of the measurement, which is very useful in anomaly detection.

Site 1	Site 2	Site 3	Site 4	Site 5	Site 6	Site 7	Site 8	Site 9	ET_TIME
5549.35	5659.8	5763.96	5824.96	5877.34	5501.67	5699.48	5739.73	5540.88	6/20/15 8:07
5410.93	5524.85	5631.59	5688.9	5707.29	5356.96	5555.87	5612.81	5428.14	6/23/15 8:59
5493.44	5571.64	5671.82	5760.63	5794.19	5456.9	5618.04	5647	5462.18	6/27/15 7:57
5436.46	5552.35	5689.99	5784.46	5802.86	5460.92	5645.25	5648.27	5389.47	7/6/15 9:01
5595	5682	5796	5878	6004	5450	5724	5892	5699	7/10/15 9:39
5587.58	5693.32	5829.78	5954.44	6019.11	5571.12	5772.03	5817.37	5567.42	7/13/15 20:12

Table 1-2: Nanospec data logging spreadsheet.

1.7 Calculation of Basic Statistics

The raw data collected from the Nanospec 9200 tool as shown in Table 1-2 needs to be manipulated further in order to make meaningful implications of the underlying trends and patterns. This section introduces the method that is used to calculate three statistical quantities:

i. The mean thickness of the nine sites on a single wafer ($\bar{x}^*$)
ii. The standard deviation of the nine sites on a single wafer (s)
iii. The wafer non-uniformity parameter (NU)

The nine sites that the Nanospec 9200 tool measures on a single wafer are distributed in a radial pattern from the center as can be seen in the spatial distribution diagram in Figure 1-6. Generally, in a radial distribution wafer measuring pattern, the calculation of any statistics on the sites measured on a wafer have to take into account the wafer area represented by each site for accurate analysis [10]. Figure 1-8 shows the wafer areal representation of each site on a nine site radial distribution pattern. The wafers used for the purposes of this study have a diameter of six inches.

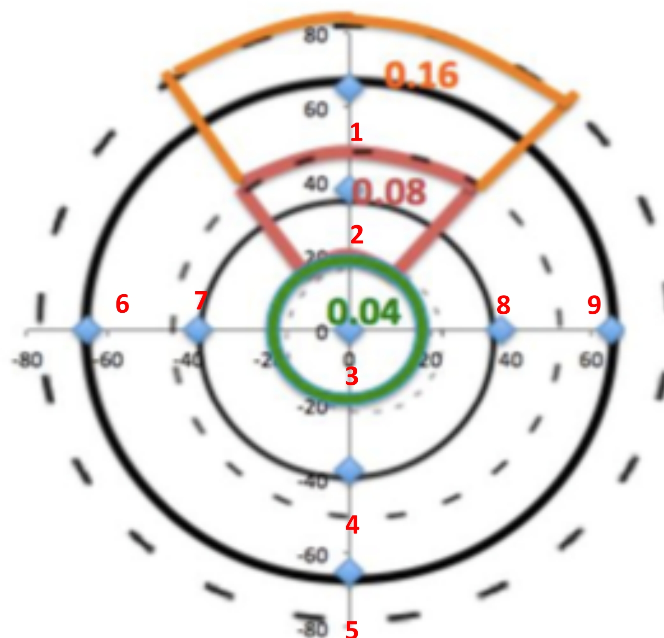

Figure 1-8: Areal Representation Ratio of nine sites on the wafer.

In Figure 1-8, site 3 represents the area bounded by the green circle (4% of the total wafer area), sites 2, 4, 7, and 8 each represent the area bounded by the red segments (32% of the total wafer area), and sites 1, 6, 5, and 9 each represent the area bounded by the orange segments (64% of the total wafer area).

The mean ($\bar{x}^*$) [11] taking into account the areal representation of each site is calculated as follows:

$$\bar{x}^* = \frac{\sum_{i=1}^{N} w_i x_i}{\sum_{i=1}^{N} w_i}$$

Equation 1-1

where x_i is the wafer thickness measured at each site, w_i is the weighted area associated with that site and N is the number of sites.

The standard deviation (s) [11] taking into account the areal representation of each site is calculated as follows:

$$s = \sqrt{\frac{\sum_{i=1}^{N} w_i}{\left(\sum_{i=1}^{N} w_i\right)^2 - \sum_{i=1}^{N} w_i^2} \cdot \sum_{i=1}^{N} w_i (x_i - \bar{x}^*)^2}$$

Equation 1-2

where x_i is the wafer thickness measured at each site, w_i is the weighted area associated with that site, N is the number of sites, and $\bar{x}^*$ is the mean.

The wafer non-uniformity parameter (*NU)* [12] taking into account the areal representation of each site is calculated as follows:

$$NU = \frac{s}{\bar{x}^*}$$

Equation 1-3

where s is the standard deviation and $\bar{x}^*$is the mean. The wafer non-uniformity parameter will be henceforth expressed as a percentage.

1.8 Problem Statement

Semiconductor fabrication facilities need to maintain extremely high yields in order to maximize profitability. As a result, fabrication centers need to have a thorough understanding of their process capabilities and implement strategies that will minimize process variations to the best of their ability. Characterization and control of process variations in semiconductor manufacturing processes is the most challenging and crucial aspect for any fabrication facility given the dimensions (nanometers) at which chips are currently made. Small process variations can completely destroy modern devices. Moreover, many etching and deposition processes have multiple inputs and process steps where each input and process step can be a source of variation. This can quickly lead to a variation stack up if process control methods are not implemented appropriately. In semiconductor manufacturing, process variations manifest in multiple and interconnected ways, including variations observed within each wafer (wafer non-uniformity), variations between wafers (run-to-run), variations between batches of wafers (batch-to batch), and variation between machines executing the same process with the same parameters (machine-to-machine). An example of wafer non-uniformity and run-to-run variation in the plasma ashing process done on a Gasonics machine is shown in Figure 1-9. The columns represent the amount of photoresist removed at each site on a wafer while the rows represent the measurements taken on different wafers. The ideal scenario is that a target of 6000 Angstroms of photoresist stripped is achieved on every site of every wafer.

Within wafer variation

Site 1	Site 2	Site 3	Site 4	Site 5	Site 6	Site 7	Site 8	Site 9	ET_TIME
5549.35	5659.8	5763.96	5824.96	5877.34	5501.67	5699.48	5739.73	5540.88	6/20/15 8:07
5410.93	5524.85	5631.59	5688.9	5707.29	5356.96	5555.87	5612.81	5428.14	6/23/15 8:59
5493.44	5571.64	5671.82	5760.63	5794.19	5456.9	5618.04	5647	5462.18	6/27/15 7:57
5436.46	5552.35	5689.99	5784.46	5802.86	5460.92	5645.25	5648.27	5389.47	7/6/15 9:01
5595	5682	5796	5878	6004	5450	5724	5892	5699	7/10/15 9:39
5587.58	5693.32	5829.78	5954.44	6019.11	5571.12	5772.03	5817.37	5567.42	7/13/15 20:12

Run to Run Variation

Measurements are in Angstroms

Figure 1-9: An example of within-wafer non-uniformity and run-to-run variation observed on the plasma ashing process.

The combined effect of the shrinking of device critical dimensions, increase in component density per chip, and more complex functionality requirements has resulted in semiconductor manufacturers needing to seek new methods to continuously monitor, update, and improve their process capabilities. Analog Devices Inc. is in a similar situation where the company is revaluating its current process control capabilities and wants to incorporate newer methods including real-time process control, automatic feedback control, and cloud-based analytics to improve its process monitoring capabilities. Currently the company uses traditional control charts to monitor its processes, but the process engineers at the company are convinced that the current charts are deficient in timely detection of unnatural drifts and mean shifts that could have negative consequences on future product lines. An "x-bar" control chart for tracking the average amount of photoresist removed during the plasma ashing process on the Gasonics tool with the current control limits is shown in Figure 1-10. There are clear mean shifts and variations are as high as 20% in the process that are not being detected by the current limits which is a cause of concern.

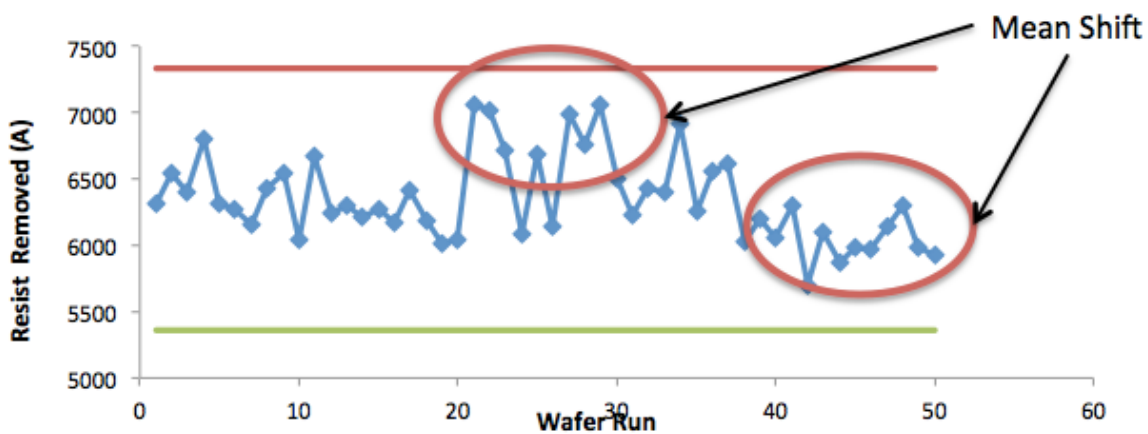

Figure 1-10: X-bar control chart monitoring the plasma ashing process showing clear mean shifts.

The goal of this project is to introduce Analog Devices Inc. to new process control methodologies that will provide them with a rigorous analysis and understanding of their current

process capabilities on the plasma ashing process done on the Gasonics tool. The three main areas of focus are as follows:

i. Recalculate and propose new control limits on current charts or develop new charts monitoring new variables that are a true representation of the natural variation of the plasma ashing process (Nilgianskul's thesis [3]).
ii. Characterize and quantify the response of the amount of photoresist removed and the spatial uniformity of the wafer in the plasma ashing process with respect to the controllable input parameters on an individual machine basis (The focus of this thesis*)*.
iii. Compare the performance of two Gasonics machines and propose machine-matching strategies to reduce or eliminate the differences in their performances and ensure that the machines function at their optimal level (Haskaraman's thesis [4]).

Analog Devices Inc. will then use the proposed methods, results, and findings to improve process capabilities on other tools and processes in the fabrication center.

1.9 Outline of Thesis

Chapter 1 is the introduction that provides background information on Analog Devices Inc. and introduces the reader to general semiconductor fabrication processes, the plasma ashing process, and the problem statement that this thesis aims to address. Chapter 2 provides a theoretical review of the key concepts and mathematical techniques of statistical process control, design of experiments, and statistical hypothesis testing which have been compiled from various literature sources. Chapter 3 discusses the motivation, the methods, and the reasoning behind selecting the necessary experimental designs and formulating the statistical regression models that can predict the behavior of the response variable to a high degree of confidence over a range of the controllable factors. Chapter 4 provides a comprehensive analysis on the outcomes of the experiments performed using the methods outlined in Chapter 3. Chapter 5 outlines the specific contributions made to Analog Devices Inc. from the insights obtained from the design of experiments analysis. Chapter 6 presents the conclusion of the thesis and the scope for future work.

Chapter 2: Theoretical Review of Key Concepts

This chapter will give a brief introduction to the theory behind key concepts that are relevant to the construction of this thesis and the overall project in general. The ideas presented in this chapter have been compiled from a variety of literature sources. The key topics described are statistical process control, analysis of variance, design of experiments, and statistical hypothesis testing.

2.1 Statistical Process Control

Statistical process control (SPC) is used to monitor and control variations in a manufacturing process. Controlling process variations is important in a manufacturing environment because decreased variability in a process reduces scrap and rework rates leading to lower costs and improved product quality.

2.1.1 Origin of SPC

Walter A. Shewhart at Bell Laboratories introduced the SPC method in the early 1920s. Later in 1924, Shewhart developed the control chart and coined the phrase “a state of statistical control” which can actually be derived from the concept of exchangeability developed by logician William Ernest Johnson in the same year in one of his works called *Logic, Part III: The Logical Foundations of Science* [13]. The theory was first put in use in 1934 at the Picatinny arsenal, an American military research and manufacturing facility located in New Jersey. After seeing the success of this project, the US military further enforced statistical process control methods among its other divisions and contractors during the outbreak of the Second World War [14].

2.1.2 Shewhart Control Charts

A Shewhart control chart plots a measured parameter that is an indicator of the process performance over a period of time. These plots are then bounded by control limits which are, as a rule-of-thumb, three standard deviations away from the mean on either side. An example of a control chart is shown in Figure 2-1 [15].

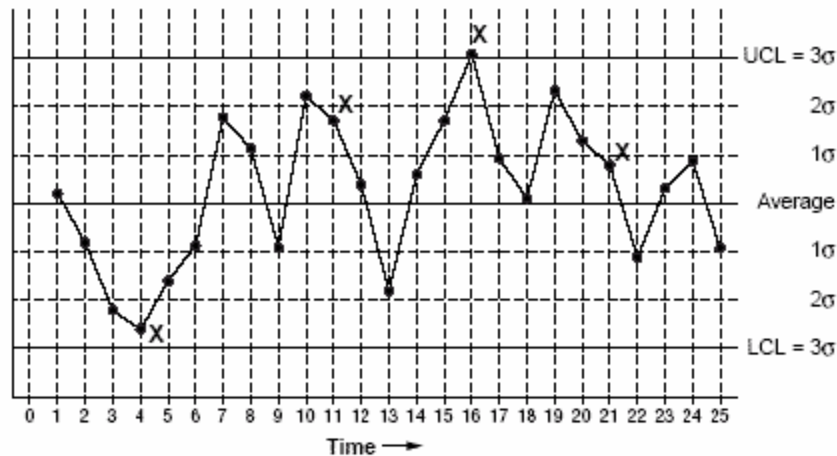

Figure 2-1: Example of a Shewhart control chart. Points marked with X's are points that would be rejected based on Western Electric rules.

Control charts can either be plotted as a run chart or an x-bar chart. The run chart plots each measurement separately while the x-bar control chart plots the average of several measurements. Other statistics like variance, range, and standard deviation are also plotted in addition to the x-bar chart.

The goal of plotting control charts is to monitor the state of the manufacturing process and detect when it is out of control. Assuming that the data plotted is normally distributed, which is the case for most processes, the chance that any single point would lie above the upper control limit (UCL) or below the lower control limit (LCL) (three standard deviations above or below the mean) would be less than 0.3%. Assuming that a set of data is normally distributed with mean μ and variance σ^2, UCL and LCL can be expressed as:

$$UCL = \mu + 3\sigma$$

Equation 2-1

$$LCL = \mu - 3\sigma$$

Equation 2-2

The probability of a point lying beyond the limits for any normally distributed data set can be solved for.

$$P(X > UCL) = P\left(Z > \frac{UCL - \mu}{\sigma}\right) = P(Z > 3) \approx 0.0013$$

$$P(X < UCL) = P\left(Z < \frac{\mu - LCL}{\sigma}\right) = P(Z < 3) \approx 0.0013$$

$$P(X > UCL||X < LCL) = P(X > UCL) + P(X < LCL) \approx 0.0013 + 0.0013 \ \approx 0.0027$$

$$P(\text{point lies outside control limit}) \sim 0.3\%$$

Equation 2-3

Besides the upper and lower control limit rule, there are other rules (Western Electric) that could be used as guidelines to suspect when the process is out of control. These include 1) if two out of three consecutive points lie either two standard deviations above or below the mean 2) four out of five consecutive points lie either a standard deviation above or below the mean 3) nine consecutive points fall on the same side of the centerline/mean [15].

2.2 Analysis of Variance

Analysis of variance (ANOVA) is a statistical hypothesis testing method used to compare the mean values of populations at more than two levels of a factor to determine the effect of that factor. The methodology for a "fixed effects model ANOVA"(assume a constant effect τ between the levels of the factor) for a single factor at a levels is presented below and equal number of observations n are taken at each level. The observed response y_{ij} where j is the observation number and i is the level of the factor can be modeled statistically as:

$$y_{ij} = \mu + \tau_i + \varepsilon_{ij}$$

Equation 2-4

where μ is the overall mean of the population, τ_i is the fixed effect at level i of the factor and ε_{ij} is the random error term ($i=1,2,\ldots,a$ and $j=1,2,\ldots,n$) [16]. The hypothesis that will be tested is as follows:

$$H_O = \tau_1, \tau_2, \ldots, \tau_a = 0 \text{ (Null Hypothesis)}$$

$$H_1: \tau_i \neq 0 \text{ for atleast 1 } i$$

Equation 2-5

If the null hypothesis is true, changing the levels of the factor has no influence on the overall mean of the response. The total variation in the data can be measured by the total sum of squares (SS_{total}) which can be partitioned in the ANOVA analysis into the differences between the sum of squares ($SS_{treatments}$) of the level means ($\bar{y}_i = \sum_{j=1}^{j=n} \frac{y_{ij}}{n}$) and overall population mean ($\bar{\bar{y}} = \sum_{i=1}^{i=a} \sum_{j=1}^{j=n} \frac{y_{ij}}{an}$) and the differences of sum of squares (SS_{error}) of observations within a level (y_{ij}) and the level mean ($\bar{y}_i$). As a result of this partitioning, one can understand the effect of different levels of a factor from $SS_{treatments}$ and the variation due to random error within a level due to SS_{error}. An important assumption in the ANOVA analysis is that the variances of observations across all levels of the factor must be the same. Using the above information the standard ANOVA table can be constructed as shown in Table 2-1 [16].

Variation Source	**Sum of Squares**	**Degrees of Freedom**	**Mean Square**	**F-value**
Between Levels	$SS_{treatments} = n \sum_{i=1}^{i=a} (\bar{y}_i - \bar{\bar{y}})^2$	*a-1*	$MS_{treatments} = \frac{SS_{treatments}}{a-1}$	$\frac{MS_{treatments}}{MS_{error}}$
Within Levels	$SS_{error} = \sum_{i=1}^{i=a} \sum_{j=1}^{j=n} (y_{ij} - \bar{y}_i)^2$	*a(n-1)*	$MS_{error} = \frac{SS_{error}}{a(n-1)}$	
Total	$SS_{total} = SS_{treatments} + SS_{error}$	*an-1*		

Table 2-1: A standard ANOVA table for a single factor fixed effect model.

The F-test can then be used to test the hypothesis described in Equation 2-5 at a chosen significance level. The standard ANOVA table and method can be extended to include more than one factor which then is known as multivariate analysis of variance (MANOVA). MANOVA is extensively used in design of experiments analysis to test for the significance of factor effects on a response variable. Statistical software programs like JMP and Minitab are used to construct the ANOVA and MANOVA tables [17], [18].

In semiconductor manufacturing, extra attention will be paid to the concept of nested analysis of variance. In nested variance analysis, the fixed effect assumption no longer holds true. Nested variance analysis will determine the significance of the variance between and within groups and subgroups of data [19]. For instance, assume there are W groups of data (an example would be observations made wafer-to-wafer*)* with M data points in each of those groups (observations made within each wafer), the mean squared sum between groups (MS_W) and within groups (MS_E) can be calculated as follows.

$$MS_W = \frac{SS_W}{W-1}$$

Equation 2-6

$$MS_E = \frac{SS_E}{W(M-1)}$$

Equation 2-7

where:

$SS_W =$ squared sum of deviations of group means from grand mean

$SS_E =$ squared sum of deviations of each data point from its group mean

Note that SS_W sums up the grand-group mean deviation for every individual point. So in this case, each squared difference between grand to group mean difference is multiplied by M before summing them together. The significance of the between-group variation could then be determined, given that the ratio MS_W/MS_E approximately follows the F-distribution.

It is important to note that the observed variance of the group averages does not reflect the actual wafer-to-wafer variance because of the existence of sub-variation (group variance).

The observed variation between the group averages $\sigma_{\bar{w}}^2$ can be written as a linear combination of the true variance σ_w^2 and the group variance σ_M^2.

$$\sigma_{\bar{w}}^2 = \sigma_w^2 + \frac{\sigma_M^2}{M}$$

Equation 2-8

Hence the true group-to-group variance can be expressed as:

$$\sigma_w^2 = \sigma_{\bar{w}}^2 - \frac{\sigma_M^2}{M}$$

Equation 2-9

From this, both the group-to-group component and the within-group component can be expressed as a percentage of the total variance. This variance decomposition is useful in differentiating between measurements made among wafers and within wafers.

2.3 Design of Experiments

Design of experiments (DOE) is a statistical method used to quantify the effects of process input parameters on the process output parameter (response variable). The output parameter should give a strong indication of the process performance for a DOE analysis to be useful. DOEs are powerful in identifying process causality within a certain manufacturing process. This information could then be used to tune the process inputs in order to optimize the outputs to achieve production goals. The focus of a DOE analysis is on planning a series of experiments in order to characterize the process in the most efficient manner. Several experimental designs have been proposed and developed over the years for a variety of different purposes like screening insignificant process parameters, optimizing a response variable, and making a process less vulnerable to nuisance factors.

Factorial experimental designs used in this thesis allow for the modeling and analysis of several factors and their interactions. These designs are built upon the foundation of analysis of variance and orthogonality. An analysis of variance table or the normal probability plot of the factor effects is used to identify the most significant factor effects on the response variable.

Orthogonality is defined as the relative independence of multiple variables that is vital to deciding which parameters can be varied simultaneously to get the same response of the output parameter. Regression analysis is used for model building purposes [16], [20].

Full factorial experiments are time consuming and may not be always possible to do in a practical industrial setting. Therefore to reduce the number of runs, fractional factorial experimental designs are used. Such designs are good for effects screening purposes but not all of the terms can be modeled in a fractional factorial experiment. These designs require aliasing or confounding of main effects and interactions and this may reduce the fidelity of the regression model. In most cases, the higher order interactions are typically less significant than lower-order interactions and so smart decisions in choosing the aliasing relationships can significantly improve the outcome of the experiment. Table 2-2 shows the full factorial (2^3) experimental design for a process with three variable input parameters (A, B, and C) varied at two levels (2^3) [16].

Run	A	B	AB	C	AC	BC	ABC
1	-1	-1	+1	-1	+1	+1	-1
2	+1	-1	-1	-1	-1	+1	+1
3	-1	+1	-1	-1	+1	-1	+1
4	+1	+1	+1	-1	-1	-1	-1
5	-1	-1	+1	+1	-1	-1	+1
6	+1	-1	-1	+1	+1	-1	-1
7	-1	+1	-1	+1	-1	+1	-1
8	+1	+1	+1	+1	+1	+1	+1

Table 2-2: 2^3 full factorial experimental design. -1 indicates a low setting while +1 represents the high setting of the input parameter.

By defining the following identity relation and aliases:

$$I = \text{ABC}$$

$$\text{A} = \text{BC}$$

$$\text{B} = \text{AC}$$

$$C = AB$$

a fractional factorial experimental design can be constructed out of the full factorial design in Table 2-2. Table 2-3 shows the fractional factorial design. If through prior process knowledge it is determined that only the main effects need to be modeled, then the design in Table 2-3 is more practical than the full factorial experiment.

Run	Factors		
	A	B	C
1	-1	-1	+1
2	+1	-1	-1
3	-1	+1	-1
4	+1	+1	+1

Table 2-3: 2^{3-1} factorial experimental design.

2.4 Statistical Hypothesis Testing

A statistical hypothesis test compares at least two sets of data that can be modeled by known distributions. Then assuming that those data follow the proposed distributions, the probability that a particular statistic calculated from the data occurs in a given range can be determined. This probability is also referred to as the P_{value} and is ultimately the basis to either accept or reject the current state or the null hypothesis. The acceptance/rejection cutoff is marked by a pre-determined "significance level". Generally, the decision as to what significance level to use would depend on the consequences of either rejecting a true null hypothesis (type I error) versus accepting a false null hypothesis (type II error) [16]. The three upcoming sub-sections will outline the statistical hypothesis tests used in this project.

2.4.1 Z-Test for Detecting Mean Shift

The Z-test refers to any hypothesis test whereby the distribution of the test statistic under the null hypothesis is modeled by the normal distribution. This becomes useful in many cases

(including this project) because of the central limit theorem. With the central limit theorem, means of a large number of samples of independent random variables approximately follow a normal distribution. Mathematically, the sample mean of any distribution of mean μ of sample size n and standard deviation σ would be normally distributed with the same mean and standard deviation $\frac{\sigma}{\sqrt{n}}$, or $\sim N\left(\mu, \frac{\sigma}{\sqrt{n}}\right)$.

For instance, when testing for whether the mean of a given process (with default mean μ and standard deviation σ) has shifted, the following hypotheses can be formed [16].

$$H_0: \mu = \mu_0$$

$$H_1: \mu \neq \mu_0$$

Equation 2-10

The null hypothesis H_0 is assumed to hold with the true mean μ being equal to the assumed mean μ_0. Now given a set of data with sample mean $\bar{x} > \mu_0$, the test statistic Z could be calculated.

$$Z = \frac{\bar{x} - \mu_0}{\sigma/\sqrt{n}}$$

Equation 2-11

The P_{value} can then be deduced as follows.

$$P_{value} = P(\bar{x} > \mu_0) = P(z > Z)$$

Equation 2-12

Given a significance level α, the null hypothesis would be rejected if $P_{value} < \alpha/2$ or, equivalently, if $Z > Z_{\alpha/2}$ then the alternative hypothesis H_1 would be accepted indicating that the mean has shifted.

The probability of encountering a type I error would be the significance level α itself, i.e. P (Type I Error) = α. Given an alternative mean μ_1, the distribution of the alternative hypothesis could be written as $\bar{x} \sim N(\mu_1, \sigma/\sqrt{n})$. Hence the probability of making a type II error could be calculated as

$$P(\text{Type II Error}) = P(\bar{x} < \bar{x}_{critical})$$

Equation 2-13

where $\bar{x}_{critical}$ is the $\bar{x}$ that corresponds to $Z_{1-\alpha/2}$ under the old mean μ_0.

$$\bar{x}_{critical} = \mu_0 + Z_{1-\frac{\alpha}{2}} \cdot \sigma$$

Equation 2-14

Therefore, continuing from Equation 2-14

$$P(\text{Type II Error}) = P\left(Z < \frac{\mu_0 - \mu_1}{\sigma} + Z_{1-\frac{\alpha}{2}}\right)$$

Equation 2-15

As previously mentioned, the significance level would depend on the tolerance for these two errors. For instance, if the detection of a mean shift would trigger an alarm and it is very costly to encounter a false alarm, then a lower α would be desired in order to minimize *P* (Type I Error). However, if it is very crucial to detect the mean shift even at the cost of incurring several false alarms, then a higher α would be desirable to minimize *P* (Type II Error).

Note that the example presented is a two-sided test because the P_{value} is tested against the probability of the sample mean being too far from the mean on either side. If it was a one sided test, then the alternative hypothesis would be $H_1: \mu > \mu_0$ or $H_1: \mu < \mu_0$, the P_{value} would be compared to α and the null hypothesis would be rejected if $Z_0 > Z_\alpha$ (no ½ factor on α). The format of other tests will follow a similar structure to the example above but with different formulas for calculating the test statistics and their probabilities.

2.4.2 F-test

Rather than detecting a mean shift, the F-test determines whether the ratio of the variance of two sets of data is statistically significant. Following the same method as in the previous Z-test example, the F-test begins with formulating hypotheses around the variance (s_1^2 *and* s_2^2) of two sets of data [16].

$$H_0: s_1^2 = s_2^2$$

$$H_1: s_1^2 \neq s_2^2$$

Equation 2-16

The test statistic F_0 in this case is simply the ratio of the variances where the numerator is the greater of the two variances, $s_1^2 > s_2^2$. F_0 can approximately be modeled by the F-distribution.

$$F_0 = \frac{s_1^2}{s_2^2}$$

Equation 2-17

The null hypothesis H_0 would be rejected under a certain significance level α if $F_0 > F_{n_1-1,n_2-1,\alpha}$ where n_1 and n_2 represent the sample sizes of the first and second data sets respectively. Alternatively, the P_{value} could be calculated and tested directly against the significance level. The calculation of the P_{value} is shown in Equation 2-18 below.

$$P_{value} = P(F > F_0)$$

Equation 2-18

This is a one-sided test. To modify this into a two-tailed test, F_0 would simply be compared with $F_{n_1-1,n_2-1,\alpha/2}$. Typically for testing whether or not two variances are different, a two-tailed test would not be used.

2.4.3 Bartlett's Test

Bartlett's test is used to determine whether k samples are sampled from distributions with equal variances. The null and alternative hypotheses can be formulated as follows.

$$H_0: s_1^2 = s_2^2 = s_3^2 \dots = s_k^2$$

$$H_1: s_i^2 \neq s_j^2, \text{for at least one pair } (i, j)$$

Equation 2-19

Given the k samples with sample sizes n_i, and sample variances s_i^2, the test statistic T can be written as follows [21].

$$T = \frac{(N-k)\ln\left(s_p^2\right) - \sum_{i=1}^{k}(n_i - 1)\ln\left(s_i^2\right)}{1 + \frac{1}{3(k-1)}\left(\sum_{i=1}^{k}\left(\frac{1}{n_i - 1}\right) - \frac{1}{N-k}\right)}$$

Equation 2-20

where N is the total number of data points combined and s_p^2 is the pooled estimated variance.

$$N = \sum_{i=1}^{k} n_i$$

Equation 2-21

$$s_p^2 = \frac{1}{N-k}\sum_{i}^{k}(n_i - 1)s_i^2$$

Equation 2-22

T can be approximated by the chi-squared distribution. H_0 would therefore be rejected under a significance level α if $T > \chi^2_{k-1,\alpha}$.

Chapter 3: Design of Experiments - Methodology

This chapter discusses the motivation, the method, and the thought process of selecting the necessary experimental designs and formulating the statistical regression models that can model the response of the output variable to a high degree of confidence over a range of input parameters or factors. The DOEs studied in this thesis were conducted using the partial qualification recipes on two Gasonics machines. The response variables under consideration are the amount of photoresist removed and the wafer non-uniformity parameter.

3.1 Motivation and Need for Design of Experiments

Variations are an inherent part of any manufacturing process, and an important objective of any process engineer is to develop a solid understanding of these variations so that significant improvements can be made in areas like throughput, product quality, and machine health. SPC techniques and Shewhart control charts discussed in Nilgianskul's thesis [3] are important tools for detecting unnatural variations in a process. However, when an out-of-control point is detected on a control chart, it may be at times difficult, time consuming, and costly to identify and fix the root cause of the problem if there is a lack of understanding of the properties of the underlying process variations and input-output parameter relationships. This calls for a need to develop mathematical or statistical models, where the response of the output can be quantified with respect to each of the inputs that can be varied on a particular process as well as the interactions between these inputs. Developing such a quantitative model allows for the identification of the most significant factors or factor interactions that affect the output response of the process, thereby enabling effective root cause analysis of problems that leads to both time and cost savings.

DOE is an effective and widely used statistical model building method applicable to many processes and industries. The basic principle of a DOE analysis is to use statistical methods including hypothesis testing, ANOVA, and regression analysis to model how systematic changes made to the inputs of a process affect the response of the output. DOEs have been

effectively used in screening factor effects, process optimization, process robustness, and determining process capability metrics [20].

Processes in the semiconductor manufacturing industry have many variable input parameters that can affect the output of the process. For example, in the plasma ashing process using the partial ashing recipe, which is studied in this thesis, six distinct factors, are identified that could have a significant impact on the amount of photoresist removed from a wafer and the wafer non-uniformity. Variations in any of these factors or a combination of the factors could have a significant impact on both response variables, and this leads to complications in troubleshooting the root causes of problems if a rigorous analysis of the input-output parameter relationships is not conducted. Figure 3-1 shows a block diagram which portrays how the input parameters relate to the output in the plasma ashing process on the Gasonics machine. A PID controller is used to keep the input parameters at their necessary set points throughout the duration of the process.

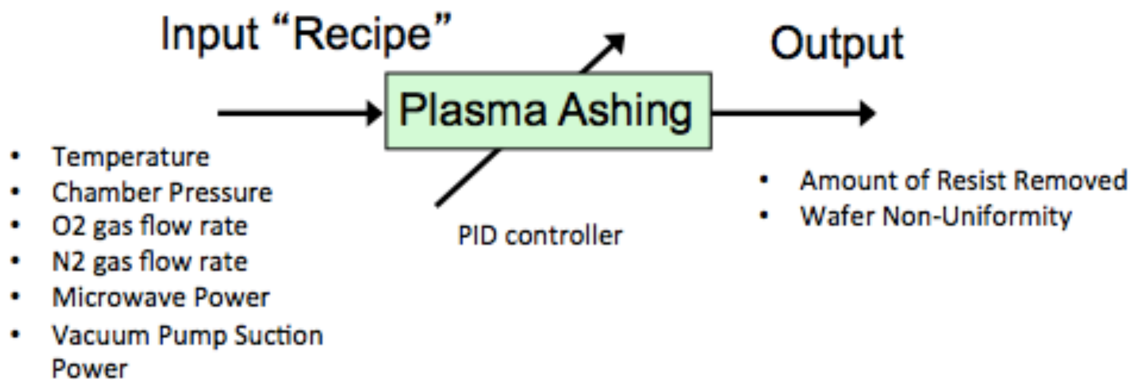

Figure 3-1: Plasma ashing process block diagram.

Theoretical equations that take into account the physics and chemistry of the process, while useful as a starting point in root cause analysis or process optimization, generally do not provide a complete picture, as they fail to consider the inherent variations in a process such as those variations that come from the build of a machine or properties of raw materials ordered from different suppliers. Therefore, a DOE analysis that provides a statistical model to relate the input factors to the output, taking into account the process variations, is a preferred method for

factor screening, root cause analysis, and process optimization. For a theoretical review of DOE, refer to Section 2.3.

Analog Devices Inc. is interested in formally implementing a DOE methodology on processes in their Wilmington, MA fabrication facility to aid in effective root cause analysis of unnatural process variations, and in strategies for designing recipes for optimal machine matching as outlined in Haskaraman's thesis [4].

3.2 A Standard Methodology for Design of Experiments

While DOEs are an effective tool in statistical model building, constructing a high fidelity model using a DOE method can be time consuming and draining on resources, especially in an industrial setting. Therefore smart assumptions and decisions must be made during the pre-experimental planning stage, as described by Montgomery [16], that includes the stages of the choice of factors and levels, selection of the response variable, and the choice of the experimental design.

When there are multiple factors of interest in a process that could significantly impact the response of the output, as is the case with the plasma ashing process on the Gasonics machine for the partial recipe (six factors as shown in Figure 3-1), a factorial experimental design (full or fractional) is used. In a full factorial experimental design, each replicate of the experiment is run at all possible combinations of the levels of the factors under consideration. Full factorial experiments are generally tedious, time consuming and not practical in an industry setting if the numbers of levels or factors are large. For example, if a full factorial experiment is performed on the plasma ashing process at two levels for each of the six process factors, then the total number of treatments that need to be run in a single replicate is 64 (2^6). Therefore fractional factorial experimental designs are much more common in such cases as they save both time and cost. Fractional factorial experimental designs may yield lower fidelity models than full factorial designs, but calculated decisions taken about choosing the runs in the design table (balanced and orthogonal designs) and the aliasing and confounding structure can overcome this challenge in most cases. The rules in statistics that work in favor of fractional factorial designs and that are

used in determining the aliasing and confounding structure to obtain a high fidelity model are as follows [20]:

i. ***Sparsity of Effects:*** This principle states that there usually are only a small number of factors that explain the majority of the variance in a process if a large number of factors are under consideration.
ii. ***Hierarchy of Effects:*** This principle states that usually lower order factors and interactions will contribute more to the response of the output than the higher order terms. For example, main effects are usually more significant than two factor interactions and two factor interactions are more significant than three factor interactions, etc.
iii. ***Inheritance of Effects:*** This principle states that the interactions between factors are most likely to have a strong influence on the response of the output if those individual factors each have a strong influence on the response of the output.

The most common approach to doing a DOE analysis that involves multiple factors is to choose a fractional factorial experimental design that helps model the main effects and lower order interactions, and that aliases the higher order interactions. Such an experiment is used to identify the most significant factors affecting the response of the output, and if required, further experiments can be done to refine the model using only the significant factors.

In the case of the partial plasma ashing recipe on the Gasonics machine, Analog Devices Inc. is primarily interested in determining the most significant factors that could affect the amount of photoresist removed and the non-uniformity across the wafer. The company is also interested in quantifying how a unit change in one of the significant factors or a combination of factors can affect the amount of photoresist removed at each of the nine sites measured on the wafer as described Section 1.6, and if there is an optimal set of parameters that would minimize the non-uniformity within each wafer while maintaining the target photoresist removal of 6000 Angstroms.

The general methodology of conducting a DOE analysis, keeping in mind the semiconductor industry and what was recommended to Analog Devices Inc., is outlined below. These recommendations are focused on DOE analysis particularly for screening non-significant factors and process characterization [16].

i. ***Selection of the process and response variable:*** There should be a clear understanding about the shortcomings of a particular process and ways in which a DOE analysis can be effective in alleviating some parts or all of the current shortcomings. It is important to choose a response variable that can provide the most useful information about the process under study, and that the response variable is a measured quantity with good gauge repeatability and capability. Using a measured quantity directly as a response variable as opposed to a quantity that is calculated using a theoretical equation is preferable because of potential errors in the theoretical equation assumptions. As a result, the derived quantity may not be a pure mathematical transformation of the measured value.

ii. ***Selection of the factors and levels:*** The choice of input factors to be studied, the range over which each input factor is varied, and the levels at which they are investigated are key steps in a DOE analysis. Leveraging prior process knowledge both in the theoretical and practical sense is important in this step. Generally, if the experiment is being done for screening or process characterization purposes then the number of factor levels is kept low. However, if a high fidelity model is needed, then the number of factor levels and replicates required may be more. The tradeoff between model accuracy and the time and cost of running the experiments must be considered during the stage of selecting the factors and levels.

iii. ***Experimental design choice:*** This step is linked with the purpose of the experiment. If the experiment is run with the purpose of screening factors or process characterization, then a fractional factorial design with an acceptable resolution and aliasing structure is generally chosen and preferred. However, if a more accurate statistical model is needed or a response surface needs to be generated, then a full factorial design or other available designs like the central composite design must be chosen [20]. This stage also involves choosing the number of replicates needed, running center points to determine lack of fit, randomizing the run order, and accounting for restrictions such as blocking.

iv. ***Performing the experiment and data collection:*** Before performing the experimental runs it is crucial to check the process equipment and tool conditions and to make sure everything is functioning as per expectations. The gauge capability of the measuring tools should also be verified. A few test and validation runs before running the actual experiments may be useful for gauge and machine validation. While performing the

experiments, it is necessary to monitor the process for any anomalies that could jeopardize the DOE. Clear instructions in the form of standard operating procedures must be given to the operators running the experiments to avoid any human error.

v. ***Data analysis and model validity:*** Several statistical software packages exist for analyzing the results of a DOE. In this thesis, the results were analyzed using the JMP software [17]. The key statistical concepts behind a DOE analysis are discussed in Section 2.3. Regression analysis is used to fit a model to the data obtained from a DOE [16]. For validating the model, analytical techniques (residual analysis and lack of fit analysis) as well as physical validation like post experimental runs are recommended.

vi. ***Reiteration of the experiment:*** If the data analysis shows that the results are not satisfactory or the model is not accurate enough, then a refinement of the model may be necessary. The general approach to refining a model is to select the most significant factors deduced from the previous analysis and redesign a new DOE based on those factors either by doing a full factorial analysis or if a significant lack of fit exists, choosing a design that allows the calculation of higher order terms (central composite design, three level factorial design, etc.).

3.3 Experimental Designs for Linear Models

The partial recipe for the plasma ashing process as described in Section 1.5 has six controllable factors that could have a significant impact on the amount of photoresist removed and the wafer non-uniformity. Since a full factorial experimental design at two levels would have needed 64 runs for each replicate, it was therefore decided to do a 2^{6-2} resolution IV fractional factorial experiment with center points to test for curvature. Each run including the center point would be replicated three times. Table 3-1 shows the six factors and the specific levels at which the experimental runs are performed, while Table 3-2 shows the fractional factorial design run table.

Parameter	Variable	Low(-1)	High(+1)	Center (0)
Temperature	A(Celsius)	220	250	235
Pressure	B (mTorr)	1600	2400	2000
Power	C (Watts)	1100	1400	1250
Pump Speed	D (k/min)	4.8	7.2	6
O2	E (SCCM)	3000	4500	3750
N2	F (SCCM)	300	450	375

Table 3-1: The controllable factors and the levels at which they are run.

	Temperature	Pressure	Power	Pump speed	O2	N2
Treatment	A	B	C	D	E	F
1	-1	-1	-1	-1	-1	-1
2	+1	-1	-1	-1	+1	-1
3	-1	+1	-1	-1	+1	+1
4	+1	+1	-1	-1	-1	+1
5	-1	-1	+1	-1	+1	+1
6	+1	-1	+1	-1	-1	+1
7	-1	+1	+1	-1	-1	-1
8	+1	+1	+1	-1	+1	-1
9	-1	-1	-1	+1	-1	+1
10	+1	-1	-1	+1	+1	+1
11	-1	+1	-1	+1	+1	-1
12	+1	+1	-1	+1	-1	-1
13	-1	-1	+1	+1	+1	-1
14	+1	-1	+1	+1	-1	-1
15	-1	+1	+1	+1	-1	+1
16	+1	+1	+1	+1	+1	+1
17	0	0	0	0	0	0

Defining Relation

I=ABCE=BCDF=ADEF

Table 3-2: The 2^{6-2} resolution IV factorial design run table.

The main purpose of doing the 2^{6-2} resolution IV fractional factorial design experiment is to screen out the non-significant factors and formulate a regression model for the amount of

photoresist removed and the within-wafer non-uniformity. A resolution IV fractional factorial design allows for the modeling of the main effects and two factor interactions while confounding the higher order terms. A two level fractional factorial experimental design allows for the formulation of a linear regression model [16]. An example of a linear regression model that includes the two factor interaction terms is shown below:

$$y = \beta_0 + \sum_{i=1}^{i=n} \beta_i x_i + \sum_{j=1}^{j=n} \sum_{k=1}^{k=n} \beta_{jk} x_j x_k + \varepsilon$$

Equation 3-1

where x_i is a main factor effect, $x_j x_k$ is a two factor interaction effect, ε is the random error term, and β_0, β_i, β_{jk} are the model coefficients. Regression analysis aims to minimize the random error term ε and provide the best estimate of the response variable y. Therefore the prediction equation becomes:

$$\hat{y} = \beta_0 + \sum_{i=1}^{i=n} \beta_i x_i + \sum_{j=1}^{j=n} \sum_{k=1}^{k=n} \beta_{jk} x_j x_k$$

Equation 3-2

where $\hat{y}$ is the estimate of the response variable y and the rest of the terms are the same as described in equation 3-1.

As discussed in Section 1.6, the Nanospec 9200 tool measures and records the amount of photoresist removed from nine sites on a single wafer. Therefore it is possible to build a regression model for the amount of photoresist removed from each site from a single DOE analysis. From a practical process-monitoring standpoint, looking at nine different regression models for each of the nine sites is tedious and difficult, and therefore it may be necessary to combine each of the nine models into a single model that would be the best predictor of the amount of photoresist removed and wafer non-uniformity during a particular run. Guo and Sachs have proposed the multiple response surface methodology which will be one of the approaches explored in this thesis to combine each of the nine regression models into a single

model for predicting the average amount of photoresist removed and the wafer non-uniformity [12]. The methodology is outlined below.

i. Build a regression model for the amount of photoresist removed from each of the nine sites on a single wafer from the results of the DOE as shown below.

$$\hat{y}_1 = \beta_{01} + \beta_{11}A + \beta_{21}B + \cdots + \beta_{p1}F + \beta_{q1}AB + \cdots + \beta_{x1}EF$$

$$\hat{y}_2 = \beta_{02} + \beta_{12}A + \beta_{22}B + \cdots + \beta_{p2}F + \beta_{q2}AB + \cdots + \beta_{x2}EF$$

.

.

.

$$\hat{y}_9 = \beta_{09} + \beta_{19}A + \beta_{29}B + \cdots + \beta_{p9}F + \beta_{q9}AB + \cdots + \beta_{x9}EF$$

Equation 3-3

where $\hat{y}_1$, $\hat{y}_2 \ldots \hat{y}_9$ are the estimates of the response variable at each site which is the amount of photoresist removed. A, B, …, F and AB, …, EF are the variables that represent the main factor effects and two factor interactions and have been defined in Table 3-2. $\beta_{01}, \beta_{11}, \ldots, \beta_{x1}$ are the model coefficients for site 1, and a similar notation is adopted for the model coefficients of the other sites.

ii. Combine the nine models outlined above to best represent and estimate the average amount of photoresist removed from a wafer and the within-wafer non-uniformity based on the methods outlined in Section 1.7. The following equations demonstrate the methodology of using the areal representation of the sites in the calculation of the combined model.

$$\bar{y} = \frac{\sum_{i=1}^{i=9} w_i \hat{y}_i}{\sum_{i=1}^{i=9} w_i}$$

Equation 3-4

where $\bar{y}$ is the combined model for predicting the average amount of photoresist removed from a single wafer, $\hat{y}_i$ is the individual site regression model, and w_i is the weighted area factor associated with that site [11], [12].

$$\hat{s} = \sqrt{\frac{\sum_{i=1}^{i=9} w_i}{\left(\sum_{i=1}^{i=9} w_i\right)^2 - \sum_{i=1}^{i=9} w_i^2} \cdot \sum_{i=1}^{i=9} w_i(\hat{y}_i - \bar{y})^2}$$

Equation 3-5

where $\hat{s}$ is the standard deviation of the estimates of the amount of photoresist removed at each site, $\bar{y}$ is the combined model for predicting the average amount of photoresist removed from a single wafer, $\hat{y}_i$ is the individual site regression model, and w_i is the weighted area factor associated with that site [11], [12].

$$NU = \frac{\hat{s}}{\bar{y}}$$

Equation 3-6

where NU (will be expressed as a percentage) is the estimate of the within-wafer non-uniformity, $\hat{s}$ is the standard deviation of the estimates of the amount of photoresist removed at each site, and $\bar{y}$ is the combined model for predicting the average amount of photoresist removed from a single wafer [12].

Another approach to modeling the within-wafer non-uniformity is the single response surface methodology described by Guo and Sachs [12]. In this method, the same 2^{6-2} resolution IV fractional factorial design experiment outlined in Table 3-2 is used, but instead of using the amount of photoresist removed as the response variable, the within-wafer non-uniformity will be used as the response variable. This means that the within-wafer non-uniformity will be calculated for each experimental run and a regression equation would be directly fit to those calculated values.

Chapter 4 presents a comprehensive analysis of both the single response surface and multiple response surface methods on the plasma ashing process and recommendations are made to Analog Devices Inc. on the best method to adopt.

3.4 Experimental Designs for Non-Linear Models

While two level fractional factorial experiments are valuable in determining the most significant factors, the regression models that are generated from such designs may be severely deficient in accuracy. In most cases, the lack of accuracy can be attributed to either a significant factor that was not considered during the experiment or the existence of curvature (higher order terms) that models obtained from a two level fractional factorial experimental design cannot generally account for. Therefore, it is critical to perform replicated center point tests when performing a two level fractional factorial experiment to test for the presence of curvature.

If it is determined from the center point tests that curvature exists, then the model must be refined to account for the higher order terms if precise prediction of the response variable is the objective. Several experimental designs like the central composite design are available and widely used to build non-linear regression models [20]. A three or higher-level factorial design experiment can also be used to account for the non-linear terms in a regression model.

The initial regression model formulated with the single response surface approach for the wafer non-uniformity using the 2^{6-2} resolution IV fractional factorial design experiment needs further refinement. It is observed from the screening experiment that the wafer temperature and the oxygen gas flow are the two most significant factors affecting the wafer non-uniformity in the plasma ashing process (Chapter 4). To refine the model, a three level full factorial experiment is done using only wafer temperature and oxygen gas flow as the two factors. The other four controllable factors were kept constant at the values outlined in the partial recipe (Table 1-1). The levels of each of the factors are shown in Table 3-3 while the 3^2 full factorial design table is shown in Table 3-4.

Parameter	Variable	Low (0)	Mid(1)	High(2)
Temperature	A (Celsius)	220	235	250
O2	B (SCCM)	3000	3750	4500

Table 3-3: The controllable factors and specific levels at which the 3^2 full factorial experiments are run.

Treatment	Temperature A	O2 B
1	0	0
2	1	0
3	2	0
4	0	1
5	1	1
6	2	1
7	0	2
8	1	2
9	2	2

Table 3-4: 3^2 full factorial design run table.

Doing a 3^2 full factorial experiment allows for the modeling of quadratic terms to account for the curvature in the response surface and this generally improves the fidelity of the model. The regression model relating the best estimate of the within-wafer non-uniformity ($\widehat{NU}$) to the wafer temperature (A) and oxygen gas flow (B) is as follows:

$$\widehat{NU} = \beta_0 + \beta_1 A + \beta_2 B + \beta_3 AB + \beta_4 A^2 + \beta_5 B^2$$

Equation 3-7

An in-depth analysis of the results of this experiment is presented in Chapter 4.

Chapter 4: Design of Experiments - Analysis

This chapter provides a comprehensive analysis of the outcomes of the DOEs that are described in Chapter 3. It explains the methods and the strategies needed to build and validate the statistical regression models. JMP statistical software and MATLAB are used to carry out the analysis [17], [22].

The DOEs are conducted on two separate Gasonics machines that are codenamed G53000 and G63000. Sufficient care is taken to keep the experimental conditions and run orders the same for both the machines. This is important because one of the broader goals of this project is to document the similarities and contrasts between machines running the same process with the same recipe. This chapter also comments on the similarities and contrasts between the G53000 and G63000 machines running the plasma ashing process with the partial recipe. Haskaraman's work [4] describes strategies for machine matching or ways in which the contrasts between the two machines can be reduced or eliminated.

The response variables that are under study are the amount of photoresist removed and the within-wafer non-uniformity. The within-wafer non-uniformity is modeled using both the multiple response surface and the single response surface methods described by Guo and Sachs [12]. The outcomes from both these methods have also been compared in this chapter. A methodology for conducting a thorough analysis of the outcomes of a DOE experiment has also been presented to Analog Devices Inc.

4.1 G53000: Multiple Response Surface Model

The multiple response surface approach combines the nine individual site models for the amount of photoresist removed from a wafer into a single model using equations 3-4 and 3-5. The wafer non-uniformity response can also be predicted from the individual site models using equation 3-6. The formulation of the regression models for each site is done in JMP. The in-depth analysis and diagrams that are presented in this section are only for site 3 which is the center of the wafer unless other wise mentioned, as all of the nine site models share similar

characteristics and properties. Important information or any anomalies from the other site models are highlighted appropriately. Table 4-1 shows the replicate runs, replicate mean, and the replicate variance of the amount of photoresist removed from site 3 in each treatment combination of the 2^{6-2} resolution IV factorial design table (Table 3-2).

Run Number	Treatment	Replicate-1	Replicate-2	Replicate-3	Replicate Mean	Replicate Variance
1	[-–-–-–]	4856.76	5034.65	5015.66	4969.0	9542.4
2	[+–--+–]	7086.73	7215.62	7000.04	7100.8	11767.1
3	[-+––++]	4838.02	4950.27	4870.11	4886.1	3342.6
4	[++-–-+]	6755.86	6855.54	6820.59	6810.7	2557.9
5	[--+-++]	5125.77	5286.27	5205.1	5205.7	6440.3
6	[+–+–-+]	7676.91	7772.08	7706.86	7718.6	2368.0
7	[–++-––]	5358.5	5451.42	5455.37	5421.8	3005.6
8	[+++–+-]	7564.78	7646.79	7636.46	7616.0	1995.1
9	[++–+––]	4920.65	4852.84	4989.95	4921.1	4700.0
10	[+––+++]	6800.71	6891.25	6896.94	6863.0	2915.0
11	[–+–++–]	4827.51	4953.79	4968.08	4916.5	5985.1
12	[++-+–-]	6863.56	6886.65	6950.7	6900.3	2038.2
13	[––+++-]	5095.41	5113.55	5302.28	5170.4	13123.9
14	[+-++-–]	7751.52	7705.83	7881.85	7779.7	8342.8
15	[-+++–+]	5306.48	5121.4	5379.1	5269.0	17656.3
16	[++++++]	7351.49	7428	7413.61	7397.7	1653.3
Center	[000000]	5976.93	5896.23	6097.22	5990.1	10229.9

Table 4-1: Values of replicate runs, replicate mean, and replicate variance for amount of photoresist stripped from a wafer in the G53000 machine.

The 2^{6-2} resolution IV factorial design table is cataloged as one of the standard designs in JMP. The value for the amount of photoresist removed for each treatment combination and replicate is tabulated in JMP and the model script is run with the “standard least squares” personality and “effects screening” emphasis. The treatment combination pattern in Table 4-1 follows the pattern outlined in Table 3-2. Figure 4-1 shows the JMP screen that aids in configuring the regression model parameters.

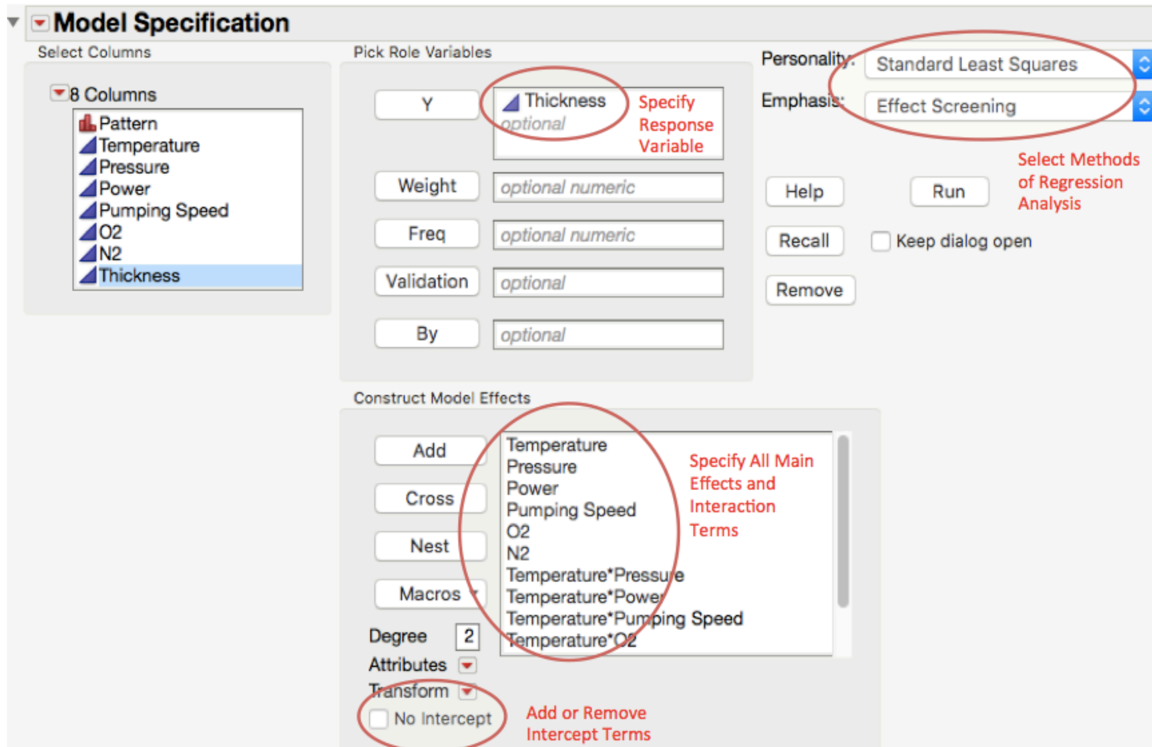

Figure 4-1: Specifying model parameters in JMP.

After all the terms of the model have been specified and the model is run, JMP compiles and generates an analysis report with the coefficients of the regression model. The key features that must be looked at in the JMP analysis report for a fractional factorial screening design in order to make sure that the DOE is valid and can be used to draw meaningful implications are as follows.

i. Effects Screening Assumptions

Screening designs assume that the effects under consideration are uncorrelated and if the design is replicated, then the variances across all runs must be equal [20]. If both these assumptions hold, then multivariate analysis of variance (MANOVA) can be used to screen out the non-significant factors as some software packages do. However, there may be cases where either one or both of these assumptions do not hold. JMP is capable of testing for both these assumptions in the analysis report and adjusting for any deficiencies if they exist. In the regression model report of site 3, JMP concludes that all the factors are uncorrelated but the variances across all runs are not equal. However, a Bartlett's test for equal variances done at a

95% confidence level shows that the variances are equal (T = 7.66, $\chi^2_{0.95,16}$ = 7.96). JMP allows the option of screening factors with or without adjusting for the assumption of equal variances. The effects screening normal probability plot for both the cases is shown in Figure 4-2 and 4-3. Both the plots show the same significant factors with the same hierarchy so the Bartlett's test conclusion is not wrong and MANOVA could have been used to screen factors in this case. It can be concluded that JMP tests for equality of variance at a higher confidence level than the 95% confidence level used in the Bartlett's test. If some other statistical software package is used that uses MANOVA to screen factors, the Bartlett's test is useful to test the equality of variance hypothesis, while a principle component analysis can be used to test for correlation among multiple factors [23]. In subsequent analysis in this thesis, the JMP conclusions will be used to validate the effects screening assumptions.

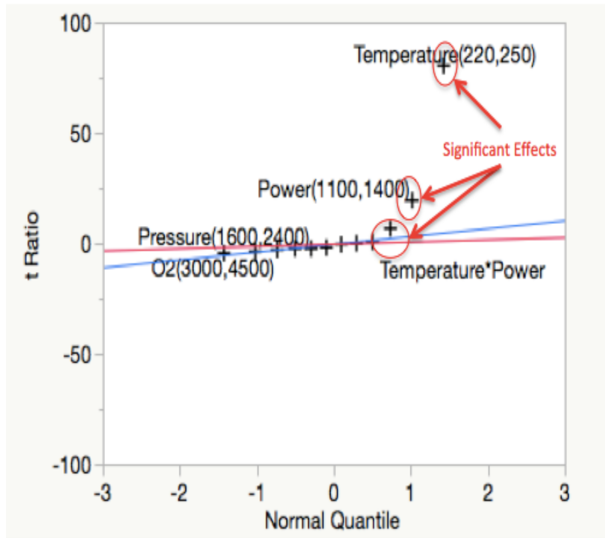

Figure 4-2: Normal probability plot of effects affecting photoresist strip rate standardized to have equal variances across all runs in the G53000 machine.

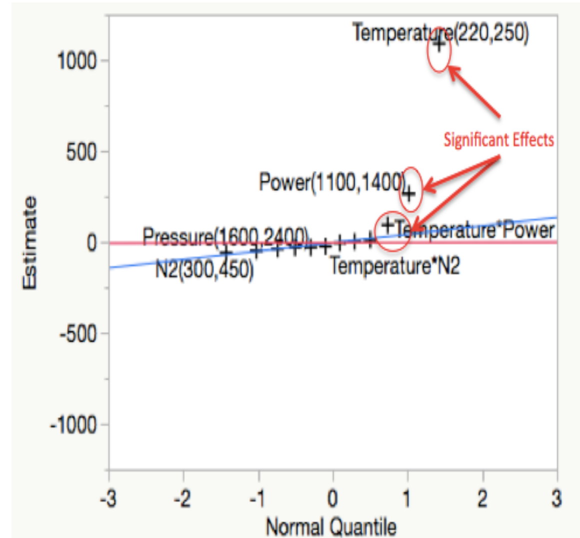

Figure 4-3: Normal probability plot of effects affecting photoresist strip rate not standardized that have unequal variances across all runs in G53000 machine.

The most significant effects are the ones that violate the normality assumption. The greater the violation from the normality assumption, the greater is the significance of the effect [16]. Wafer temperature, power, and the two factor interaction between wafer temperature and power

are the most significant effects that influence the amount of photoresist removed in the plasma ashing process on the G53000 machine.

ii. Alias Structure and Singularity

It is important to validate the alias structure and singularity terms in a fractional factorial screening design experiment. The alias structure is specified while making the initial DOE run table. The aim of the 2^{6-2} resolution IV factorial design experiment is to model all the main effects and two factor interactions [16]. However, there does exist a singularity term as shown in Figure 4-4 where there is a linear dependency between the interaction of wafer temperature and oxygen flow and the interaction of chamber pressure and power.

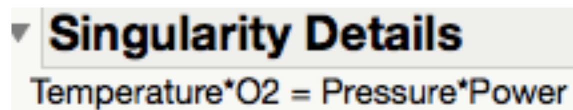

Figure 4-4: Singularity report as seen in JMP.

Singularity terms indicate confounding between factors or interactions, and one must be cautious while including them in a regression model should they be significant. Engineering judgment must be applied in such cases. In the case of the regression model for site 3, it is unlikely that the two factor interaction between temperature and oxygen and the two factor interaction between pressure and power will have a significant impact on the predicted outcome. This is because the main effects of oxygen and pressure have virtually no impact on the amount of photoresist removed as shown by the normal probability plots, and based on both the principles of hierarchy of effects and inheritance of effects, it is even more unlikely that the singularity terms in this model will have a significant impact on the amount of photoresist removed. However, should a singularity term be deemed to be statistically significant and should they be interaction terms between the main effects, then the choice of the interaction term to be selected should be the one with the most significant main effects. For example, in this case the interaction between wafer temperature and oxygen will be chosen over the interaction between the chamber pressure and power, since the effect of temperature is more significant than the effect of power and the effect of oxygen is more significant than the effect of chamber pressure.

iii. Lack of Fit Analysis

The analysis report in JMP contains a graph that plots the values predicted by the regression model versus the actual values obtained from the experiment and fits a curve to it as shown in Figure 4-5.

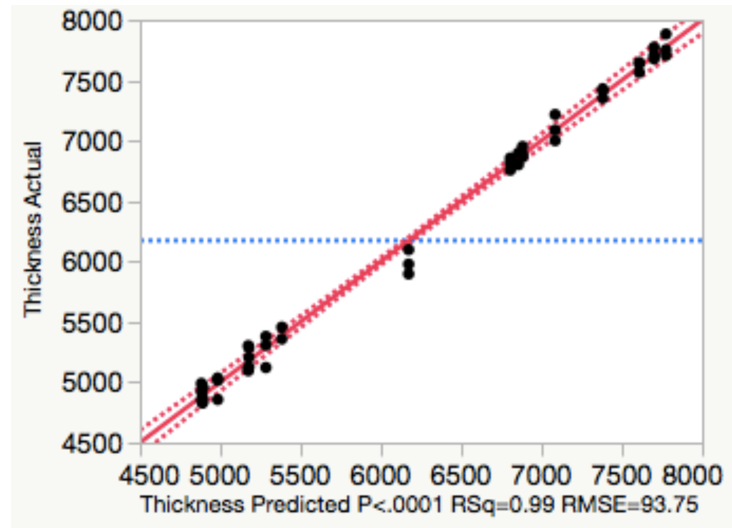

Figure 4-5: Observed values versus model predicted values plot for amount of photoresist removed from site 3 of the wafer in the G53000 machine.

The adjusted R^2 value for this plot is 0.992 which indicates that there is very little variation of the data not explained by the model, confirming that the model has good precision. The actual values of the residuals, however, must be checked for model accuracy analysis. A low R^2 value would have indicated that the regression model either has significant curvature or a missing factor leading to poor precision. If center points are entered in the design table, JMP also performs the curvature test. In this case there is some curvature especially around the center points as can be seen from Figure 4-5 and the residual analysis, but these center points do not deviate much from the overall natural variation in the process and therefore the lack of fit can be ignored. Table 4-2 gives the adjusted R^2 values for each site model for the observed values versus the predicted values plot for the amount of photoresist removed.

Sites	Adjusted R^2 Value
Site-1	0.993
Site-2	0.993
Site-3	0.993
Site-4	0.994
Site-5	0.988
Site-6	0.993
Site-7	0.995
Site-8	0.986
Site-9	0.989

Table 4-2: Adjusted R^2 values for observed versus predicted plot for the amount of photoresist removed from all sites on a wafer in the G53000 machine.

It can be concluded from the adjusted R^2 values, that the regression models for each site show good precision over the specified range of the input factors in the DOE.

iv. Model Coefficients

The analysis report in JMP also provides the regression model coefficients for the factors in decreasing order of significance as shown in Figure 4-6. The model is restricted to main effects and two factor interactions and second order (squared) terms are excluded based on the results of the lack of fit analysis. The "Estimate" column gives the model coefficients for each factor.

Term		Estimate	Std Error	t Ratio	Prob>|t|
Temperature(220,250)		1089.1965	13.53165	80.49	<.0001*
Power(1100,1400)		263.21562	13.53165	19.45	<.0001*
Temperature*Power		91.450625	13.53165	6.76	<.0001*
Temperature*Pressure		-60.28063	13.53165	-4.45	<.0001*
N2(300,450)		-50.16063	13.53165	-3.71	0.0007*
O2(3000,4500)		-39.62812	13.53165	-2.93	0.0057*
Pumping Speed(4.8,7.2)		-31.93771	13.53165	-2.36	0.0235*
Pressure(1600,2400)		-31.89896	13.53165	-2.36	0.0237*
Temperature*N2		-25.70146	13.53165	-1.90	0.0651
Temperature*O2	Biased	10.647708	13.53165	0.79	0.4362
Temperature*Pumping Speed		-6.235208	13.53165	-0.46	0.6476
Pressure*Pumping Speed		0.5485417	13.53165	0.04	0.9679
Pressure*Power	Zeroed	0	0	.	.

Figure 4-6: Model coefficients and hierarchy of significance of factors affecting the amount of photoresist removed from a wafer in the G53000 machine (site 3 of wafer).

This regression model assumes that the values entered for each factor as an input will be "coded", i.e., all the inputs entered into the model for each factor must be between -1 and +1. JMP also has a feature called "prediction expression" that shows the regression model without the coded inputs, allowing a user to enter absolute values of the input factors if required. The intercept value or the β_0 term for the site 3 regression model is 6172.739. This value is provided in a separate table in JMP and must not be accidently ignored when building the regression model. As expected, the two factor interactions of temperature and oxygen and pressure and power are confounded because of the singularity and alias structure. In this case, the pressure and power interaction is zeroed and the temperature and oxygen term is retained but may be biased due to this term also potentially containing some of the zeroed term's effects.

JMP analyzes the significance of factors by calculating the t-ratio as shown in the "t-ratio" column in Figure 4-6. The greater the magnitude of the absolute t-ratio from 0, the more significant is the factor and the t-test hypothesis is tested at a 1% (orange) and 5% (red) significance level. The bar chart in Figure 4-6 shows the t-ratio with vertical lines at a 0.05 significance level. P_{values} can also be used to determine the significance of effects and in this case the lower the P_{value}, the more significant that effect is. JMP also has a separate table in the analysis report where one can compare the significance of effects using the P_{values}.

Table 4-3 shows the main effects at a 1% (red) and 5% (orange) significance level and the model coefficients for each of the nine sites. The "x" symbol indicates those factors that were not significant to the site regression model.

Sites	Temperature	Pressure	Power	Pumping Speed	Oxygen	Nitrogen
Site 1	1107.2	x	243.9	x	x	-38.3
Site 2	1081.5	x	253.6	x	-37.56	-46.48
Site 3	1089.2	-31.9	263.2	-31.9	-39.6	-50.2
Site 4	1078.8	-37.5	250.8	-41.3	x	-47.5
Site 5	1111.3	x	273.8	-62.8	x	-42.1
Site 6	1078.3	x	213.9	x	x	-50.1
Site 7	1077.4	x	253.1	-33.1	-27.5	-44.9
Site 8	1050.6	-39.7	272.6	-47	-53.7	-43.6
Site 9	1023.2	x	225.7	-39.1	x	-31.7

Table 4-3: Model coefficients for all nine sites for the amount of photoresist removed from a wafer in the G53000 machine.

It can be clearly seen that wafer temperature and power are the most significant effects in all nine sites. The model coefficients give an idea of the hierarchy of significance. Table 4-4 shows the most significant two factor interaction effects on the amount of photoresist removed. It is also observed that the two factor interaction between wafer temperature and power is the most significant effect and present in all of the nine sites. This is consistent with the inheritance of effects principle because the main factors of wafer temperature and power have the most significant effect on the amount of photoresist removed in the plasma ashing process.

Sites	Significant 2-factor interactions
Site-1	Temperature*Power, Temperature*O2, Temperature*Pressure
Site-2	Temperature*Power, Temperature*Pressure
Site-3	Temperature*Power, Temperature*Pressure
Site-4	Temperature*Power, Temperature*Pressure
Site-5	Temperature*Power, Temperature*O2,Temperature*Pressure
Site-6	Temperature*Power, Temperature*Pressure
Site-7	Temperature*Power, Temperature*Pressure, Temperature*N2
Site-8	Temperature*Power, Temperature*Pressure
Site-9	Temperature*Power, Temperature*Pressure, Temperature*N2

Table 4-4: List of significant two factor interactions for the amount of photoresist removed from a wafer in the G53000 machine.

v. Residual Analysis

A residual is defined as the difference between the predicted model value and the observed value [16]. A residual analysis gives an idea of the stochastic or random error, while the regression coefficients account for the deterministic portion of the model [24]. Consistent low values of the residuals can give some reassurance about the accuracy of the regression model. A residual analysis includes the following tests [16], [24].

1. Checking if the residuals follow a normal distribution, as they are indicative of random error.

2. Plotting residual versus predicted values to look for any trends or patterns. The residuals should be randomly scattered in this plot and should be centered on the zero line throughout the range of fitted values in the ideal case, and should not be systematically high or low. Depending on a case-by-case basis, other residual plots such as residual versus run order (time series), residual versus a particular input factor, etc. may also be generated to obtain more specific information about the process behavior.

Figures 4-7 and 4-8 show the normal probability plot of the residuals and the residual versus predicted plot for site 3.

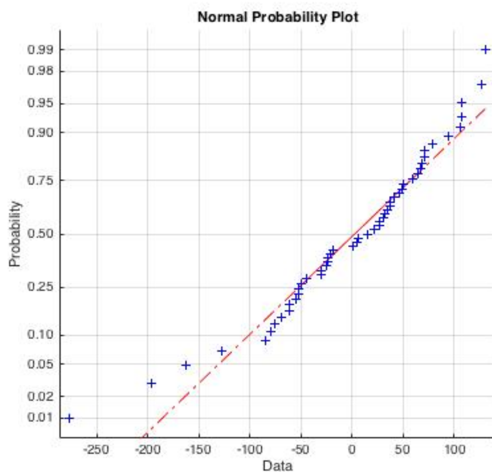

Figure 4-7: Normal probability plot of residuals for amount of photoresist removed from a wafer in the G53000 machine (site 3).

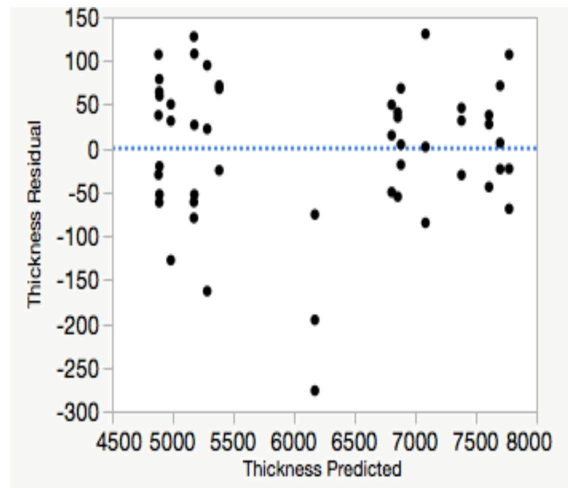

Figure 4-8: Residual versus predicted plot for amount of photoresist removed from a wafer in the G53000 machine (site 3).

The normal probability plot of the residuals indicates that there seems to be no significant deviation from the normality assumption for the residuals. The residual versus predicted plot indicates that the residuals are randomly scattered around the zero line everywhere except the center points where a consistent negative trend is observed. This indicates the presence of curvature in the model and higher order terms are required to fine-tune the model if further model accuracy is required. However, if the extreme value among the three center point residuals is considered, the model is off by 276 Angstroms in this worst case, which is 4.7% of the target value of 6000 Angstroms. From a practical perspective, this value was acceptable to Analog

Devices Inc. and there was no need to do an additional DOE to refine the model. In such cases engineering judgment must be used to determine if the model needs refinement or not.

vi. Post Experiment Physical Validations

Once the experiment was completed and the regression model was formulated, additional wafers were run on the G53000 machine at various combinations of the input factors, and the observed values are compared with the values obtained from the regression model. The model accurately predicts the response at all the sites for most of the test cases within 150 Angstroms, which is within the range of the stochastic error, and the worst-case error is a center point at 350 Angstroms. Doing such additional runs after the experiment further validates the regression model.

vii. Modeling of the within-wafer non-uniformity

After all of the regression models for the individual sites are formulated and validated, the models can be combined to give a single value of the average amount of photoresist removed from a wafer according to equation 3-4. Using the regression models of the nine sites, the within-wafer non-uniformity can also be predicted according to equations 3-5 and 3-6. The within-wafer non-uniformity has spatial characteristics and in most cases a regression model formulated with the wafer non-uniformity as the response variable using traditional methods is non-linear [12]. The hope is that the structure of equations 3-5 and 3-6 may be able to account for the non-linear terms. Table 4-5 below shows a number of test cases that are used to check the accuracy of predicting the within-wafer non-uniformity using the multiple response surface methodology. The key column of interest is the "% Difference" which is calculated as follows:

$$\%\, Difference = \frac{|Predicted\ Value - Observed\ Value|}{Observed\ Value} * 100$$

Equation 4-1

Run Number	Treatment	Observed Non-Uniformity	Predicted Non-Uniformity	Residuals	% Difference
1	[-–––––]	3.99	4.05	0.06	1.47
2	[+––-+–]	3.14	2.78	-0.36	11.45
3	[-+––++]	3.35	2.99	-0.36	10.75
4	[++-––+]	3.06	2.84	-0.22	7.28
5	[--+-++]	3.94	3.91	-0.03	0.80
6	[+–+–-+]	3.31	3.42	0.11	3.30
7	[–++-––]	3.98	4.15	0.17	4.36
8	[+++–+-]	2.82	2.8	-0.02	0.56
9	[-+–+––]	4.09	3.32	-0.77	18.75
10	[+––+++]	2.92	2.61	-0.31	10.47
11	[–+–++–]	3.16	2.46	-0.70	22.23
12	[++-+–-]	3.02	2.51	-0.51	16.88
13	[––+++-]	3.68	3.52	-0.16	4.28
14	[+-++-–]	3.46	3	-0.46	13.40
15	[-+++–+]	3.80	3.55	-0.25	6.49
16	[++++++]	2.80	2.57	-0.23	8.13
17	[000000]	3.01	2.99	-0.02	0.66
18	[-0+0+0]	3.75	3.46	-0.29	7.73
19	[00+000]	2.81	3.19	0.38	13.52
20	[+0+0+0]	4.28	2.78	-1.50	35.05
21	[+0+000]	3.21	2.9	-0.31	9.66
22	[-0+0-0]	3.83	4.02	0.19	4.96
23	[00+0+0]	3.37	3.02	-0.35	10.39

Table 4-5: Test cases for a variety of treatment combinations to validate the wafer non-uniformity model using the multiple response surface method.

The treatment combination codes (-, +, 0) refer to the low, high, and center point values of the 2^{6-2} resolution IV factorial design run table shown in Table 3-2. The values highlighted in red in the % Difference column refer to those runs where the difference between the observed values (i.e., non-uniformity calculated from the actual measurements done on a wafer after it has undergone the ashing process for a particular treatment combination) and the predicted values (i.e., non-uniformity predicted by combining the nine site regression models for a particular treatment combination) exceeded by 10%. As can be seen from the table above, the multiple response surface model for the wafer non-uniformity predicts some values with good accuracy but most of the values are off by more than 5% with the worst-case scenario being 35.05%. The model does predict the general trend correctly which proves that some of the non-linearity is being accounted for, however, the model is not accurate enough and should not be used for predictive purposes. There are several possible hypotheses as to why this could be the case. The

first one is that certain factors that may be statistically significant for modeling the response of the within-wafer non-uniformity may not be significant for modeling the response of the amount of photoresist removed. Therefore ignoring these factors could lead to a deficiency in the model for the within-wafer non-uniformity since this model was based off the regression models for the amount of photoresist removed. The second hypothesis is that certain non-linearity terms may not have been captured by the structure of equations 3-5 and 3-6 leading to the model deficiency. A third hypothesis is that the lack of fit created by neglecting the second order curvature terms in the site models more severely impacts the non-uniformity prediction. Another hypothesis, that seems to be the most likely case, is that the replication error in each of the nine site models could have a substantial effect on the predicted outcome of the within-wafer non-uniformity. It may therefore be necessary to review the calculation of the non-uniformity parameter and this hypothesis is explored further.

The wafer non-uniformity parameter calculated from the multiple response surface method is a ratio of two random variables: the weighted standard deviation of the amount of photoresist removed from the nine sites on the wafer, and the weighted average of the amount of photoresist removed from the nine sites on the wafer. The site regression models are combined to predict the wafer non-uniformity according to equations 3-4, 3-5, and 3-6. The errors associated in predicting both the random variables can therefore stack up and be more profound in the non-uniformity prediction. Figures 4-9, 4-10, 4-11, and 4-12 show the observed and predicted values at each site for the amount of photoresist removed and the non-uniformity prediction error (% Difference column in Table 4-5) associated with that treatment combination for the best case, worst case, and two intermediate scenarios. It can be seen that the non-uniformity prediction error is the lowest if the observed and prediction curves overlap at each site (Figure 4-9). Differences in the mean and the standard deviation between the two curves increase the non-uniformity prediction error. In Figure 4-10, the values for the amount of photoresist removed are consistently over predicted because the treatment combination for that run is near the center point where some curvature exists. These plots also indicate that significant differences in the shapes of the observed and predicted curves (Figure 4-12) have a stronger influence on the non-uniformity prediction error than shifts in the mean (Figure 4-10). The graphs also indicate that the site models are better at predicting the shape or the variation in the amount of photoresist removed from a wafer than the mean value.

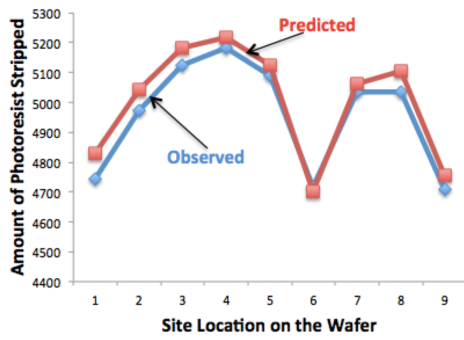

Figure 4-9: Observed and predicted values of the amount of photoresist stripped at each site for treatment combination [--+-++]. The non-uniformity prediction error is 0.8%.

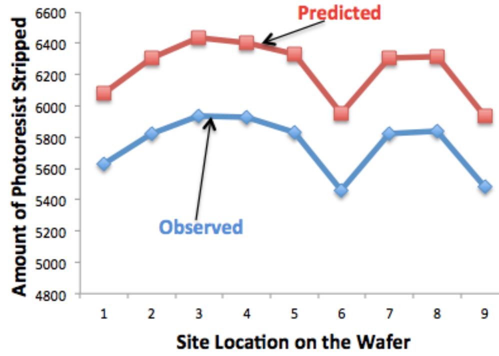

Figure 4-10: Observed and predicted values of the amount of photoresist stripped at each site for treatment combination [00+000]. The non-uniformity prediction error is 13.52%.

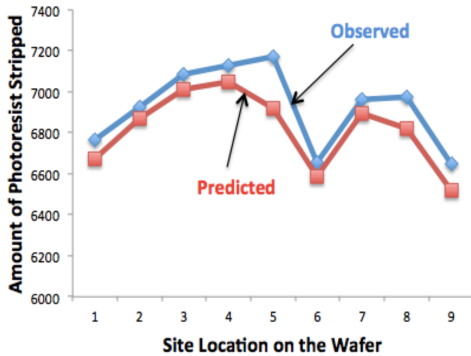

Figure 4-11: Observed and predicted values of the amount of photoresist stripped at each site for treatment combination [+---+-]. The non-uniformity prediction error is 11.45%.

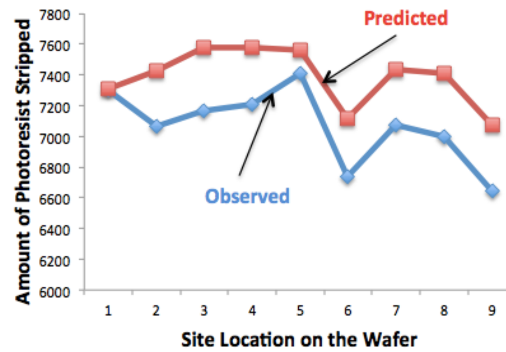

Figure 4-12: Observed and predicted values of the amount of photoresist stripped at each site for treatment combination [+0+0+0]. The non-uniformity prediction error is 35.05%.

A possible alternative for future consideration is to use the weighted standard deviation as the within-wafer non-uniformity metric, rather than normalizing the standard deviation to the mean. This would decouple the error in the within-wafer variation shape from the error in the mean, and enable more robust analysis of the two parameters separately.

An alternative to the multiple response surface method explored next is to model the within-wafer non-uniformity using the single response surface method in the hope of achieving greater accuracy.

4.2 G53000: Single Response Surface Model

To formulate a more accurate model and to better understand the factors that have a significant impact on the within-wafer non-uniformity, the single response surface method is used where the within-wafer non-uniformity parameter is calculated for each of the experimental runs of the 2^{6-2} resolution IV factorial design table and a regression model is directly fit on these values. Table 4-6 shows the individual replicates, the replicate means and the replicate variances that are used to construct the design table. A similar method of analysis as outlined in Section 4.2 for modeling the individual nine site regression models will be followed.

Run Number	Treatment	Replicate-1	Replicate-2	Replicate-3	Replicate Mean	Replicate Variance
1	[-–––-–]	3.99	3.56	3.90	3.82	0.053
2	[+––-+–]	3.14	3.06	2.99	3.06	0.005
3	[-+––++]	3.35	3.31	3.18	3.28	0.008
4	[++-–-+]	3.06	3.05	3.07	3.06	0.000
5	[--+-++]	3.94	3.76	3.61	3.77	0.027
6	[+–+–-+]	3.31	3.32	3.46	3.36	0.007
7	[–++-––]	3.98	3.96	3.92	3.95	0.001
8	[+++–+-]	2.82	2.78	2.70	2.77	0.004
9	[++–+––]	4.09	3.67	3.63	3.80	0.063
10	[+––+++]	2.92	3.19	2.88	2.99	0.029
11	[–+–++–]	3.16	3.40	3.40	3.32	0.019
12	[++-+–-]	3.02	2.90	3.10	3.01	0.010
13	[––+++-]	3.68	3.58	3.99	3.75	0.047
14	[+-++-–]	3.46	3.11	3.42	3.33	0.038
15	[-+++–+]	3.80	3.25	3.73	3.59	0.090
16	[++++++]	2.80	2.72	2.62	2.71	0.008
Center	[000000]	3.01	2.88	3.37	3.09	0.063

Table 4-6: Values of replicate runs, replicate mean, and replicate variance for wafer non-uniformity observed on the G53000 machine.

i. Effects Screening Assumptions

JMP indicates that the factor effects are not correlated but the equality of variance assumption across all experimental runs does not hold. JMP accounts for this in the normal probability plot shown in Figure 4-13 that is used to screen out the less significant factors. The wafer temperature, oxygen gas flow, and chamber pressure are the most significant effects affecting the within-wafer non-uniformity on the G53000 machine.

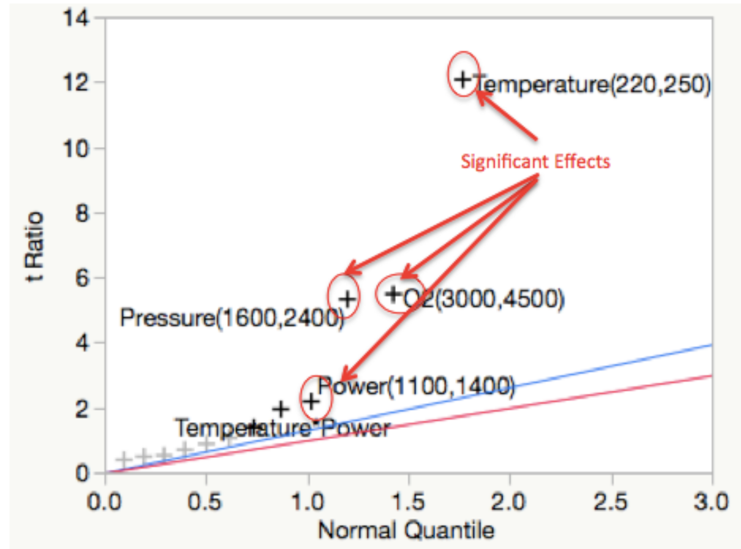

Figure 4-13: Normal probability plot of effects affecting wafer non-uniformity standardized to have equal variances across all runs in the G53000 machine.

ii. Alias Structure and Singularity

The alias structure is analyzed and there is a singularity term in the model which results from the linear dependency between the two factor interactions of temperature and oxygen and power and pressure. Since temperature and oxygen are both very significant factors that influence the within-wafer non-uniformity, the two factor interaction between temperature and oxygen will be included in the model if this potentially biased term is deemed to be statistically significant at a 5% significance level.

iii. Lack of Fit Analysis

The plot of the observed values versus the predicted values for the within-wafer non-uniformity is shown in Figure 4-14. The adjusted R^2 value for the linear fit in the plot is 0.80. The acceptance of this fit depends upon the precision needed in predicting the response variable. The adjusted R^2 value indicates that this model cannot accurately account for as much as 20% of the variation in the data and therefore it cannot be used if a highly precise model is needed. This plot also indicates that including higher order terms may better fit the data and lead to more precise predictions.

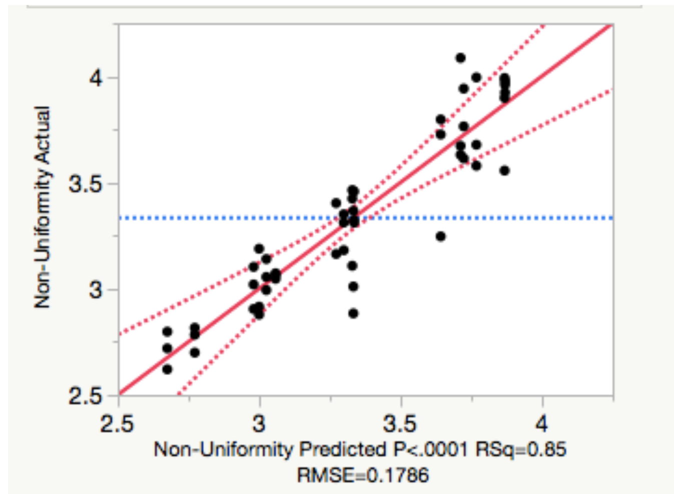

Figure 4-14: Observed values versus model predicted values plot for the wafer non-uniformity observed on the G53000 machine.

iv. Model Coefficients

The summary of the model coefficients in the hierarchy of their significance is shown in Figure 4-15. The value of the intercept term is 3.33 and this regression model also assumes that the values entered as inputs will be coded. Wafer temperature, oxygen, and chamber pressure are the main effects that are highly significant followed by power.

Term		Estimate	Std Error	t Ratio	Prob>|t|
Temperature(220,250)		-0.31119	0.025777	-12.07	<.0001*
O2(3000,4500)		-0.141228	0.025777	-5.48	<.0001*
Pressure(1600,2400)		-0.137071	0.025777	-5.32	<.0001*
Power(1100,1400)		0.0562696	0.025777	2.18	0.0353*
Temperature*Power		-0.050198	0.025777	-1.95	0.0589
Pumping Speed(4.8,7.2)		-0.035723	0.025777	-1.39	0.1739
N2(300,450)		-0.02747	0.025777	-1.07	0.2933
Temperature*N2		0.0226359	0.025777	0.88	0.3854
Pressure*Pumping Speed		-0.017906	0.025777	-0.69	0.4915
Temperature*Pressure		-0.013448	0.025777	-0.52	0.6049
Temperature*O2	Biased	-0.012612	0.025777	-0.49	0.6275
Temperature*Pumping Speed		0.009913	0.025777	0.38	0.7027
Pressure*Power	Zeroed	0	0	.	.

Figure 4-15: Model coefficients and hierarchy of significance of factors affecting the wafer uniformity observed on the G53000 machine.

v. ***Residual Analysis***

Figures 4-16 and 4-17 show the normal probability plot of the residuals and the residual versus predicted plot for the within-wafer non-uniformity model.

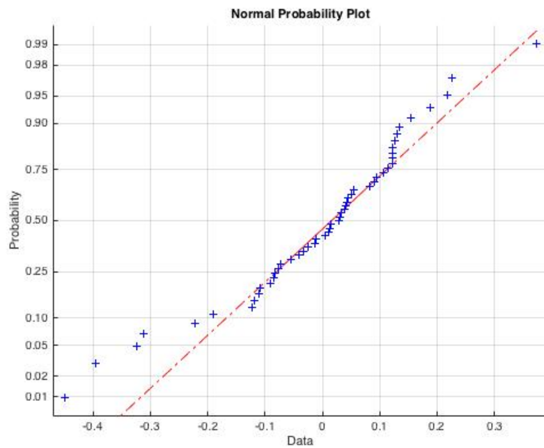

Figure 4-16: Normal probability plot of residuals for wafer non-uniformity observed on the G53000 machine.

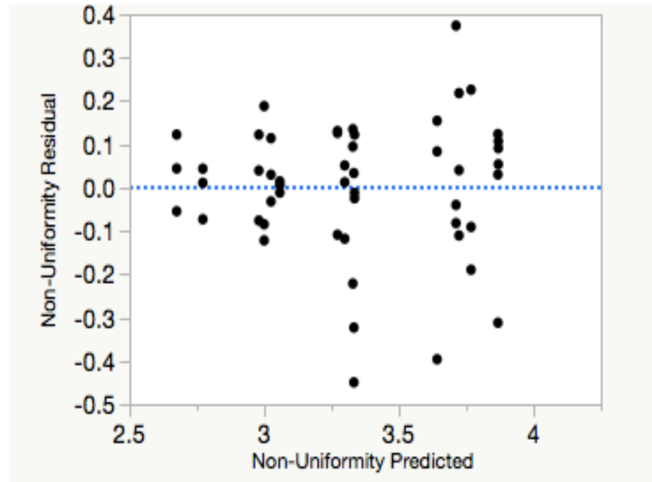

Figure 4-17: Residual versus predicted plot for wafer non-uniformity observed on the G53000 machine.

By looking at the normal probability plot of the residuals, it can be seen that plotted points appear to bend up and to the left of the normal line indicating that the distribution has a long tail to the right (right skew) [25]. However, since most of the residual points lie either on or close to the normal line, the deviation from the normality assumption is not that substantial and the residuals can be assumed to follow a normal distribution. In the residual versus the fitted value plot, an interesting trend is observed. The variance of the residuals about the zero line increases with the increase in the fitted values of the within-wafer non-uniformity. This means that the current linear model is better at predicting the wafer non-uniformity at lower values than at higher values and therefore this model cannot be used to predict the wafer non-uniformity response across the range of the input factors. This indicates that the model has room for improvement either by considering additional factors or including non-linear terms.

vi. Post Experiment Validation Runs

The post experiment validation runs were done primarily to compare this single response surface linear model to the multiple response surface model and to check if there are any improvements in predicting the response of the within-wafer non-uniformity. The same treatment combinations are used and the residuals and the % Difference are calculated and the results tabulated in Table 4-7.

Run Number	Treatment	Observed Non-Uniformity	Predicted Non-Uniformity	Residuals	% Difference
1	[-–-–-–]	3.99	3.87	-0.12	3.09
2	[+–-–+–]	3.14	3.03	-0.11	3.63
3	[-+–-–++]	3.35	3.30	-0.05	1.52
4	[++-–-+]	3.06	3.06	0.00	0.16
5	[--+-++]	3.94	3.72	-0.22	5.53
6	[+–+–-+]	3.31	3.34	0.02	0.75
7	[–++-––]	3.98	3.87	-0.11	2.69
8	[+++–+-]	2.82	2.77	-0.04	1.54
9	[-+–+––]	4.09	3.71	-0.37	9.15
10	[+––+++]	2.92	3.00	0.08	2.91
11	[–+–++–]	3.16	3.27	0.11	3.45
12	[++-+–-]	3.02	2.98	-0.04	1.30
13	[––+++-]	3.68	3.77	0.09	2.48
14	[+-++-–]	3.46	3.33	-0.13	3.88
15	[-+++–+]	3.80	3.64	-0.15	4.06
16	[++++++]	2.80	2.68	-0.12	4.37
17	[000000]	3.01	3.33	0.32	10.74
18	[-0+0+0]	3.75	3.6	-0.15	4.00
19	[00+0+0]	2.81	3.39	0.58	20.64
20	[+0+0+0]	4.28	2.89	-1.39	32.48
21	[+0+000]	3.21	3.02	-0.19	5.92
22	[-0+0-0]	3.83	3.89	0.06	1.57
23	[00+0+0]	3.37	3.25	-0.12	3.56

Table 4-7: Test cases for a variety of treatment combinations to validate the wafer non-uniformity model using the single response surface method on the G53000 machine.

Comparing the values of % Difference in Table 4-5 and Table 4-7, the single response surface model is definitely the better predictor of within-wafer non-uniformity than the multiple response surface model. However runs 17, 19, and 20 in Table 4-7 do lead to an error of more than 10% in the model and this indicates that there are areas over the range of the input factors where the model fails. It is interesting to note that chamber pressure and oxygen, which

significantly affect the within-wafer non-uniformity (Figure 4-11), were not included in building the regression models of six out of nine sites and five out of nine sites respectively (Table 4-3) as they did not significantly impact the amount of photoresist removed. This may have also added to the loss of adequacy of the multiple response surface model in addition to the replication error in the mean value.

4.3 G53000: Quadratic Response Surface Model

The failure of the single response surface linear model and the multiple response surface model to predict the wafer non-uniformity with reasonable accuracy at some instances over the range of the input factors indicates that the lack of explicit higher order terms can have a negative impact. If the regression model for the wafer non-uniformity is to be further improved, then these higher order terms need to be included in the model. After consulting with the process engineers at Analog Devices Inc., it was decided that a 3^2 full factorial DOE (Table 3-4) with a single replicate would be done using the single response surface method. The two input factors chosen are the wafer temperature and oxygen (Table 3-3) as these two are the most significant factors determined from the screening experiment. The other parameters are kept constant at the values outlined in the partial recipe (Table 1-1). The initial analysis of the response of the within-wafer non-uniformity from previous models showed that the wafer non-uniformity varied only between 3%-4% over the acceptable range of the input parameters. Therefore, there was no need to build a highly precise model to predict the within-wafer non-uniformity. However, the engineers at Analog Devices Inc. were interested in seeing if the within-wafer non-uniformity could be minimized and if so, at what values of the input factors could this be achieved. A 3^2 full factorial DOE would allow for the modeling of a quadratic response surface that is capable of detecting maxima or minima [20]. This experiment only required nine runs and this was important because there were constraints on the amount of time the machine could be switched off from the active production state and the availability schedules of the team performing the experiments. Table 4-8 shows the within-wafer non-uniformity response of each run.

Run Number	Treatment	Non-Uniformity
1	[0,2]	3.76
2	[2,1]	3.21
3	[0,0]	3.82
4	[1,0]	3.55
5	[1,1]	2.81
6	[2,0]	3.18
7	[1,2]	3.37
8	[2,2]	4.28
9	[0,1]	3.43

Table 4-8: Values of wafer non-uniformity obtained from the 3^2 full factorial experimental runs done on the G53000 machine.

To analyze the outcomes of the above experiment, the following steps are taken:

i. Lack of Fit Analysis

The plot of the observed values versus the predicted values for the within-wafer non-uniformity is shown in Figure 4-18. The adjusted R^2 value for the plot is 0.66 indicating a poor fit. It was anticipated that the quadratic model would improve on the single response surface linear model but this was not the case. A reason for this anomaly could be the exclusion of the factors of chamber pressure and power, which significantly affect the response of the within-wafer non-uniformity as seen in Figure 4-15. This indicates that excluding key factors from a DOE can significantly reduce the fidelity of the regression model formulated from that DOE.

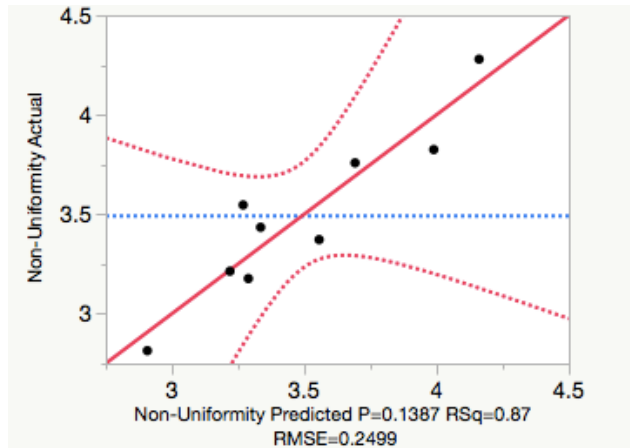

Figure 4-18: Observed values versus model predicted values plot for the wafer non-uniformity quadratic model obtained from the experiments done on the G53000 machine.

ii. Model Coefficients

The summary of the model coefficients obtained from this DOE is shown in Figure 4-19. It is to be noted that the model coefficients in this case represent the absolute values of the input parameters and not the coded variables, as was the case in the screening designs. In a full factorial experiment with three or more levels, JMP automatically accounts for the coded values which was not the case with the previous screening designs and this difference must be noted.

Term	Estimate	Std Error	t Ratio	Prob>|t|
(Oxygen-3750)*(Oxygen-3750)	8.9877e-7	3.141e-7	2.86	0.0645
(Temperature-235)*(Oxygen-3750)	2.5981e-5	1.111e-5	2.34	0.1013
(Temperature-235)*(Temperature-235)	0.0016446	0.000785	2.09	0.1273
Oxygen	0.0001915	0.000136	1.41	0.2539
Temperature	-0.003864	0.006801	-0.57	0.6097

Figure 4-19: Quadratic model coefficients of factors affecting the wafer non-uniformity observed on the G53000 machine.

iii. Residual Analysis

Figures 4-20 and 4-21 show the normal probability plot of the residuals and the residual versus predicted plot for the within-wafer non-uniformity quadratic model.

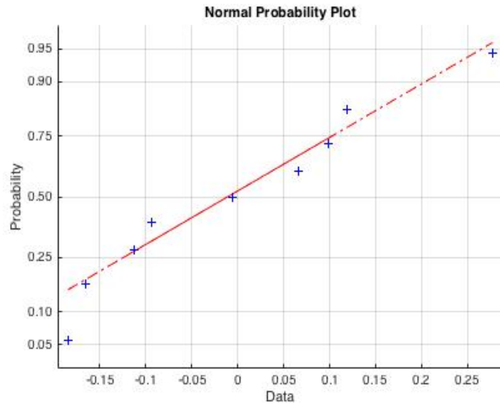

Figure 4-20: Normal probability plot of residuals for wafer non-uniformity observed on the G53000 machine (quadratic model).

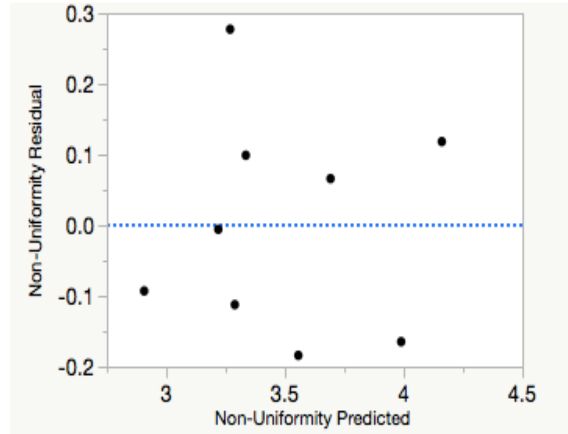

Figure 4-21: Residual versus predicted plot for wafer non-uniformity observed on the G53000 machine (quadratic model).

These plots show that the residuals do follow a normal distribution and are randomly distributed above and below the zero line, indicating that a quadratic model is a good fit for the within-wafer non-uniformity and further indicates that the lack of accuracy in predictions comes from not including the significant factors of pressure and power. The values of the individual residuals and the % Difference between the predicted values and the observed values is tabulated in Table 4-9.

Run Number	Treatment	Observed Non-Uniformity	Predicted Non-Uniformity	Residuals	% Difference
1	[0,2]	3.76	3.69	-0.07	1.75
2	[2,1]	3.21	3.22	0.01	0.18
3	[0,0]	3.82	3.99	0.16	4.31
4	[1,0]	3.55	3.27	-0.28	7.82
5	[1,1]	2.81	2.91	0.09	3.31
6	[2,0]	3.18	3.29	0.11	3.54
7	[1,2]	3.37	3.56	0.18	5.46
8	[2,2]	4.28	4.16	-0.12	2.76
9	[0,1]	3.43	3.34	-0.10	2.88

Table 4-9: Test cases for a variety of treatment combinations to validate the wafer non-uniformity quadratic model obtained from the experiments done on the G53000 machine.

iv. Response Surface and Optimal Parameters

One advantage of doing a DOE that includes interaction or higher order terms is the ability to plot a multivariate response surface [16], [20]. These response surfaces are particularly useful in process optimizations when a response variable needs to be maximized or minimized over a certain range of the input parameters. In this case, the goal is to minimize the within-wafer non-uniformity, and with the help of the "prediction profiler" and "surface profiler" tools in JMP, the response surface can be plotted and the response variable can be optimized. Figure 4-22 shows the 3-D quadratic response surface of the within-wafer non-uniformity in relation to the controllable factors of wafer temperature and oxygen, while Figure 4-23 shows the prediction profiler where a user can manually vary the input factors over the operational range and see how the response variable changes.

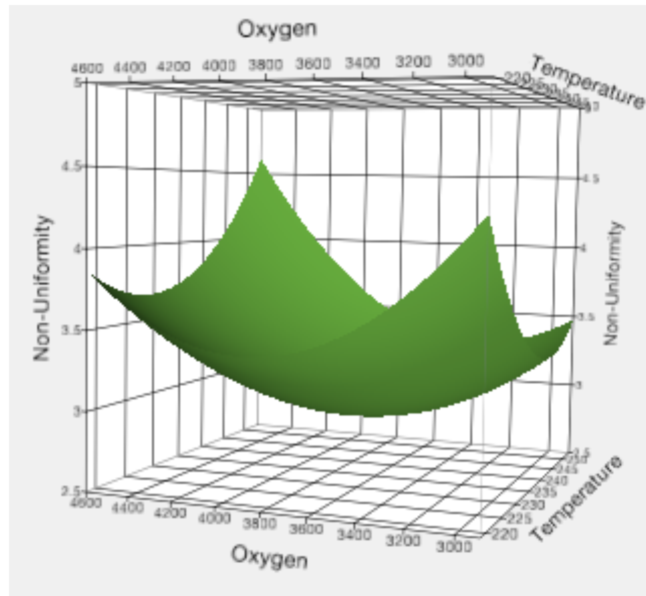

Figure 4-22: Quadratic response surface for wafer non-uniformity with temperature and oxygen as controllable factors obtained from the experiments done on the G53000 machine.

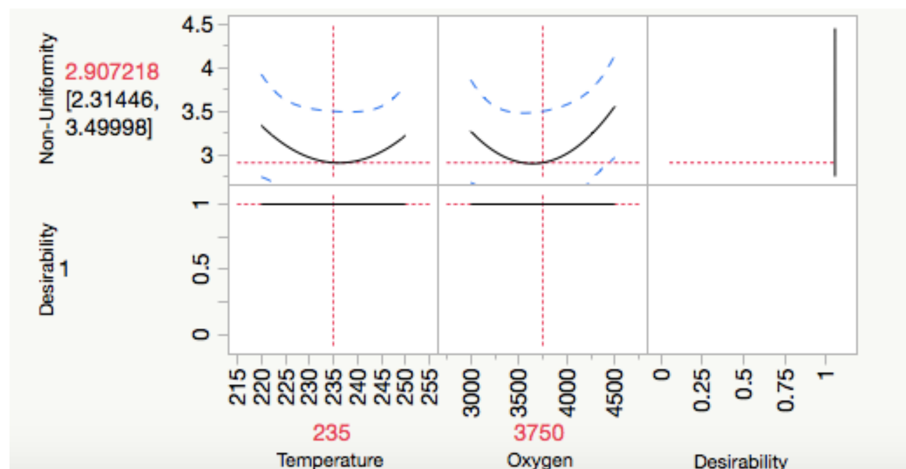

Figure 4-23: Prediction profiler for the response of wafer non-uniformity to temperature and oxygen for the G53000 machine.

The optimal value of the within-wafer non-uniformity is found to be 2.89% at a wafer temperature value of 236.67 degrees Celsius and oxygen gas flow value of 3617 SCCM while all of the other factors are kept at the values outlined in the partial recipe (Table 1-1).

4.4 G63000: Multiple Response Surface Model

The same experimental design and analysis approach that was used in Section 4.1 to build the regression models for the amount of photoresist removed and the within-wafer non-uniformity in the plasma ashing process using the multiple response surface method (Section 3.3) will be used on another Gasonics machine codenamed G63000. In this case too, the detailed analysis and diagrams presented in this section are for site 3 which is at the center of the wafer unless stated otherwise. The individual nine site models share similar characteristics and properties and any anomalies are highlighted appropriately. Table 4-10 shows the mean and the variance of the amount of photoresist removed from site 3 in each treatment combination of the 2^{6-2} resolution IV factorial design table (Table 3-2).

Run Number	Treatment	Replicate-1	Replicate-2	Replicate-3	Replicate Mean	Replicate Variance
1	[––-–-–]	4468.55	4629.97	4399.69	4499.40	13971.17
2	[+––-+–]	6533.5	6664.9	6547.99	6582.13	5190.64
3	[-+––++]	4606.59	4650.73	4588.86	4615.39	1015.10
4	[++-–-+]	6114.31	6235.44	6177.72	6175.82	3670.82
5	[--+-++]	4841.56	4923.26	4927.19	4897.34	2337.14
6	[+–+–-+]	6992.5	7189.87	6976.87	7053.08	14094.70
7	[–++-––]	5025.61	4990.73	4931.65	4982.66	2255.92
8	[+++–+-]	7004.75	7012.77	7070.95	7029.49	1305.28
9	[++–+––]	4557.47	4492.56	4502.06	4517.36	1228.97
10	[+––+++]	6568.45	6381.02	6590.1	6513.19	13218.86
11	[–+–++–]	4761.13	4619.5	4628.48	4669.70	6289.29
12	[++-+–-]	6354.05	6199.38	6267.8	6273.74	6007.19
13	[––+++-]	4911.02	4768.62	5197.33	4958.99	47673.91
14	[+-++-–]	7389.92	7137.32	7182.26	7236.50	18158.17
15	[-+++–+]	4997.5	4807.37	4994.29	4933.05	11849.80
16	[++++++]	6983.06	6807.88	6987.86	6926.27	10517.31
Center	[000000]	5676.67	5988.34	5927.83	5864.28	10229.90

Table 4-10: Values of replicate runs, replicate mean, and replicate variance for amount of photoresist stripped from a wafer in the G63000 machine.

The values in Table 4-10 are tabulated in JMP and the analysis report is generated. Since this is a fractional factorial screening design, the following features are analyzed to validate the DOE:

i. Effects Screening Assumptions

The JMP analysis report concludes that all the factors are uncorrelated but the variances of the replicates across all the runs are not the same. Therefore the condition of unequal variances must be accounted for in determining the significance of the factors under consideration. Figure 4-24 shows the normal probability plot of the effects for site 3.

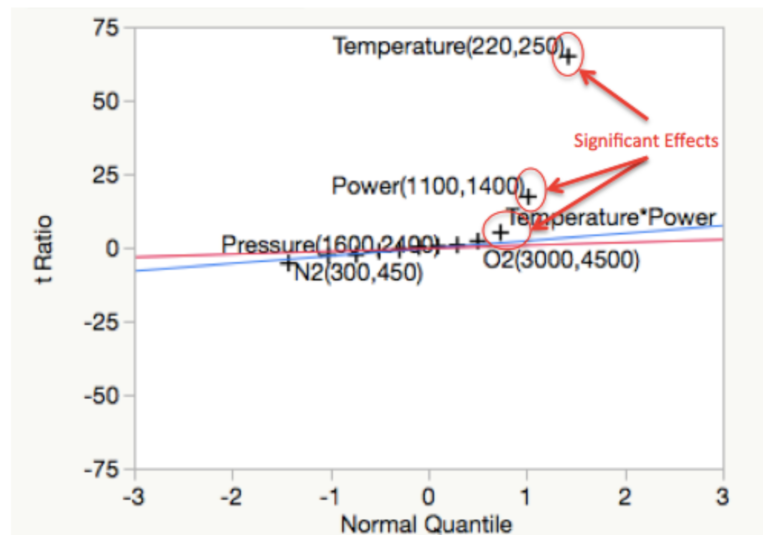

Figure 4-24: Normal probability plot of effects affecting photoresist strip rate standardized to have equal variances across all runs in the G63000 machine.

Wafer temperature, power, and the two factor interaction between wafer temperature and power are the most significant effects that influence the amount of photoresist removed in the plasma ashing process on the G63000 machine. These are the same factors in the same hierarchy that influenced the amount of photoresist removed on the G53000 machine.

ii. Alias Structure and Singularity

The alias structure is validated while making the design table in JMP and the JMP analysis report shows that there exists a singularity term where there is a linear dependency between the interaction of wafer temperature and oxygen and the interaction of chamber pressure and power.

In this case too, the interaction between wafer temperature and oxygen is chosen over the interaction between the chamber pressure and power, since the effect of temperature is more significant than the effect of power, and the effect of oxygen is more significant than the effect of chamber pressure, if any of the singularity terms are deemed to be statistically significant.

iii. Lack of Fit Analysis

The values predicted by the regression model versus the observed values from the experiment are plotted in Figure 4-25.

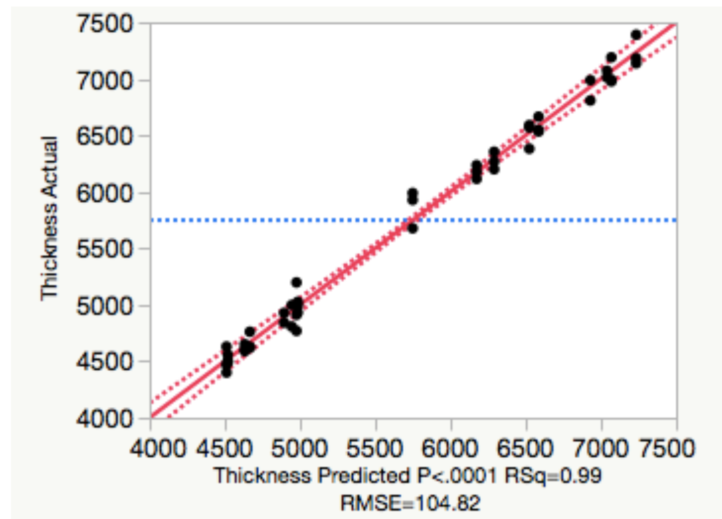

Figure 4-25: Observed values versus model predicted values plot for amount of photoresist removed from site 3 of the wafer in the G63000 machine.

A linear function is fitted to the values plotted on the graph and the adjusted R^2 value is 0.989 indicating that the regression model for site 3 is a precise model. The center point curvature test did not indicate the presence of any statistically significant non-linearity. This was not the case with the G53000 machine. Table 4-11 gives the adjusted R^2 values for each site model for the observed values versus the predicted values plot for the amount of photoresist removed.

Sites	Adjusted R^2 Value
Site-1	0.99
Site-2	0.99
Site-3	0.989
Site-4	0.987
Site-5	0.983
Site-6	0.99
Site-7	0.989
Site-8	0.989
Site-9	0.988

Table 4-11: Adjusted R^2 values for observed values versus predicted values plot for the amount of photoresist removed from all sites on a wafer in the G63000 machine.

It can be concluded from the adjusted R^2 values, that the regression models for each site are precise models over the specified range of the input factors in the DOE. The accuracy of the models must be confirmed from the residual analysis.

iv. Model Coefficients

The regression model coefficients for the factors in decreasing order of significance are shown in Figure 4-26.

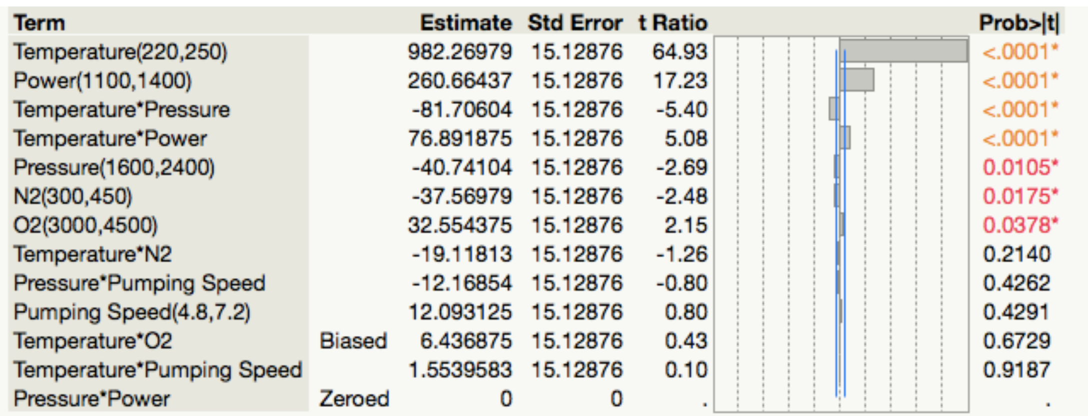

<table>
<tr><th>Term</th><th></th><th>Estimate</th><th>Std Error</th><th>t Ratio</th><th>Prob>|t|</th></tr>
<tr><td>Temperature(220,250)</td><td></td><td>982.26979</td><td>15.12876</td><td>64.93</td><td><.0001*</td></tr>
<tr><td>Power(1100,1400)</td><td></td><td>260.66437</td><td>15.12876</td><td>17.23</td><td><.0001*</td></tr>
<tr><td>Temperature*Pressure</td><td></td><td>-81.70604</td><td>15.12876</td><td>-5.40</td><td><.0001*</td></tr>
<tr><td>Temperature*Power</td><td></td><td>76.891875</td><td>15.12876</td><td>5.08</td><td><.0001*</td></tr>
<tr><td>Pressure(1600,2400)</td><td></td><td>-40.74104</td><td>15.12876</td><td>-2.69</td><td>0.0105*</td></tr>
<tr><td>N2(300,450)</td><td></td><td>-37.56979</td><td>15.12876</td><td>-2.48</td><td>0.0175*</td></tr>
<tr><td>O2(3000,4500)</td><td></td><td>32.554375</td><td>15.12876</td><td>2.15</td><td>0.0378*</td></tr>
<tr><td>Temperature*N2</td><td></td><td>-19.11813</td><td>15.12876</td><td>-1.26</td><td>0.2140</td></tr>
<tr><td>Pressure*Pumping Speed</td><td></td><td>-12.16854</td><td>15.12876</td><td>-0.80</td><td>0.4262</td></tr>
<tr><td>Pumping Speed(4.8,7.2)</td><td></td><td>12.093125</td><td>15.12876</td><td>0.80</td><td>0.4291</td></tr>
<tr><td>Temperature*O2</td><td>Biased</td><td>6.436875</td><td>15.12876</td><td>0.43</td><td>0.6729</td></tr>
<tr><td>Temperature*Pumping Speed</td><td></td><td>1.5539583</td><td>15.12876</td><td>0.10</td><td>0.9187</td></tr>
<tr><td>Pressure*Power</td><td>Zeroed</td><td>0</td><td>0</td><td>.</td><td>.</td></tr>
</table>

Figure 4-26: Model coefficients and hierarchy of significance of factors affecting the amount of photoresist removed from a wafer in the G63000 machine (site 3 of wafer.)

In this case too, JMP expects the input values to be entered as coded variables where each factor is varied from -1 to +1. The intercept value or the β_0 term for the site 3 regression model is 5748.73. Wafer temperature and power are the most significant main effects while the interactions between wafer temperature and pressure and the wafer temperature and power are the most significant two factor interactions.

Table 4-12 shows the main effects at a 1% (red) and 5% (orange) significance level and the model coefficients for each of the nine sites. The "x" symbol indicates the non-significant terms in the regression models. Wafer temperature and power are the most significant main effects in all the nine sites. It is interesting to note that the vacuum pump speed has no significant effect at all on the amount of photoresist removed in the plasma ashing process using the partial recipe on the G63000 machine.

Sites	Temperature	Pressure	Power	Pumping Speed	Oxygen	Nitrogen
Site 1	1026.3	-37.9	246.2	x	42.6	-34.2
Site 2	985.1	-55.3	256.4	x	x	-39.2
Site 3	982.3	-40.7	260.7	x	32.5	-37.6
Site 4	939.5	-37.5	245.5	x	72.9	x
Site 5	913.9	x	233.2	x	134.5	x
Site 6	934.9	x	227.9	x	181.6	x
Site 7	960	-36.2	247.5	x	93.4	-31.8
Site 8	970	x	259.6	x	x	-38.3
Site 9	959.3	x	249.8	x	31.4	-32

Table 4-12: Model coefficients for all nine sites for the amount of photoresist removed from a wafer in the G63000 machine.

Table 4-13 shows the most significant two factor interaction effects on the amount of photoresist removed. The two factor interaction between the wafer temperature and power is a significant effect in every site thus consistent with the inheritance of effects principle.

Sites	Significant 2-factor interactions
Site-1	Temperature*Power, Temperature*Pressure
Site-2	Temperature*Pressure, Temperature*Power
Site-3	Temperature*Pressure, Temperature*Power
Site-4	Temperature*Power, Temperature*Pressure
Site-5	Temperature*Power, Temperature*Pressure, Temperature*O2
Site-6	Temperature*Power, Temperature*O2, Temperature*Pressure
Site-7	Temperature*Power, Temperature*Pressure
Site-8	Temperature*Pressure, Temperature*Power
Site-9	Temperature*Power, Temperature*Pressure

Table 4-13: List of significant two factor interactions for the amount of photoresist removed from a wafer in the G63000 machine.

v. Residual Analysis

Figures 4-27 and 4-28 show the normal probability plot of the residuals and the residual versus predicted plot for site 3. The normal probability plot of the residuals indicates that there seems to be no significant deviation from the normality assumption for the residuals as all of the residuals lie on or close to the normal line. The residual versus the predicted plot indicates that the residuals are randomly scattered around the zero line and no significant obvious trend is observed. The stochastic error in the plasma ashing process carried out on the G63000 machine is around 220 Angstroms which is more than what was observed on the G53000 machine (150-180 Angstroms).

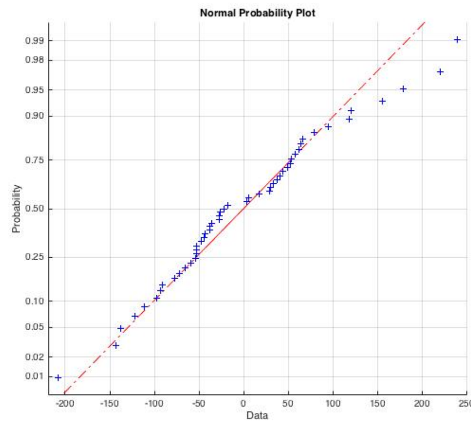

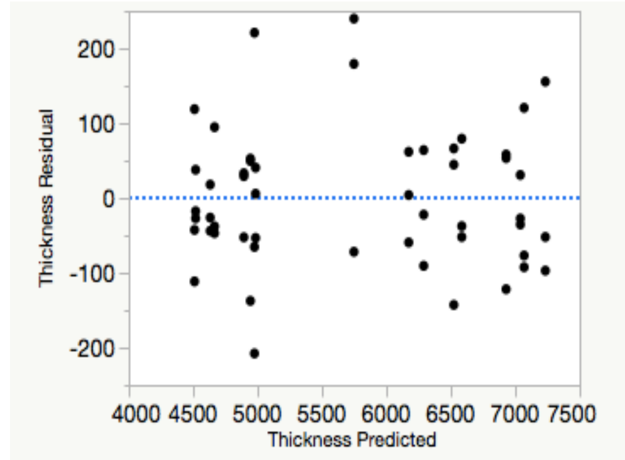

Figure 4-27: Normal probability plot of residuals for amount of photoresist removed from a wafer in the G63000 machine (site 3).

Figure 4-28: Residual versus predicted plot for amount of photoresist removed from a wafer in the G63000 machine (site 3).

vi. Post Experiment Validation Runs

After the experiment was completed and the regression model was formulated, a few additional wafers were processed in the G63000 machine at various combinations of the input factors and the observed values are compared with the values obtained from the regression model. The model accurately predicts all the values within the stochastic error of the process of 220 Angstroms.

vii. Modeling of the within-wafer non-uniformity

The individual regression models are again combined to give a single value of the amount of photoresist removed from a wafer and the within-wafer non-uniformity according to equations 3-4, 3-5, and 3-6. Again, a number of test cases are formulated to check the accuracy of predicting the within-wafer non-uniformity using the multiple response surface methodology. The key column of interest % Difference is calculated using equation 4-1.

Run Number	Treatment	Observed Non-Uniformity	Predicted Non-Uniformity	Residuals	% Difference
1	[-–-–-–]	3.67	4.50	0.83	22.74
2	[+––-+–]	2.09	4.53	2.44	117.06
3	[-+––++]	1.82	3.69	1.87	102.86
4	[++-–-+]	3.50	3.97	0.47	13.50
5	[--+-++]	2.42	4.50	2.08	85.89
6	[+–+–-+]	3.95	4.43	0.48	12.19
7	[–++-––]	4.68	4.87	0.19	4.11
8	[+++–+-]	1.22	3.73	2.51	206.04
9	[-+–+––]	3.47	3.92	0.45	12.99
10	[+––+++]	2.00	4.20	2.20	110.11
11	[–+–++–]	1.92	3.46	1.54	79.85
12	[++-+–-]	4.22	3.65	-0.57	13.56
13	[––+++-]	2.45	4.23	1.78	72.86
14	[+-++-–]	4.00	4.17	0.17	4.25
15	[-+++–+]	4.57	4.07	-0.50	11.03
16	[++++++]	1.08	3.34	2.26	209.19
17	[000000]	2.60	3.94	1.34	51.61
18	[-0+0+0]	2.37	3.6	1.23	51.90
19	[00+000]	2.84	3.99	1.15	40.49
20	[+0+0+0]	2.37	3.83	1.46	61.60
21	[+0+000]	2.79	3.88	1.09	39.07
22	[-0+0-0]	4.50	4.44	-0.06	1.33
23	[00+0+0]	2.69	3.94	1.25	46.47

Table 4-14: Test cases for a variety of treatment combinations to validate wafer non-uniformity model obtained from the experiments done on the G63000 machine.

The treatment combination codes (-, +, 0) refer to the low, high, and center point values of the 2^{6-2} resolution IV factorial design run table shown in Table 3-2. The values highlighted in red in the % Difference column refer to those runs where the difference between the observed values and the predicted values exceeded 10%. In the case of the G63000 machine, the model to predict the within-wafer non-uniformity using the multiple response surface method is extremely poor. Most of the test cases show significant differences between the predicted values and the observed values. The main reasons as to why this may be the case is that the non-linear response surface described by the prediction model is completely different from what the actual response surface may be or there could be strong effects of factors that affect the within-wafer non-uniformity that were not a part of the DOE. The failure of the multiple response surface model to accurately predict the wafer non-uniformity on the G63000 machine indicates that there are significant differences in the mean and standard deviation between the actual amount of photoresist removed from the nine sites and the predicted amount of photoresist removed from

the nine sites. Figures 4-29, 4-30, 4-31, and 4-32 show the observed and predicted values at each site for the amount of photoresist removed and the non-uniformity prediction error (% Difference in Table 4-14) associated with that treatment combination for the best case, worst case, and two intermediate scenarios.

The non-uniformity prediction error is lower when the observed and predicted curves overlap. The plots also indicate that differences in standard deviation (Figure 4-32) have a stronger influence on the non-uniformity prediction error than the differences in the mean. It is consistently observed that there are significant differences in the observed and predicted values of the amount of photoresist removed at site 8 of the wafer in all treatment combinations and this must be investigated further as there may be some other factors relating to the current state of the machine near site 8 (e.g. gas flow leaks) which may have jeopardized the prediction capability of the site regression model. The plots also show that the site models are capable of capturing the shape of the variation in the amount of photoresist removed from a wafer. Again a possible alternative for future consideration is to use the weighted standard deviation as the within-wafer non-uniformity metric, rather than normalizing the standard deviation to the mean. This will help to decouple the errors in the models for both the standard deviation and the mean, and enable more robust analysis of the parameters.

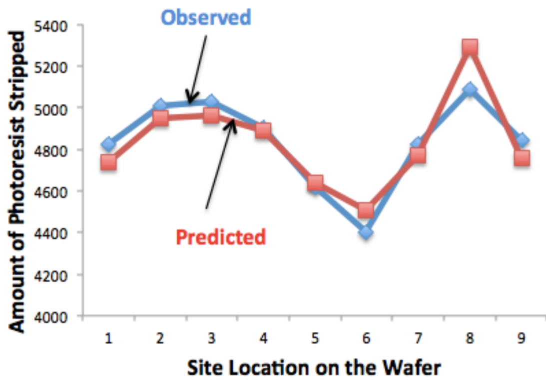

Figure 4-29: Observed and predicted values of the amount of photoresist stripped at each site for treatment combination [-++---]. The non-uniformity prediction error is 4.11%.

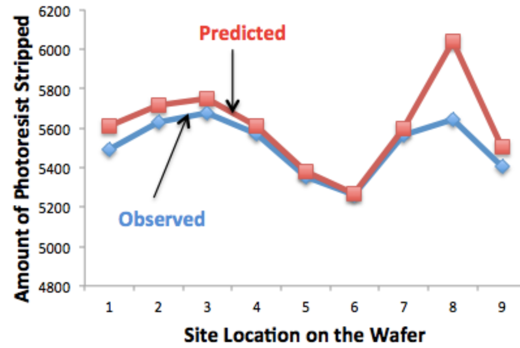

Figure 4-30: Observed and predicted values of the amount of photoresist stripped at each site for treatment combination [000000]. The non-uniformity prediction error is 51.61%.

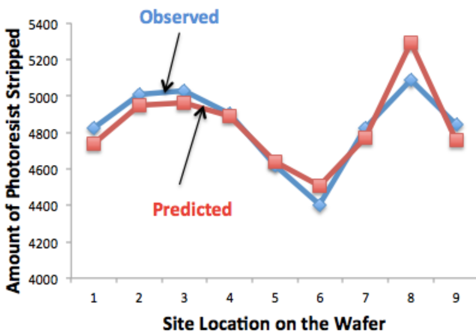

Figure 4-31: Observed and predicted values of amount of the photoresist stripped at each site for treatment combination [++-+--]. The non-uniformity prediction error is 13.56%.

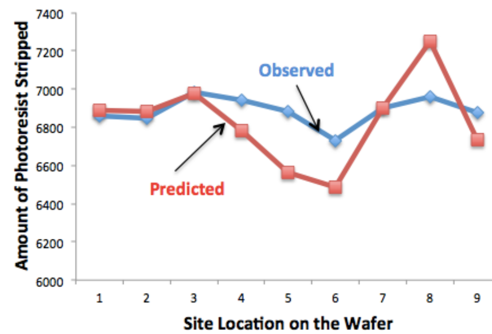

Figure 4-32: Observed and predicted values of amount of the photoresist stripped at each site for treatment combination [++++++]. The non-uniformity prediction error is 209.19%.

Another approach to model the within-wafer non-uniformity is to use the single response surface method and is presented next. This model may provide a better understanding of the significant factors affecting the response of the wafer non-uniformity on the G63000 machine.

4.5 G63000: Single Response Surface Model

In an effort to better understand the significant factors that affect the wafer non-uniformity on the G63000 machine, the single response surface method described in Section 3.3 is used to model the wafer non-uniformity using the 2^{6-2} resolution IV factorial design table. Table 4-15 shows the individual replicates, the replicate means and the replicate variances that are used to construct the design table. The same structure of analysis that was used in previous screening designs will be followed.

Run Number	Treatment	Replicate-1	Replicate-2	Replicate-3	Replicate Mean	Replicate Variance
1	[-––––]	3.67	3.96	4.05	3.89	0.04
2	[+––-+–]	2.09	2.56	2.67	2.44	0.09
3	[-+––++]	1.82	2	2.1	1.97	0.02
4	[++-––-+]	3.5	4.14	4.43	4.02	0.23
5	[--+-++]	2.42	2.72	2.74	2.63	0.03
6	[+–+–-+]	3.95	4.56	4.48	4.33	0.11
7	[–++-––]	4.68	5.13	4.92	4.91	0.05
8	[+++–+-]	1.22	1.84	1.67	1.58	0.10
9	[++–+––]	3.47	3.86	3.6	3.64	0.04
10	[+––+++]	2	2.74	2.39	2.38	0.14
11	[–+–++–]	1.92	2.18	2.34	2.15	0.04
12	[++-+–-]	4.22	4.7	4.5	4.48	0.06
13	[––+++-]	2.45	2.89	2.74	2.69	0.05
14	[+-++-–]	4	4.69	4.48	4.39	0.13
15	[-+++–+]	4.57	4.47	4.61	4.55	0.01
16	[++++++]	1.08	1.87	1.47	1.47	0.16
Center	[000000]	2.6	3.27	3.09	2.99	0.12

Table 4-15: Values of replicate runs, replicate mean, and replicate variance for wafer non-uniformity observed on the G63000 machine.

i. Effects Screening Assumptions

In this case too, JMP concludes that the effects are not correlated but the equality of variance assumption across all experimental runs does not hold. Therefore, this was accounted for in the normal probability plot shown in Figure 4-25. The oxygen flow is the only significant main effect affecting the within wafer non-uniformity on the G63000 machine, followed by the two factor interaction between wafer temperature and power.

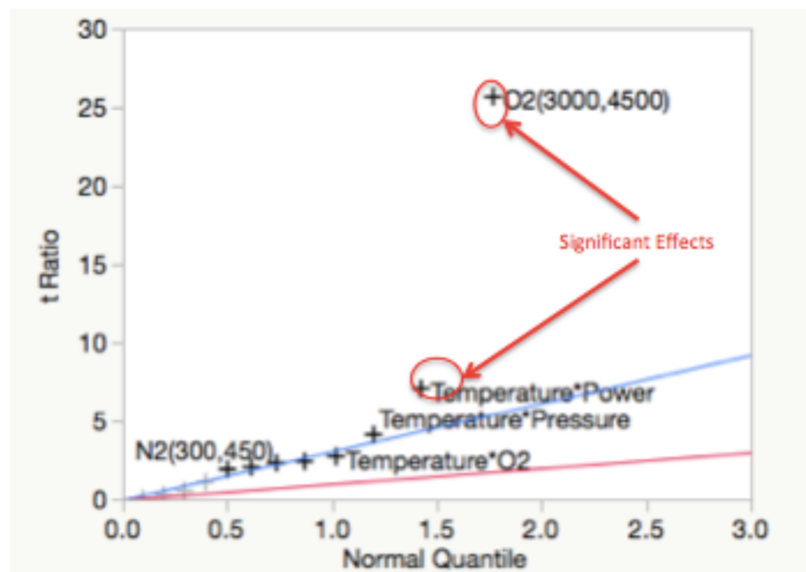

Figure 4-33: Normal probability plot of effects affecting wafer non-uniformity standardized to have equal variances across all runs in the G63000 machine.

ii. Alias Structure and Singularity

The alias structure is verified when constructing the design table and there is a singularity term in the model which is the linear dependency between the two factor interactions of wafer temperature and oxygen and power and pressure. Since oxygen is the most significant factor that influences the within-wafer non-uniformity, the two factor interaction between temperature and oxygen will be included in the model if the biased term is deemed to be statistically significant at a 5% significance level.

iii. Lack of Fit Analysis

The plot of the observed values versus the predicted values with a linear fit curve for the within-wafer non-uniformity is shown in Figure 4-34. The adjusted R^2 value for the linear fit in the plot is 0.94 which indicates that this model cannot account for as much as 6% of the variation in the data over the range of the input factors. The linear model using the single response surface method is a significant improvement on the previous model that was formulated using the multiple response surface method. While this linear model can be used to obtain a general idea of the within-wafer non-uniformity for different combinations of the input factors, a non-linear response surface is still needed to optimize the process.

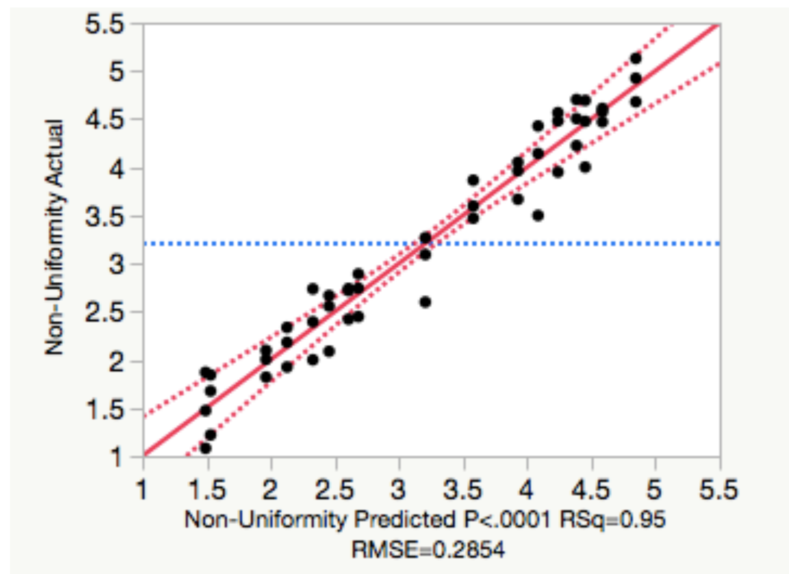

Figure 4-34: Observed values versus model predicted values plot for the wafer non-uniformity observed on the G63000 machine.

iv. Model Coefficients

The summary of the model coefficients in the hierarchy of their significance is shown in Figure 4-35. The value of the intercept term is 3.21 and this regression model also assumes that the values entered as inputs will be coded. Oxygen flow is the single most significant main effect by looking at the absolute t-ratio and small variations in oxygen flow over the wafer in the G63000 machine can significantly alter the within-wafer non-uniformity parameter.

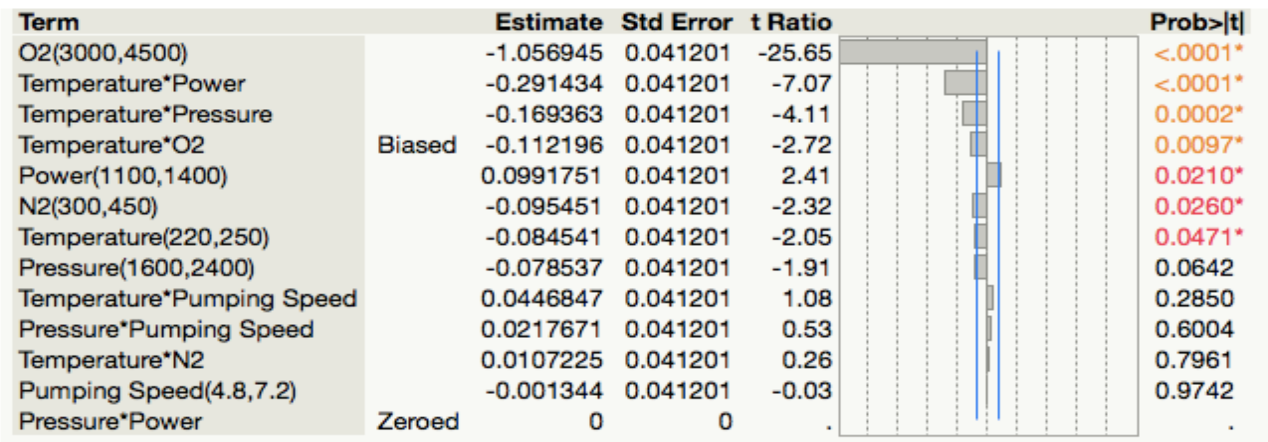

Term		Estimate	Std Error	t Ratio	Prob>|t|
O2(3000,4500)		-1.056945	0.041201	-25.65	<.0001*
Temperature*Power		-0.291434	0.041201	-7.07	<.0001*
Temperature*Pressure		-0.169363	0.041201	-4.11	0.0002*
Temperature*O2	Biased	-0.112196	0.041201	-2.72	0.0097*
Power(1100,1400)		0.0991751	0.041201	2.41	0.0210*
N2(300,450)		-0.095451	0.041201	-2.32	0.0260*
Temperature(220,250)		-0.084541	0.041201	-2.05	0.0471*
Pressure(1600,2400)		-0.078537	0.041201	-1.91	0.0642
Temperature*Pumping Speed		0.0446847	0.041201	1.08	0.2850
Pressure*Pumping Speed		0.0217671	0.041201	0.53	0.6004
Temperature*N2		0.0107225	0.041201	0.26	0.7961
Pumping Speed(4.8,7.2)		-0.001344	0.041201	-0.03	0.9742
Pressure*Power	Zeroed	0	0	.	.

Figure 4-35: Model coefficients and hierarchy of significance of factors affecting the wafer non-uniformity observed on the G63000 machine.

v. Residual Analysis

Figures 4-36 and 4-37 show the normal probability plot of the residuals and the residual versus predicted plot for the within-wafer non-uniformity model. By looking at the plots, one can conclude that the residuals are normally distributed and the error is stochastic. This indicates that the failure of the linear model to account for the 6% of the variation may be due to additional factors at work since there is no obvious trend in the residual pattern that suggests lack of fit. If one is convinced through prior process knowledge that all the process parameter factors were accounted for in the experiment, then the machine must be checked for other factors that could jeopardize the results of the DOE like potential gas flow leaks, sensor failure, etc.

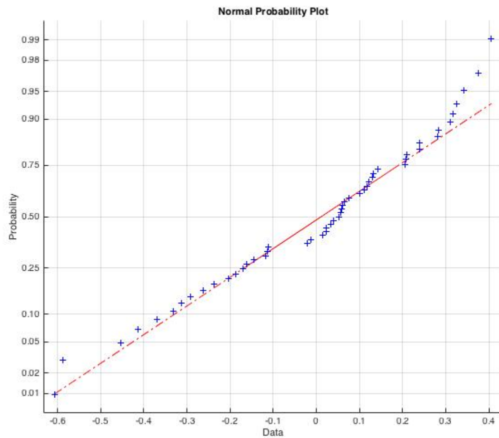

Figure 4-36: Normal probability plot of residuals for wafer non-uniformity observed on the G63000 machine.

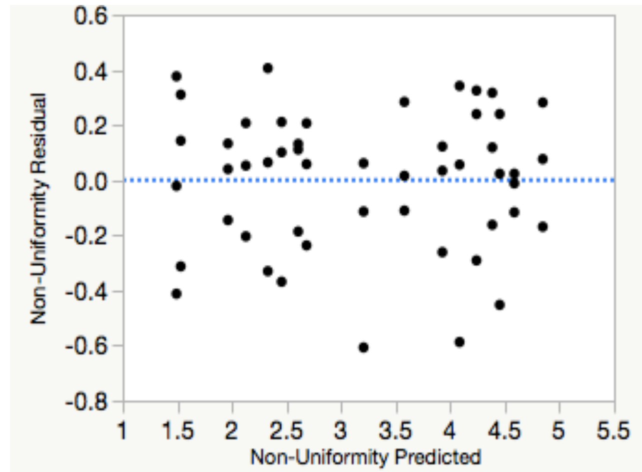

Figure 4-37: Residual versus predicted plot for wafer non-uniformity observed on the G63000 machine.

vi. Post Experiment Validation Runs

The post experiment validation runs were done primarily to see the improvement of using the single response surface method over the multiple response surface method using the same treatment combinations over the range of the input factors. Table 4-16 shows the calculated residuals and % Difference. Table 4-16 clearly shows that the single response surface model is a far better predictor of the within-wafer non-uniformity than the multiple response surface model, but some of the treatment combination runs do show significant differences between the observed values and the predicted values. For the G63000 machine, the effect of oxygen flow over the wafer was much more significant to the response of both the amount of photoresist removed from each site as well as the within-wafer non-uniformity when compared with the G53000 machine. The quadratic response surface model presented next may be an improvement over the single response surface model due to the addition of non-linear terms.

Run Number	Treatment	Observed Non-Uniformity	Predicted Non-Uniformity	Residuals	% Difference
1	[-–-–-–]	3.67	3.93	0.26	7.13
2	[+––-+–]	2.09	2.46	0.37	17.67
3	[-+––++]	1.82	1.96	0.15	7.98
4	[++-–-+]	3.50	4.09	0.59	16.80
5	[--+-++]	2.42	2.61	0.19	7.71
6	[+–+–-+]	3.95	4.24	0.29	7.38
7	[–++-––]	4.68	4.85	0.17	3.62
8	[+++–+-]	1.22	1.53	0.31	25.69
9	[-+–+––]	3.47	3.58	0.11	3.19
10	[+––+++]	2.00	2.33	0.33	16.53
11	[–+–++–]	1.92	2.13	0.20	10.62
12	[++-+–-]	4.22	4.38	0.16	3.84
13	[––+++-]	2.45	2.68	0.24	9.68
14	[+-++-–]	4.00	4.45	0.45	11.32
15	[-+++–+]	4.57	4.59	0.01	0.26
16	[++++++]	1.08	1.49	0.41	38.18
17	[000000]	2.60	3.21	0.61	23.37
18	[-0+0+0]	2.37	2.62	0.25	10.55
19	[00+000]	2.84	3.31	0.47	16.55
20	[+0+0+0]	2.37	1.87	-0.50	21.10
21	[+0+000]	2.79	2.93	0.14	5.02
22	[-0+0-0]	4.50	4.74	0.24	5.33
23	[00+0+0]	2.69	2.25	-0.44	16.36

Table 4-16: Test cases for a variety of treatment combinations to validate the wafer non-uniformity model using the single response surface method from the experiments done on the G63000 machine.

4.6 G63000: Quadratic Response Surface Model

As was the case with G53000 machine, the process engineers at Analog Devices Inc. were interested in understanding at what combination of input parameters could the within-wafer non-uniformity be minimized. The analysis of the previous models on the G63000 machine showed that the within-wafer non-uniformity varied between 1.5%-5%, which is substantial. Therefore it was decided to build a quadratic response surface of the within-wafer non-uniformity by doing a 3^2 full factorial DOE in the hope of finding the minima. The two factors chosen were oxygen and temperature because of their significance in having an impact on the

within-wafer non-uniformity (Table 3-4). Table 4-17 shows the within-wafer non-uniformity response of each run.

Run Number	Treatment	Non-Uniformity
1	[0,2]	2.37
2	[2,1]	2.79
3	[0,0]	4.50
4	[1,0]	4.52
5	[1,1]	2.84
6	[2,0]	4.52
7	[1,2]	2.69
8	[2,2]	2.37
9	[0,1]	2.79

Table 4-17: Values of wafer non-uniformity obtained from the 3^2 full factorial experimental runs in the G63000 machine.

To analyze the outcome of the above experiment, the following steps are taken.

i. Lack of Fit Analysis

The plot of the observed values versus the predicted values for the within-wafer non-uniformity is shown in Figure 4-38. The adjusted R^2 value for the plot is 0.99 indicating a very strong fit. This indicates that there exists some amount of curvature in the response of the within-wafer non-uniformity that the previous models could have failed to take into account.

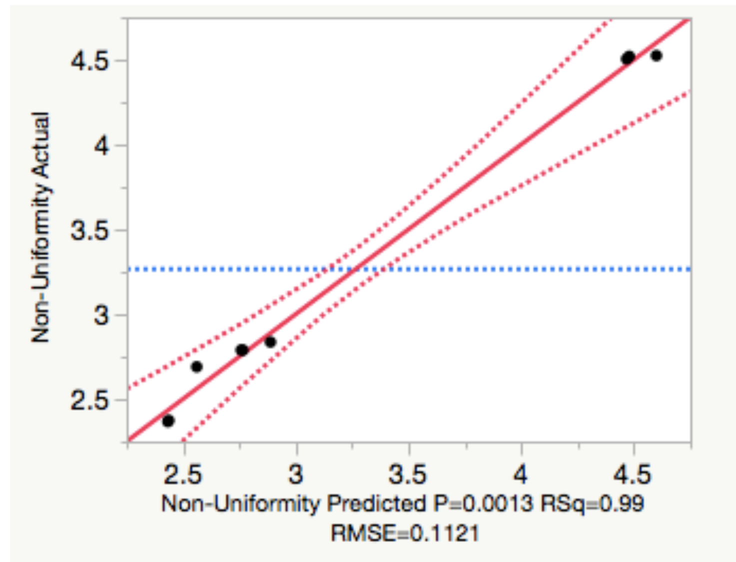

Figure 4-38: Observed values versus model predicted values plot for the wafer non-uniformity quadratic model obtained from the experiments done on the G63000 machine.

ii. Model Coefficients

The summary of the model coefficients obtained from this DOE is shown in Figure 4-31. It should again be noted that the model coefficients in this case represent the absolute values of the input parameters and not the coded variables. These coefficients again indicate that the within-wafer non-uniformity is primarily driven by the oxygen gas flow over the wafer in the G63000 machine.

Term	Estimate	Std Error	t Ratio	Prob>|t|
Oxygen	-0.001359	0.000061	-22.27	0.0002*
(Oxygen-3750)*(Oxygen-3750)	1.2305e-6	1.41e-7	8.73	0.0032*
(Temperature-235)*(Temperature-235)	-0.000561	0.000352	-1.59	0.2098
Temperature	0.0002611	0.003052	0.09	0.9372
(Temperature-235)*(Oxygen-3750)	-1.697e-7	4.984e-6	-0.03	0.9750

Figure 4-39: Quadratic model coefficients of factors affecting the wafer non-uniformity observed on the G63000 machine.

iii. Residual Analysis

Figures 4-40 and 4-41 show the normal probability plot of the residuals and the residual versus predicted plot for the within-wafer non-uniformity quadratic model. The residuals in this case do not follow a normal distribution while the residuals versus predicted plot shows higher variation of the residuals at lower values of the within-wafer non-uniformity. The deviation from the normality assumption in the residuals suggests that there was some significant factor that was not considered in the DOE. These factors may not necessarily be the process parameters and could stem from deficiencies in the current state of the machine like gas leaks, faulty sensors, and equipment nearing failure. In such cases, it is advisable to thoroughly investigate the machine for any sign of potential breakdown or failure.

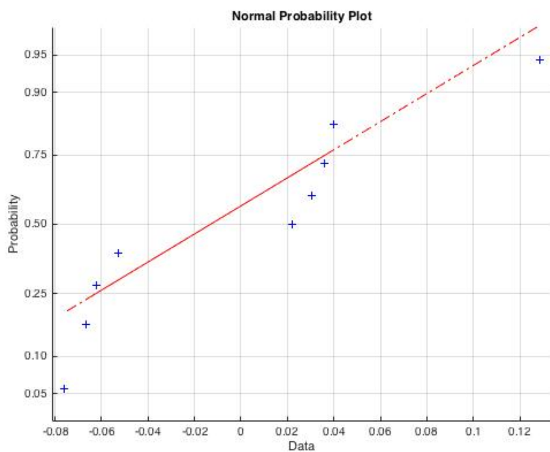

Figure 4-40: Normal probability plot of residuals for wafer non-uniformity observed on the G63000 machine (quadratic model).

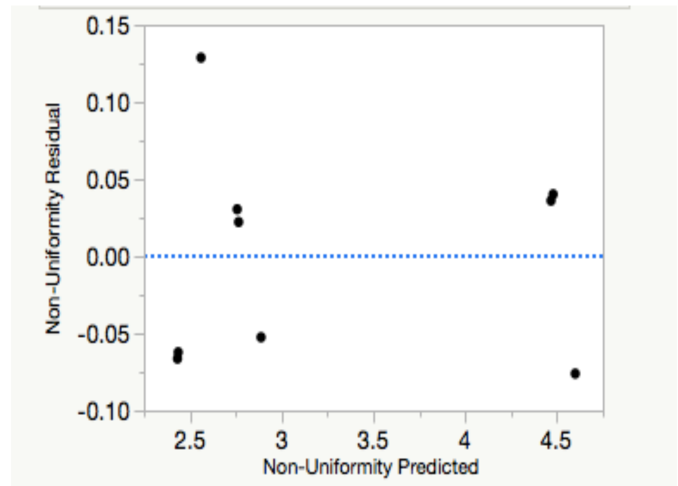

Figure 4-41: Residual versus predicted plot for wafer non-uniformity observed on the G63000 machine (quadratic model).

The values of the individual residuals and the % Difference between the predicted values and the observed values is tabulated in Table 4-18. The quadratic model is the most accurate predictor of the within-wafer non-uniformity when compared to the single response surface and multiple response surface models.

Run Number	Treatment	Observed Non-Uniformity	Predicted Non-Uniformity	Residuals	% Difference
1	[0,2]	2.37	2.43	0.07	2.81
2	[2,1]	2.79	2.77	-0.02	0.79
3	[0,0]	4.50	4.47	-0.04	0.80
4	[1,0]	4.52	4.60	0.08	1.68
5	[1,1]	2.84	2.89	0.05	1.85
6	[2,0]	4.52	4.48	-0.04	0.89
7	[1,2]	2.69	2.56	-0.13	4.78
8	[2,2]	2.37	2.44	0.06	2.62
9	[0,1]	2.79	2.76	-0.03	1.09

Table 4-18: Test cases for a variety of treatment combinations to validate the wafer non-uniformity quadratic model obtained from the experiments done on the G63000 machine.

iv. Response Surface and Optimal Parameters

In this case too, the goal of the DOE was to minimize the within-wafer non-uniformity. With the help of the prediction profiler and surface profiler tools in JMP, the response surface can be plotted and the within-wafer non-uniformity can be optimized. Figure 4-42 shows the 3-D quadratic response surface of the within-wafer non-uniformity in relation to the controllable factors of wafer temperature and oxygen, while Figure 4-43 shows the prediction profiler where a user can manually vary the input factors over the operational range and see how the response variable changes. The skewed shape of the response surface of the wafer non-uniformity in relation to the oxygen gas flow (Figure 4-42) and the deviation from the normality assumption of the residuals (Figure 4-40) suggest that there is some factor that was not captured by the DOE regarding the gas flows over the wafer during the plasma ashing process. A probable hypothesis is that the reacting chamber of the G63000 machine is not sealed properly resulting in a gas flow leak. It was recommended to the equipment engineers at Analog Devices Inc. to investigate the state of the G63000 machine further before putting the machine back online to run the product wafers.

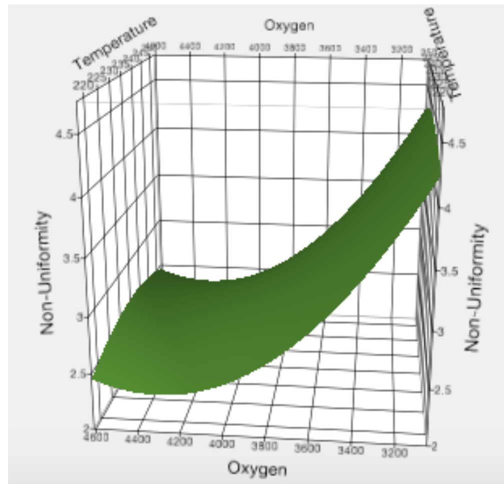

Figure 4-42: Quadratic response surface for wafer non-uniformity with temperature and oxygen as controllable factors obtained from the experiments done on the G63000 machine.

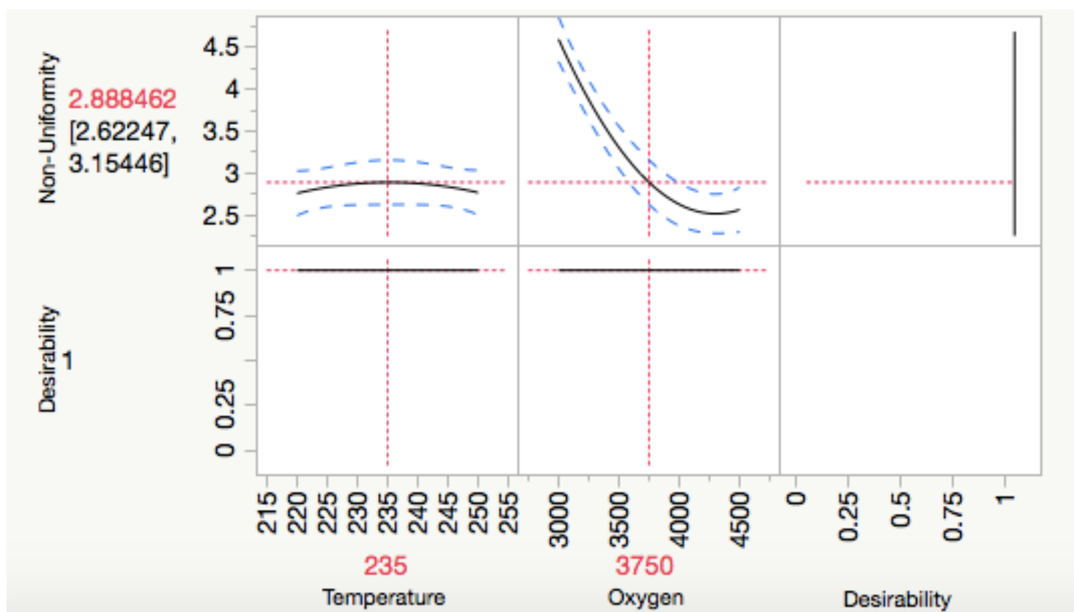

Figure 4-43: Prediction profiler for the response of wafer non-uniformity to temperature and oxygen for the G63000 machine.

The optimal value of the within-wafer non-uniformity was found to be 2.38% at a wafer temperature value of 220 degrees Celsius and oxygen value of 4367 SCCM while all of the other factors are kept at the values outlined in the partial recipe (Table 1-1).

4.8 Comparison between G53000 and G63000 Machines

The analysis of the DOEs done on the machines clearly show that differences exist between them even though the same process with the same recipe was run on both of them. The G53000 machine on an average consistently stripped 400-600 Angstroms of photoresist more than the G63000 machine, which is a significant and substantial difference. The response of the within-wafer non-uniformity parameter was completely different for both machines. Such variations between the same machines that run the same process mainly come from the intrinsic build and current state of the machines. The multiple response surface model is a better predictor of the wafer non-uniformity on the G53000 machine than the G63000 machine. Chapter 5 explains some of the reasons as to why these differences may occur between the machines while Haskaraman's work [4] describes strategies to match the performance of these machines.

Chapter 5: Contributions to Analog Devices Inc.

This chapter highlights the specific contributions made to Analog Devices Inc. from the insights obtained from the DOE analysis. Contributions were made in introducing the company to new methodologies for calculating wafer statistics, using the DOE analysis for detecting and eliminating root causes of problems, and developing new process improvement strategies.

5.1 New Methodologies for Wafer Statistics Calculation

The process engineers at Analog Devices Inc. were introduced to the concept of calculating the mean, standard deviation, and within-wafer non-uniformity by taking into account the areal representation of sites as shown by the equations in Section 1.7. Maintaining a high level of spatial uniformity in a wafer fabrication process is a key metric for many semiconductor companies. However, the correct uniformity of the wafer must be discerned by measuring only a few sites on the wafer due to time and cost considerations. It is therefore important to adopt a robust method for wafer measurement and qualification purposes that can be validated. For etching processes, Analog Devices Inc. uses the Nanospec 9200 tool to measure the thickness of wafers and in most of the processes the sites are measured in a radial pattern. The following method is proposed and validated for the plasma ashing process using the partial recipe done on the Gasonics Aura 3010 machines:

i. Measure 49 points in a radial pattern on a wafer and plot a spatial map developed by Haskaraman [4] as shown in Figure 5-1 and 5-2, when the machine of interest is believed to be in the state of process control. Also measure the same wafer using the standard measurement method that is currently used to measure the wafer non-uniformity. For the plasma ashing process using the partial recipe, the standard method is to measure nine sites in a radial pattern.

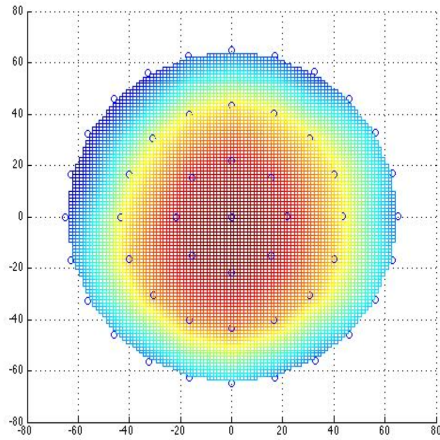

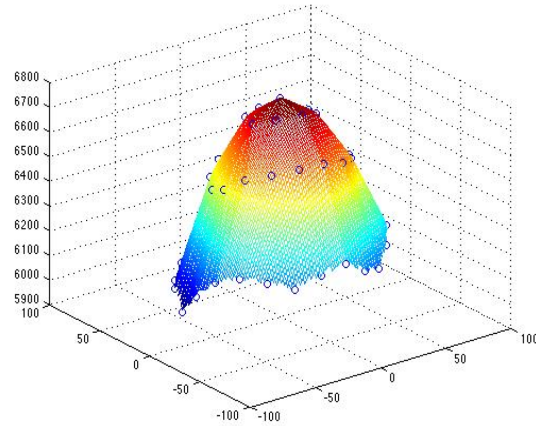

Figure 5-1: Spatial map of a wafer showing the distribution of sites. This spatial map represents a wafer that has undergone a forming test process on a Gasonics machine.

Figure 5-2: 3-D plot of a wafer showing the amount of photoresist removed at each of the 49 sites. X and Y-axes show the co-ordinate position of a site and the Z-axis plots the amount of photoresist removed at that site.

ii. Calculate the non-uniformity of this wafer using the 49-point data and the standard measurement data. In general, the statistics for calculating the site data in a radial pattern should take into account the areal representation of sites since the distribution of sites is such that each point does not represent the same area of the wafer [10]. However, it can be seen in Figure 5-1 that the number of sites is different for different rings and in this case, each site is considered to approximately represent equal areas and no weighting is necessary.

iii. Compare the two measured non-uniformities. If their magnitudes are similar then the current measurement method is a good representation of the wafer non-uniformity. It is also recommended to compare the non-uniformity of a few additional wafer runs that are measured using the standard method to the non-uniformity measured from the 49-point data for further validation.

The above method is used to validate the wafer non-uniformities after the plasma ashing process had been completed using the partial recipe on both the G53000 and G63000 machine. The wafer non-uniformity from the 49-point data on the G53000 machine is 3.04% and the G63000 machine is 3.09%. The current nine site measurement method taking into account the areal representation of sites for multiple wafer runs gives a wafer non-uniformity range of 2.8%-3.2% on both the machines. This validates the fact that the current nine site measurement method with the areal representation of sites is a good representation of the wafer non-uniformity for the plasma ashing process on the Gasonics tools. Using the 49-point data to construct a spatial map diagram is also useful in visualizing the non-uniformity of the wafer and can be used in anomaly detection. The Nanospec 9200 tool in Analog Devices Inc.'s fabrication center has been programmed to incorporate the 49-point measuring method. For processes, where the wafer non-uniformity is determined by measuring sites in a square grid pattern, a 7x7 square grid (49 points) has also been incorporated into the tool.

5.2 Root Cause Analysis and Machine Diagnostics

A DOE analysis provides insightful information on the behavior of various processes and machines taking into account the natural variation of the process and the intrinsic build and state of the machines. Information from a DOE analysis can be used to develop a structured framework and operating procedures to identify the root causes of failures and machine breakdowns, and take corrective measures in a timely and efficient way. The insights obtained from the DOE analysis done on the plasma ashing process exposed the following problems that could potentially have a detrimental impact on future product lines.

i. Lack of Temperature Control

Figures 5-3 and 5-4 show the spatial map of a wafer that has undergone the plasma ashing process using the partial recipe on the G53000 machine. The spatial map is generated by measuring the amount of photoresist removed from 49 sites on a single wafer.

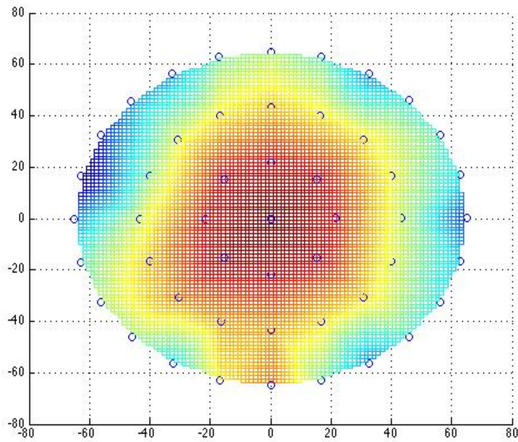

Figure 5-3: Spatial distribution map of a wafer processed in the G53000 machine using the partial recipe.

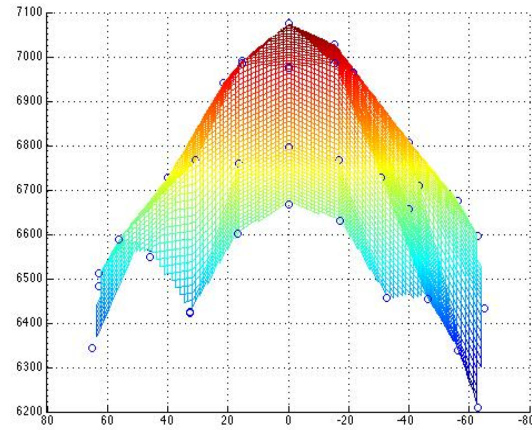

Figure 5-4: Map of the amount of photoresist removed from the wafer sites shown in Figure 5-3.

The above figure clearly shows that the amount of photoresist removed is more at and near the center of the wafer than it is at the edges of the wafer. On measuring multiple wafers, it was noted than on an average the difference between the amounts of photoresist removed at the center and at the edge of a wafer was 700 Angstroms which is 12.6% of the target value of 6000 Angstroms. It can also be seen that the G53000 machine strips much more that 6000 Angstroms of photoresist at many sites. This behavior is a cause of concern. The DOE analysis showed that the most significant factor affecting the amount of photoresist removed is the wafer temperature. This suggests that even though the partial recipe specifies a set point of 235 degrees Celsius for the wafer temperature, the temperature at the edges of the wafer is less than the temperature at the center of the wafer. Using the prediction profiler feature in JMP, it can be determined that a 1 degree Celsius increase in wafer temperature can remove approximately 80 Angstroms of photoresist more on the G53000 machine. This suggests that the difference in temperatures between the center and the edge of the wafer is approximately 8.75 degrees Celsius. To validate this hypothesis, a temperature-mapping wafer was inserted into the chamber of the G53000 machine and the process was run to check the actual temperatures. Figure 5-5 shows the temperature profile of the wafer.

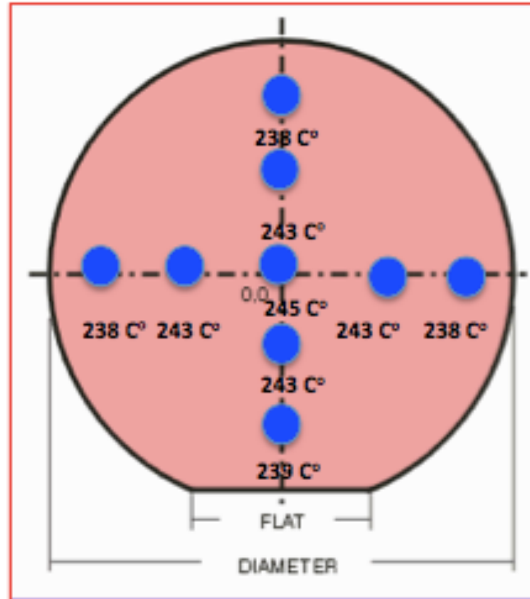

Figure 5-5: Temperature profile of a wafer being processed in the G53000 machine using the partial recipe.

The temperature profile of the wafer follows a radial pattern, and clearly shows that there is a difference of 7 degrees Celsius between the center of the wafer and the edge sites, which is very close to what the DOE predicted. It can also be seen that even though the temperature set point for the G53000 machine was 235 degrees Celsius, the actual wafer temperature is much above 235 degrees Celsius, which explains why the G53000 machine strips more photoresist than the target. The actual temperature is 10 degrees Celsius higher than the set point temperature in the center of the wafer, while at the edge points it is 3 degrees Celsius higher. The DOE predicts a difference of 12.5 degrees Celsius (1000 Angstroms) between the actual temperature and set point temperature at the center, and 3.8 degrees Celsius (300 Angstroms) difference between the actual temperature and set point temperature at the edge points.

The G63000 machine also shows similar trends. The spatial map of a wafer processed on the G63000 machine and the temperature profile obtained from the temperature-mapping wafer are shown in Figure 5-6 and Figure 5-7 respectively.

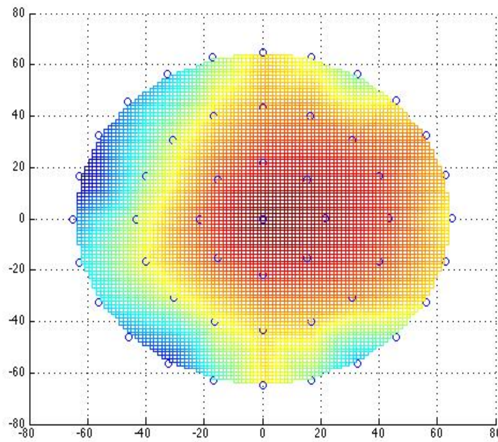

Figure 5-6: Spatial map of wafer processed in the G63000 machine using the partial recipe.

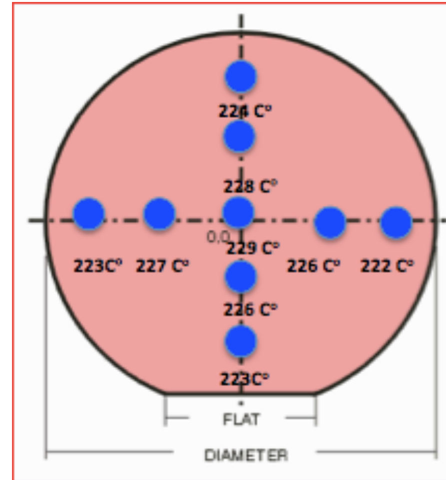

Figure 5-7: Temperature profile of a wafer being processed in the G63000 machine using the partial recipe.

The G63000 machine strips on average 400-600 Angstroms of photoresist less than the G53000 machine, and looking at the temperature profiles of the two wafers, one can clearly see that the actual temperature of the wafer on the G63000 machine is much less than the actual temperature of the wafer on the G53000 machine. The prediction profiler tool in JMP concludes that a 1 degree Celsius change in wafer temperature on the G63000 machine strips 70 Angstroms more of photoresist from the wafer. The average amount of photoresist stripped by the G63000 machine is around 300 Angstroms less than the target value of 6000 Angstroms. The difference between the wafer temperature and temperature set point at the center of the wafer is 6 degrees Celsius (DOE prediction is 4.3 degrees Celsius) and the overall average temperature difference between the wafers on the two machines is 13 degrees Celsius (DOE prediction is 8.25 degrees Celsius).

This analysis shows that the current temperature controller on the machines fails to maintain the wafer temperature at its set point throughout the duration of the process. This is an issue because failure to maintain the wafer temperature at the set point has a significant effect on both the amount of photoresist removed from the wafer and the wafer non-uniformity. The analysis also validates the result of the DOE.

Analog Devices Inc. has five Gasonics tools in operation at their Wilmington, MA fabrication center. The actual historical production data over a period of nine months for the plasma ashing process using the partial recipe was analyzed and Table 5-1 shows the statistics of the data for each machine with the control chart limits for the amount of photoresist removed.

Machine	Average Photoresist Stripped	UCL Photoresist Stripped	LCL Photoresist Stripped	Average Non-Uniformity
G23000	5367.18	5695	5039	5.10%
G43000	5783.8	6193	5375	2.70%
G53000	5669.75	6166	5175	3.70%
G63000	5688.2	6251	5126	3%
G73000	5735.13	6139	5332	3.10%

Table 5-1: Statistics of nine month actual production data from the Gasonics tools with proposed control limits.

It can be clearly seen that the G23000 machine is performing very poorly compared to the others. This anomaly was not detected until this table was made. The root cause of the issue on the machine was that the infrared heat lamps present in the machine chamber and used to heat the wafer to the desired temperature were not properly installed, showing once again that wafer temperature is the most significant factor in this process. Since the DOE analysis was already done, the process engineers instructed the equipment technicians to check the wafer temperature related equipment on the machine first, thus reducing considerable amount of machine downtime in resolving this issue. It is also important to note that the power of these heat lamps decreases over time leading to process drifts and mean shifts and therefore it is imperative to monitor this process using SPC charts over time.

ii. Effects on Wafer Non-Uniformity due to Wafer Geometry and Gas Flows

Figures 5-8 and 5-9 show the spatial maps of a wafer that has been processed by the G53000 and G63000 machines. It is interesting to note the process behavior of the plasma ashing process done on both machines at the location of the flat of the wafer, which has been highlighted in the diagrams.

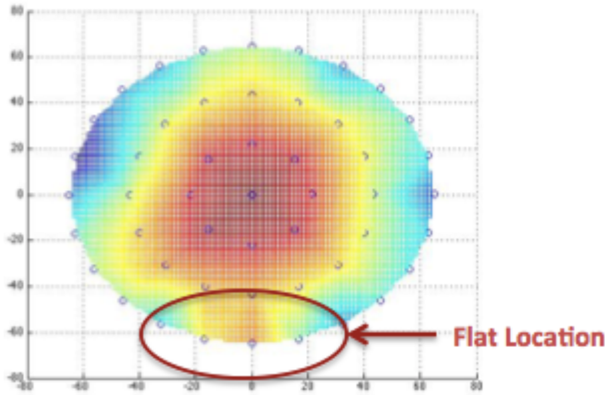

Figure 5-8: Flat effect on wafer processed in the G53000 machine using the partial recipe.

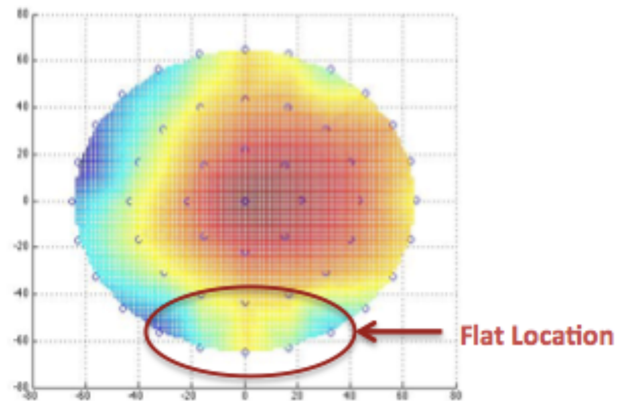

Figure 5-9: Flat effect on wafer processed in the G63000 machine using the partial recipe.

It can be seen that there is more photoresist stripped at the location of the flats than what would be expected at the edge points. This is because the temperature profiles of wafers in both the machines as shown in Figure 5-5 and Figure 5-7 clearly indicate a uniform radial pattern, i.e., temperature at sites equidistant from the center of the wafer is the same, and ideally the photoresist strip pattern should have resembled a “bull’s eye” as seen in Figure 5-1. However, due to the change in geometry of the wafer at the flat, the fluid mechanics and the heat transfer mechanisms of the gas flows over the flat may be different compared to the other parts of the wafer leading to the anomalies. To validate the fact that the presence of the wafer flat was indeed the cause of the anomalies and not the intrinsic structure of the machines, the wafer orientations were changed (wafers rotated by 90, 180, and 270 degrees) in the chamber of the machines and the process was run but the outcome was the same.

It is also interesting to note the right half of the spatial map of a wafer processed in the G63000 machine shown in Figure 5-6. The amount of photoresist removed on the right side of the wafer is much more than what would be expected given the uniform radial temperature profile. It is hypothesized that this is due to position of the vacuum pump on the machine which has an outlet close to the right hand side location of the wafer. This outlet is supposed to be sealed and the gases are to be purged from the chamber through an opening right below the wafer. However, in the case of the G63000 machine, there seems to be a leak in the outlet which is close to the right hand side of the wafer which is pulling the reacting gases towards it during

the chamber purging process leading to more photoresist stripping on the right hand side of the wafer. The equipment engineers at Analog Devices Inc. were in the process of investigating this anomaly more closely at the time this thesis was written.

These anomalies were present in all wafer runs in the past year for the plasma ashing process using the partial recipe and even exist for multiple combinations of the controllable factors in the recipe. Figures 5-10 and 5-11 shows the graphs of the amount of photoresist removed at each site on multiple wafer runs done using the partial recipe on the G53000 and G63000 machine.

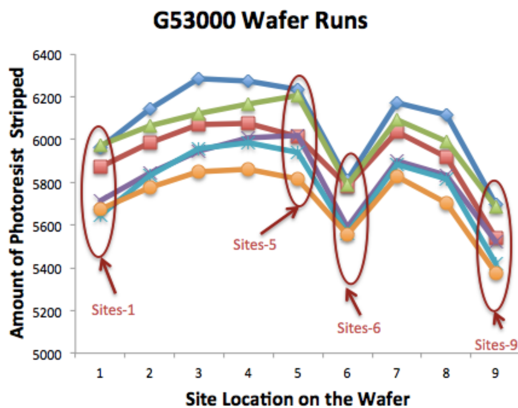

Figure 5-10: Amount of photoresist removed from each site in the plasma ashing process using the partial recipe on the G53000 machine.

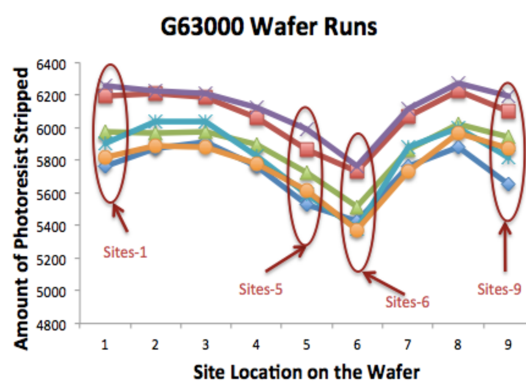

Figure 5-11: Amount of photoresist removed from each site in the plasma ashing process using the partial recipe on the G63000 machine.

The edge points shown in each of the graphs show considerable difference in the amount of photoresist removed at each site which is due to the wafer geometry and gas flow effects. Site 1 is on the topmost side of the wafer opposite the flat, site 5 lies in the wafer flat region, site 6 is on the leftmost side of the wafer, while site 9 is on the rightmost side of the wafer. It is therefore important to find a way to get rid of these effects if wafer uniformity is to be improved even further. A recommendation was made to Analog Devices Inc. to use circular wafers with notches instead of the wafers with flats but at the time this thesis was written, the company did not have

any six inch circular wafers with notches in stock and therefore the behavior of those wafers could not be tested.

iii. Faulty Sensor Calibration

The Gasonics tools rely on sensors and a PID controller to make sure that the recipe parameters are always maintained at their set points during the plasma ashing process. It is therefore necessary to ensure that these sensors are always functioning as expected. These sensors are periodically upgraded or replaced during machine maintenance operations and need to be calibrated before they become operational. Typically the manufacturer of the sensor does provide the calibration constants that simply need to be entered in the machine computer. Analog Devices Inc. in the past has had issues where the manufacturer's calibration constants were not correct. In those cases, the equipment engineers had to rely on their intrinsic process knowledge and use the method of trial and error to manually adjust the sensor calibration constants in the machine computer. Their only feedback was the SPC chart and they had to keep on running additional wafer runs until the process was back in control. This method was purely qualitative, time consuming, and costly to the company. A DOE analysis once again is useful in alleviating such issues. The prediction profiler feature in JMP provides a quantitative relationship as to how a unit change in any factor or input variable can affect the response of the output variable. Figure 5-12 shows the prediction profiler graphs from the DOE analysis done on the G53000 machine to model the response of the amount of photoresist removed from site 1 of the wafer.

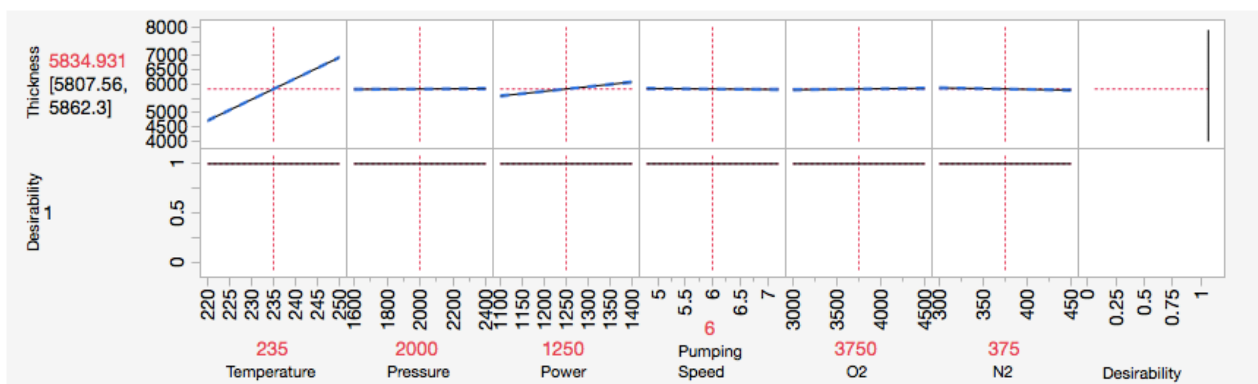

Figure 5-12: Prediction profiler for the amount of photoresist removed from site 1 of the wafer in the G53000 machine.

The graphs clearly show that wafer temperature is the most significant factor followed by power in affecting the amount of photoresist removed. Using these graphs, charts can be made that can be included in the standard operating procedures of the equipment engineers that highlight the hierarchy of significance of factors and provide quantitative relationships between the input factors and the response variable that is plotted on the SPC charts, so that the engineers have a clear idea as to what look for in case the process goes out of control. For example, should the plasma ashing process on the Gasonics tools go out of control, the equipment that controls the wafer temperature must be inspected first, followed by the equipment that controls the RF power as those two are the most significant factors affecting the process. For the G53000 machine, a unit increase in temperature results in approximately 80 Angstroms of photoresist being stripped more and a unit increase in power results in approximately 1 Angstrom of photoresist being stripped more. The other factors have negligible effects.

5.3 Process Improvement Strategies

A DOE analysis can be a powerful guide in developing strategies that can improve current processes either to save costs or optimize a response variable. For example, in the plasma ashing process, oxygen and nitrogen gases are considered as consumables. The DOE analysis for the G53000 machine shows that these gases have no significant impact on the amount of photoresist removed, therefore running these gases at their low levels (oxygen-3000 SCCM, nitrogen-300 SCCM) instead of their current levels (oxygen-3750 SCCM, nitrogen-375 SCCM) can save up to 413 SCC (partial ashing process takes about half a minute to complete, therefore the volume of combined gas used per wafer is half of 825 SCCM) of both gases combined per wafer, and the process will still achieve its target of removing 6000 Angstroms of photoresist from the wafer with a little bit of sacrifice in the wafer non-uniformity. Taking a simple hypothetical case, if the cost of in-house production and storage of both these gases was determined to be 1 cent per SCC, and 100 wafers are run everyday, and the fabrication center is open for 350 days a year, then the potential cost savings opportunity in this case would be $144,550 a year. While, the cost of consumables in the plasma ashing process is actually much less than this, in processes where the cost of consumables is high, a DOE analysis can definitely help in determining cost savings strategies.

In many processes, the input factors are generally run at higher levels to incorporate safety factors. Running equipment and tools at higher levels may cause frequent failures and breakdowns. A DOE analysis is again useful in making sure that the factors in a process are run at the appropriate levels, and this may prolong the life of equipment and tools. For example, in the DOE analysis of the G63000 machine it is determined that the vacuum pumping speed is not significant to either the amount of photoresist removed or the wafer non-uniformity. Again taking a hypothetical case, if it is observed that the vacuum pump on the G63000 machine needs frequent repair operating at its current level, then running the vacuum pump at its lower level may help in prolonging its life leading to less machine downtime and more cost savings.

For process optimization purposes, doing DOEs to construct response surfaces as done for the wafer non-uniformity on both the G53000 and G63000 machines is a useful method. Process time is another response variable that is frequently optimized to increase throughput rate.

Chapter 6: Conclusion and Future Work

This chapter presents the conclusion of the thesis and the scope for future work that can be done by Analog Devices Inc. using the methods demonstrated in this thesis.

6.1 Conclusion

The goal of this thesis is to show the benefits of doing a DOE analysis in a practical industrial setting and ways in which insights obtained from this analysis can be used by Analog Devices Inc. to their advantage. This thesis presents the advantages and limitations of various design choices, design types, and modeling techniques. The thesis also aims to show how the behavior of two machines built to do the same process with the same process parameters can be substantially different and if not accounted for could lead to problems. The work in this thesis was done in a comprehensive manner over a period of two and a half months focusing on one type of machine and one process. While doing such a comprehensive analysis in an industrial setting is difficult, it is hoped that this document can serve as pedagogical tool for process engineers at Analog Devices Inc. as they try to characterize the process variations in the rest of the processes in the fabrication center.

6.2 Future Work

The DOEs done in this thesis do not take into account the process time as a factor in the plasma ashing process. Before the actual plasma ashing process begins, there is a warm up step of 20 seconds where the machine ramps up the process parameters close or equal to the actual values in the recipe. There is no RF power in the warm up step and thus the reactive gases are not ionized. It is observed that since the temperature of the wafer is ramped up to 215 degrees Celsius for 20 seconds in this stage, the wafer is baked and the photoresist shrinks by approximately 3000 Angstroms. The process engineers believe that this could be an issue for some products as the photoresist may change chemical properties during the shrinking process

and this could have unintended negative consequences. There is also a 35 second wafer cooling time after the ashing process has been completed. Both the warm up time and wafer cooling time have been arbitrarily decided keeping the notion of safety factor in mind. There is an opportunity to optimize both these times and reduce the overall process time by doing a DOE. Reducing process time could lead to a significant improvement in throughput. It is also hoped that the process engineers at Analog Devices Inc. will use this document as a template to perform DOEs on other machines and processes in the fabrication center.

References

[1] Analog Devices Inc., "Corporate Information | Analog Devices." [Online]. Available: http://www.analog.com/en/about-adi/corporate-information.html.

[2] Analog Devices Inc., "Analog Devices Inc. Form 10-K." [Online]. Available: http://files.shareholder.com/downloads/ADI/2383156919x0x872073/9B336071-EF60-43AF-9E98-A424EEF6634C/2015_AnalogDevices_AR.FINAL_for_Posting.pdf. [Accessed: 10-Aug-2016].

[3] T. Nilgianskul, "Control of a Semiconductor Dry Etch Process using Variation and Correlation Analyses," Master's thesis, Massachusetts Institute of Technology, 2016.

[4] F. Haskaraman, "Chamber Matching in Semiconductor Manufacturing using Statistical Analysis and Run-to-Run Control," Master's thesis, Massachusetts Institute of Technology, 2016.

[5] Lam Research Corporation, "Products | Lam Research." [Online]. Available: http://www.lamresearch.com/products/products-overview.

[6] G. S. May and C. J. Spanos, *Fundamentals of Semiconductor Manufacturing and Process Control*. John Wiley & Sons, Inc, 2006.

[7] Electron Microscopy Sciences, "Plasma Ashing Applications Technical Data Sheet." [Online]. Available: https://www.emsdiasum.com/microscopy/technical/datasheet/plasma_apps.aspx.

[8] "Aura 3010 ® Operations Guide." Gasonics International.

[9] Justin BD&L, "Gasonics A3010 Dry Asher." [Online]. Available: http://www.surplushere.com/Inventory/Config/Config_Novellus-Gasonics_A3010_Asher.pdf. [Accessed: 11-Aug-2016].

[10] J. C. Davis, R. S. Gyurcsik, J. C. Lu, and J. M. Hughes-Oliver, "Robust Metric for Measuring Within-Wafer Uniformity," *IEEE Trans. Components, Packag. Manuf. Technol. Part C. Manuf.*, vol. 19, no. 4, pp. 283–289, 1996.

[11] NASA, "Giovanni-3 Operation Technical Summary: Time Series Statistics." NASA Goddard Earth Sciences Data and Information Services Center, 2009.

[12] E. Sachs and R. S. Guo, "Modeling, Optimization and Control of Spatial Uniformity in Manufacturing Processes," *IEEE Trans. Semicond. Manuf.*, vol. 6, no. 1, pp. 41–57, 1993.

[13] W. E. Johnson, *Logic-Part III-The Logical Foundations of Science*. 1924.

[14] R. E. Barlow and T. Z. Irony, "Foundations of Statistical Quality Control," in *Current Issues in Statistical Inference: Essays in Honor of D. Basu*, 1992, pp. 99–112.

[15] Western Electric Company, *Statistical Quality Control Handbook*, 2nd ed. Easton: Mack Printing Company, 1958.

[16] D. Montgomery C., *Introduction to Statistical Quality Control*, 6th ed. John Wiley & Sons, Inc.

[17] "JMP® Pro 12.1.0." SAS Institute Inc., Cary, NC.

[18] "Minitab 17 Statistical Software." Minitab, Inc., State College, PA, 2010.

[19] D. Drain, *Statistical Methods for Industrial Process Control*. Chapman & Hall/CRC.

[20] D. Montgomery C., *Design and Analysis of Experiments*, 5th ed. John Wiley & Sons, Inc, 2007.

[21] G. Snedecor and W. Cochran, *Statistical Methods*, 6th ed. Iowa State University Press, 1967.

[22] "MATLAB 8.6." The Mathworks, Inc., Natick, MA.

[23] J. Shlens, "A Tutorial on Principal Component Analysis," 2005. [Online]. Available:

http://www.cs.cmu.edu/~elaw/papers/pca.pdf. [Accessed: 09-Aug-2016].

[24] Minitab, “Patterns in Residual Plots.” [Online]. Available: http://support.minitab.com/en-us/minitab/17/topic-library/modeling-statistics/regression-and-correlation/residuals-and-residual-plots/patterns-in-residual-plots/. [Accessed: 10-Aug-2016].

[25] SkyMark Corporation, “Normal Test Plot.” [Online]. Available: http://www.skymark.com/resources/tools/normal_test_plot.asp.